NOTICES PAGE

Foreign Nation Release

This information is furnished upon the condition that it will not be released to another Nation without specific authority of the cognizant agency (Military or NASA) of the United States Government, and that the information be provided substantially the same degree of protection afforded it by the Department of Defense of the United States.

Disclaimer of Liability from Act of Transmittal

When Government drawings, specifications, or other data are used for any purpose other than in connection with a definitely related Government procurement operation, the United States Government thereby incurs no responsibility nor any obligation whatsoever; and the fact that the Government may have formulated, furnished, or in any way supplied the said drawings, specification, or other data, is not to be regarded by implication or otherwise as in any manner licensing the holder or any other person or corporation, or conveying and rights or permission to manufacture, use, or sell any patented invention that may in any be related thereto.

Any information disseminated by the Data Distribution Centers of the Interagency Data Exchange Program is intended to promote test data utilization in the National interest among groups engaged in Ballistic Missile, Space Vehicle and related programs.

Dissemination of said information does not imply verification or endorsement of the information. The originator, in submitting the material is acting in accordance with the requirements of his contract, and neither the originator nor the disseminator assumes any liability to parties adopting any product, process or practice based upon the usage of the information. Its presenting the success or failure of one (or several) part number(s), model(s), lot(s) under specific environment and output requirements, does not imply that other products not herein reported on are either inferior or superior.

Omission of Charges for Follow-on Actions

Any compliance by the report originator with requests from recipients for more detailed information on IDEP reports originated under Government contracts will be considered within the scope of present contractual obligations. Compliance with such requests will be at the discretion of the report originator and will be performed without cost or obligation to the requestor unless otherwise negotiated in advance.

Reproduction of this Report

Reproduction or duplication of any portion of this report is expressly forbidden, except by those contractors receiving it directly from the Data Centers or originator, for their internal use or the use of their sub-contractors. Reproduction or display of all or any portion of this material for any sales, advertising of publicity purposes is prohibited.

~~HSTIF~~

DRA

~~ERTS~~

(E83-10112) GEOMAGNETIC MODELING BY OPTIMAL RECURSIVE FILTERING Final Report (Business and Technological Systems, Inc.) 119 p
HC A06/MF A01
CSCL 08G
G3/43

N83-15755
Unclas
00112

BUSINESS AND TECHNOLOGICAL SYSTEMS, INC.

BTS

BTS-FR-81-147

MAY 1981

GEOMAGNETIC MODELING BY OPTIMAL RECURSIVE FILTERING

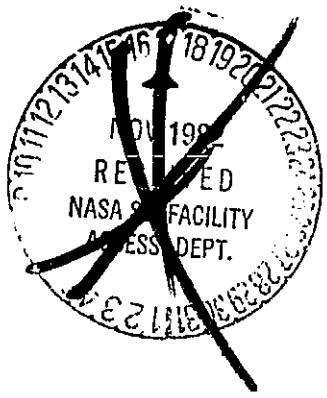

by

BRUCE P. GIBBS

RONALD H. ESTES

FINAL PEPORT
Contract NAS 5-26250

prepared for
NATIONAL AERONAUTICS AND SPACE ADMINISTRATION
GODDARD SPACE FLIGHT CENTER
Greenbelt, Maryland 20771

by
BUSINESS AND TECHNOLOGICAL SYSTEMS, INC.
Aerospace Building, Suite 440
10210 Greenbelt Road
Seabrook, Maryland 20801

Table of Contents

Page

Appendices

1.0 Introduction and Summary

1.1 Overview

Geomagnetic field models are important for a number of uses, including investigation of processes deep within the earth's interior, trend removal for anomaly studies, and the investigation of the correlation between geomagnetic and geodetic anomalies. (Field models are also used for navigation and survey purposes and charged particle trajectory calculations.) The typical method of modeling the main field and the secular variation is by least squares analysis using spherical harmonic models. An extensive review of spherical harmonic methods and main field and secular variation models is given by Barraclough [1975, 1976].

Most users of geomagnetic field models require accurate estimates of the current field. This necessitates prediction beyond the data domain of a field model and, inevitably, involves extrapolation inaccuracies caused by uncertainties in modeling changes in secular variation patterns. Due to present lack of knowledge of the underlying physical processes involved, these patterns can typically be accurately modeled by linear variations only over periods on the order of a few years.

Recursive estimation theory provides a means of combining models obtained by conventional batch least squares over deterministic periods into optimal estimates of the field model parameters at any particular time. In particular, this technique should provide more accurate field model prediction capability. This is done by using statistical information about the temporal variation in the field model to weight the individual least squares solutions for a particular time interval (here referred to as a batch estimate). Obviously, the most recent data is weighted most heavily and past data is given the least weight. However, the data from all of the conventional solutions over the deterministic periods is included in the solution so that the prediction errors should be significantly less than those for a single batch estimate. In

particular, the MAGSAT mission, with accurate vector and scalar data, will provide for a highly accurate field model for epoch 1980, and the recursive procedure will allow for improved prediction capability from the MAGSAT model by optimally incorporating past information.

Other advantages of recursive estimation include the ability to easily update the field model as new data becomes available, improve the field estimate for times in the past and also to generate an estimate of the error in the field.

1.2 Summary

The results of a preliminary study to determine the feasibility of using Kalman filter techniques for geomagnetic field modeling are given in this report. Specifically, five separate field models were computed using observatory annual means, satellite, survey and airborne data for the years 1950 to 1976. Each of the individual field models used approximately five years of data. Then these five models were combined using a recursive information filter (a Kalman filter written in terms of information matrices rather than covariance matrices.) The resulting estimate of the geomagnetic field and its secular variation was propogated four years past the data to the time of the MAGSAT data. The accuracy with which this field model matched the MAGSAT data was evaluated by comparisons with predictions from other pre-MAGSAT field models. The field estimate obtained by recursive estimation was found to be superior to all other models.

It must be emphasized that this study was not intended to be the final word on field modeling. Because of the preliminary nature of the study, several "short cuts" were taken which make the field estimate suboptimal. In particular, Kalman filtering can only be optimal when the statistics of the unmodeled field dynamics (among other quantities) are known. In this study, there statistics were obtained by an "eyeball estimate" using plots of the estimated field model coefficients and were refined using the likelihood function computed by the Kalman filter.

However, these estimates are crude at best and should really be obtained using a more sophisticated technique such as maximum likelihood estimation. (Obviously it would be preferable to use knowledge of the core dynamics but this is not well known at the present time).

Another "short cut" involves the handling of observatory "biases" and scaling of the information matrices to account for aliasing and data noise. This is discussed in detail in later sections.

Considering the limitations of this study, we believe that the results are encouraging and warrant further analyses to optimally apply recursive estimation for geomagnetic field modeling.

2.0 Mathematical Description

2.1 Deterministic Geomagnetic Models

While several organizations are currently involved in core field modeling, the basic techniques used date back to Gauss, with virtually no utilization of modern estimation methods. Typically, the magnetic field is parameterized as a scalar potential expanded in spherical harmonics

$$V = V_{internal} + V_{external}$$

$$V = \bar{a} \sum_{n=1}^{n^*} \left(\frac{\bar{a}}{r}\right)^{n+1} \sum_{m=0}^{n} (g_n^m \cos m\phi + h_n^m \sin m\phi)\, P_n^m(\theta)$$

$$+ \bar{a} \sum_{n=1}^{k} \left(\frac{r}{\bar{a}}\right)^{n} \sum_{m=0}^{n} (\gamma_n^m \cos m\phi + \delta_n^m \sin m\phi)\, P_n^m(\theta)$$

where

$\bar{a}$ = mean radius of the earth

n^* = maximum degree of the expansion

r = geocentric distance

g, h = quasi-normalized Schmidt coefficients

ϕ = east longitude

θ = colatitude

$P_n^m(\theta)$ = associated Legendre Functions (Schmidt quasi-normalized).

Here V is the potential at a point in a domain free from sources of magnetic field, and the field vector $\bar{B}$ is given by the gradient of this potential

$$\bar{B} = -\nabla V \ .$$

The coefficients g and h are typically represented deterministically as first or second order Taylor expansions in time about some epoch t_0, with a conventional least squares batch processing method (outlined in Section 2.3) used for their recovery.

While data from repeat stations, marine surveys, aeromagnetic surveys, magnetic observatories and satellites (principally the POGO series and currently MAGSAT) contribute to the determination of the geomagnetic field over a time interval about the epoch, annual means from a world-wide network of magnetic observatories (see Figure 2.1) represent the most useful data set for determining the secular variation of the internal field. The difficulty in modeling the temporal variation of the field over more than a short time interval is illustrated in Figure 2.2 for the Abisko observatory. There the solid lines represent a quadratic polynomial model for g_n^m and h_n^m over the interval 1900-1965. For prediction of the magnetic field, the selection of the temporal representation for a given data span is crucial, and the danger of extrapolating beyond the data is clear. The incorporation of annual means data into a main field model for a particular epoch suffers from the fact that the magnetic field measured at the observatory is the vector sum of the main field and a contribution due to local crustal magnetization,

$$\bar{B} = \bar{B}_{internal} + \bar{B}_{crustal}$$

where $\bar{B}_{crustal}$ may change appreciably over the distance of a few kilometers. While $\bar{B}_{internal}$ varies with time, however, $\bar{B}_{crustal}$ remains constant. Thus, models of secular variation based only on time derivatives of annual means observations

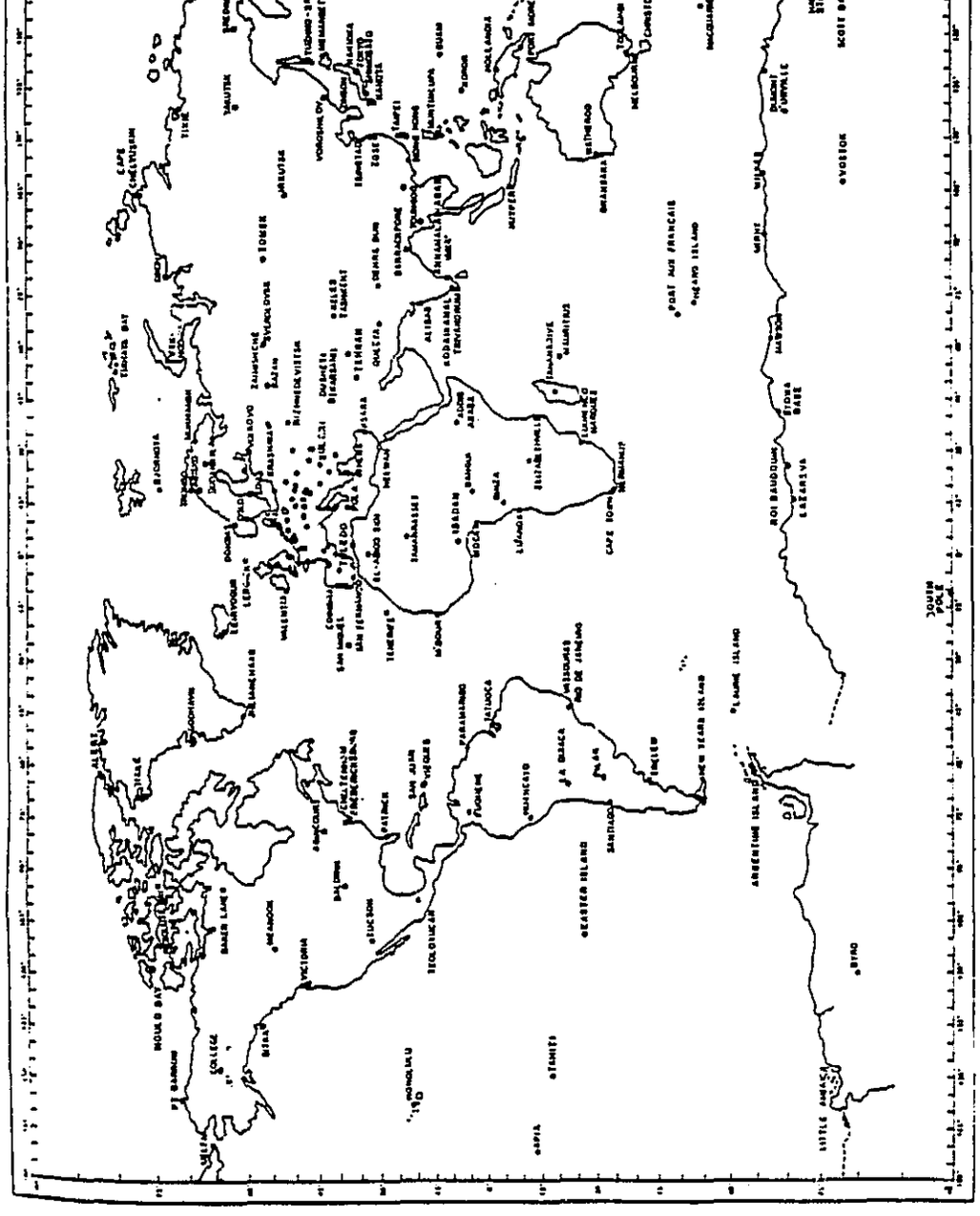

Figure 2.1 World Wide Magnetic Observatories

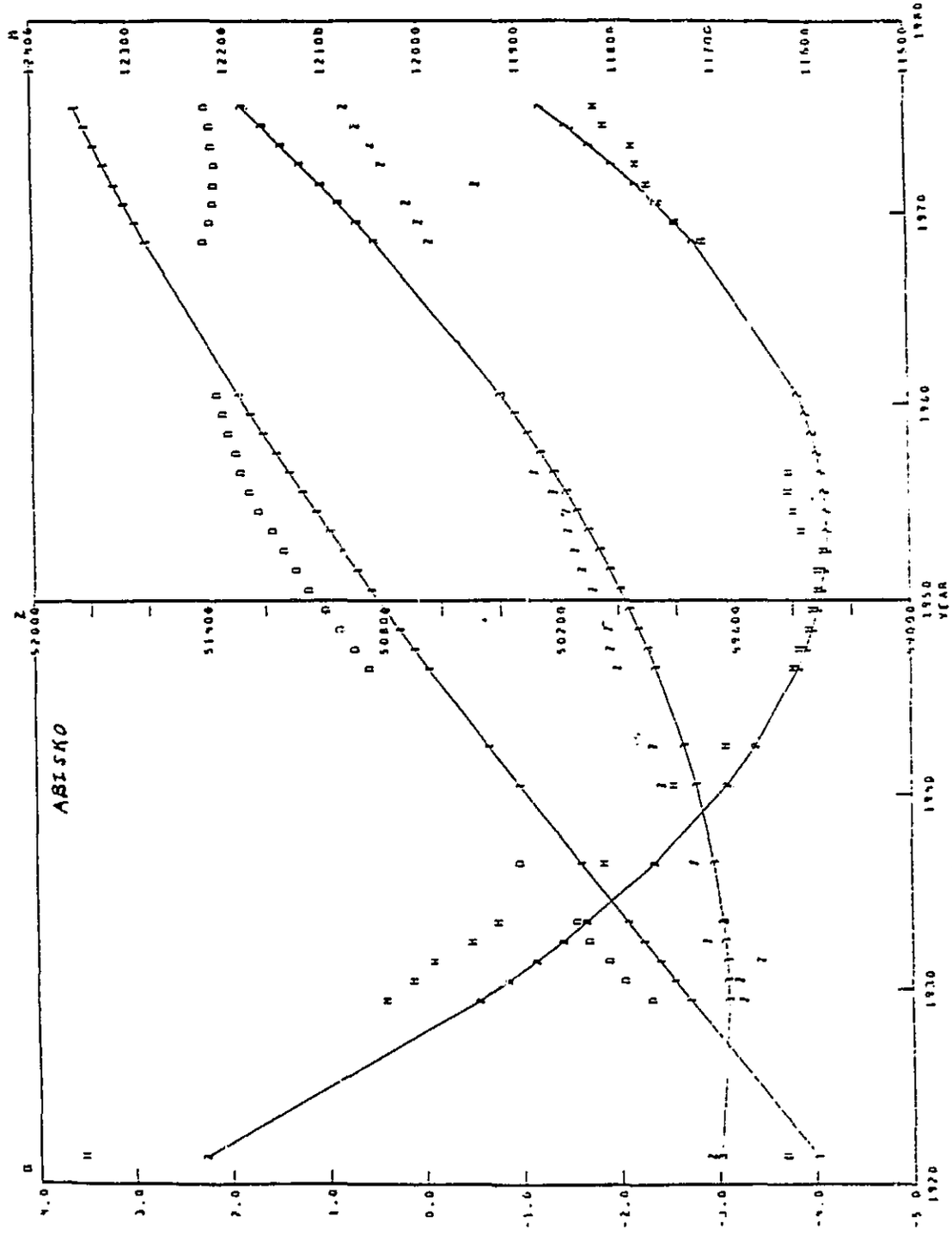

Figure 2.2 Abisko Magnetic Observatory Data

$$\dot{\bar{B}} = \dot{\bar{B}}_{internal}$$

are not influenced by the local anomalous fields, but models of the main field are aliased.

In this analyses, the main field and its secular variation were estimated simultaneously, using both annual means and other data types (satellite, airborne, survey). The annual means data is accommodated by solving for the local observatory bias, $\bar{B}_{crustal}$, at each observatory. This allows the data to properly distribute its influence among the secular variation and constant parameters of the model in a least squares sense. The local biases, which are estimated along with the field model, provide some physical measure of the local anomaly field.

2.2 Modeling The Temporal Variation of the Field

In the previous section, it was stated that the temporal variation of the core geomagnetic field has usually been modeled deterministically as a first or second order Taylor series expansion. This deterministic modeling is a necessity when conventional least squares estimation is employed. However, when Kalman filtering is used, the process can be modeled as a stochastic one. Thus the question arises as to whether some form other than a truncated Taylor series would be more appropriate for modeling the temporal variation. For example, a first or second order Markov process may be suitable. However, Markov process models are mainly useful when the data span is a significant fraction of the time constants of the process and when the process is zero mean. If the data span is much shorter than the time constants of the process, the output can be approximated quite well as the integration of initial conditions and white noise inputs for a system which does not use feedback (although the order of the system may be different than that of the Markov

process). In other words, knowledge of the time constants of a Markov process does not significantly improve the modeling of that process when the data span is much shorter than the time constants.

For the case of geomagnetic core field modeling, the shortest time constants appear to be 50 to 100 years (it is difficult to determine them accurately when only 80 years of data are available). Since we are only using 26 years of data (1950-1976), the use of a Markov model is not justified (even if it was, we do not know the time constants). Furthermore, many of the low degree coefficients in the spherical harmonic expansion are definitely not zero mean (e.g. g_{10}). Thus the "bias" in coefficients would have to be estimated separately from the Markov process, adding unnecessary complexity to the model.

For these reasons, Markov models were not used in our analyses. Rather, the stochastic contribution of the temporal variation of the spherical harmonic coefficients was modeled as one of two forms:

$$\text{low degree:} \quad \dddot{c}_i(t) = w_i(t)$$

$$\text{high degree:} \quad \ddot{c}_i(t) = w_i(t)$$

where:

c_i represents a coefficient of the spherical harmonic expansion
w_i is random noise.

Thus the expressions for c as function of time are:

$$\text{low degree:} \quad c_i(t) = c_i(t_0) + \dot{c}_i(t_0)(t-t_0) + \ddot{c}_i(t_0)(t-t_0)^2/2 + q_i(t-t_0)$$

$$\text{high degree:} \quad c_i(t) = c_i(t_0) + \dot{c}_i(t_0)(t-t_0) + q_i(t-t_0)$$

where $q_i(t-t_0)$ represents a random disturbing input (i.e. weighted integral of w(t) (See Section 2.3.3).

The dividing line used in deciding between the linear and quadratic models was set so that the differences between the data and the model appeared to be random. All coefficients of degree 7 or less used the quadratic model while the linear model was used for higher degree coefficients.

2.3 Estimation Procedure

Data available for field modeling is comprised of survey and observatory annual means values (primarily D, I, H, Z, F), oceanographic data (F), aeromagnetic data (F), and satellite data (F). With MAGSAT, there will be available satellite vector component data as well. For this preliminary study, only data from 1950 to 1976 was used. Prior to 1950, the data coverage is sparse. No data after 1976 was used so that the estimated field could be predicted to 1980 and compared with the MAGSAT data. During the period 1950 to 1976, approximately 186,000 observatory, ground survey, aeromagnetic and satellite observations are available. Oceanographic and repeat survey data were not used in this preliminary analysis because of its questionable quality and difficulty in using it properly.

The following sections describe the procedure used to compute "mini-batch" field models, the recursive estimation procedure and the calculation of the state noise matrix.

2.3.1 Mini-Batch Field Models

The recursive estimation procedure used here requires the calculation of conventional epoch field models on a "mini-batch" interval of approximately 5 years of data. The computer software used for this

purpose is that originally developed at Goddard Space Flight Center by Cain, et al, 1967 and recently modified and enhanced by Business and Technological Systems, Inc., (Estes, 1979 and 1980).

For the purpose of clarifying equations to follow, we shall summarize the equations of the conventional batch solution in matrix notation. Values of the g and h coefficients at any point in time are assumed to be in terms of the values at epoch (t_0). Since we are using only 5 years of data in each "mini-batch," the field can be adequately represented (with negligible aliasing) using only constant and linear terms, ie.

$$g(t) = g(t_0) + \dot{g}(t_0)(t-t_0)$$

$$h(t) = h(t_0) + \dot{h}(t_0)(t-t_0)$$

The maximum degree to which the constant and linear terms in the expansion was carried varied for the different mini-batches. When satellite data was available (after 1960), the constant and linear terms were carried to degree 13. However, prior to 1960, the available data would not support a solution with so many unknowns. Thus the cutoff was lower. (Details for the individual mini-batches are given in section 3.1).

For purposes of clarity in the discussion to follow, we will assume that secular velocity terms are present through $n^* = 13$. The relationship of the parameters can be written in matrix form by defining a state vector which contains the values and derivatives of the coefficients. Let

$$\underset{\sim}{x}^T = [g^{1,0}\ \dot{g}^{1,0}\ g^{1,1}\ \dot{g}^{1,1}\ h^{1,1}\ \dot{h}^{1,1} \ldots h^{13,13}\ \dot{h}^{13,13}\ b_x^1\ b_y^1\ b_z^1 \ldots b_z^{\ell}]$$

where b_x^i, b_y^i, b_z^i are "biases" in the x, y and z components of the

magnetic field at observatory i. (This accounts for localized fields) Then

$$\underline{x}(t) = \Phi(t-t_0)\ \underline{x}(t_0)$$

where

$$\Phi = \begin{bmatrix} \begin{matrix} 1 & \Delta t \\ 0 & 1 \end{matrix} & 0 & 0 & 0 \\ 0 & \begin{matrix} 1 & \Delta t \\ 0 & 1 \end{matrix} & 0 & 0 \\ 0 & 0 & \ddots & 0 \\ 0 & 0 & 0 & I \end{bmatrix}$$

Let the set of measurements during the mini-batch period be denoted by vector $\underline{y}$ of length m (m may be on the order of tens of thousands). Then $\underline{y}$ can be written as a nonlinear function of $\underline{x}$ plus random measurement noise ($\underline{y} = f(\underline{x}) + \underline{v}$). The perturbations in $\underline{y}$ ($\delta\underline{y}$) due to perturbations in $\underline{x}$ ($\delta\underline{x}$) can be written as

$$\delta\underline{y} = M\ \delta\underline{x}$$

where

$$M = \frac{\partial \underline{y}}{\partial \underline{x}} \qquad \text{(dimension mxn)} .$$

Then the weighted, least squares, differential correction estimate of $\underline{x}$ is given by

$$\hat{\underline{x}}^K = \hat{\underline{x}}^{K-1} + (M^T W^{-1} M)^{-1}\ M^T W^{-1} (\underline{y} - f(\hat{\underline{x}}^{K-1}))$$

where:

$\hat{\underline{x}}^K$ = the estimate of $\underline{x}$ at iteration K

W = the covariance matrix of the random measurement errors. If $\underline{y} = f(\underline{x}) + \underline{v}$ where $\underline{v}$ is a zero-mean, random error vector, then $W = E(\underline{v}\underline{v}^T)$ (diagonal).

Denote the converged output of mini-batch number i as $\hat{\underline{x}}_{bi}$. Then the associated covariance matrix for the error ($\Delta\hat{\underline{x}}_{bi}$) is given by

$$P_{bi} \triangleq E(\Delta\hat{\underline{x}}_{bi}\Delta\hat{\underline{x}}_{bi}^T) = (M^T W^{-1} M)_i^{-1} .$$

This matrix is produced as a by-product of the least squares calculation.

After convergence, those partitions of the information matrix ($M^T W^{-1} M = P_{bi}^{-1}$) and the state estimate $\hat{\underline{x}}_{bi}$ corresponding to the field model (spherical harmonic coefficients and derivatives) are written on tape for later use. However, this partition of the information matrix must be equal to the inverse of the corresponding partition of the covariance matrix. If the original information matrix and vector are partitioned as follows:

$$M^T W^{-1} M = \begin{bmatrix} A_1 & A_2 \\ A_2^T & A_3 \end{bmatrix}, \quad M^T W^{-1} \Delta y = \begin{bmatrix} B_1 \\ B_2 \end{bmatrix}$$

where the first partition corresponds to the spherical harmonic coefficients and the second partition corresponds to the observatory biases, then

$$P_{bi} = \begin{bmatrix} D^{-1} & -D^{-1}A_2A_3^{-1} \\ -A_3^{-1}A_2^TD^{-1} & A_3^{-1} + A_3^{-1}\ A_2^T\ D^{-1}\ A_2\ A_3^{-1} \end{bmatrix}$$

where $D = A_1 - A_2A_3^{-1}A_2^T$ is the partition of the information matrix written on the tape.

It was sometimes necessary to modify the epoch of the mini-batch after the information had already been stored. This is done using the following transformations

$$D(t) = \phi^T(t_0-t)\ D(t_0)\ \phi(t_0-t)$$

$$\hat{x}(t) = \phi(t-t_0)\ \hat{x}(t_0)$$

2.3.2 Optimal Filtering of Mini-Batch Field Models

The output from the mini-batches must be combined to produce an optimal estimate of the spherical harmonic coefficients at the epoch of the last mini-batch (1972.5). When properly done, this estimate should yield good predictions of the geomagnetic field for several years into the future. The key to combining the results of the mini-batches is to correctly weight their output. This can be done via a Kalman filter which includes the effects of process (state) noise (Gelb, 1974).

Recall that the temporal model for the spherical harmonic coefficients was assumed to be

$$\underline{x}(t) = \Phi(t-t_0)\ \underline{x}(t_0)$$

where the definition of Φ has been expanded (because of the longer time span) to include quadratic terms in addition to the constant and linear terms for coefficients of degree 7 or less. The partitions of Φ corresponding to quadratic terms are

$$\begin{bmatrix} 1 & \Delta t & \Delta t^2 \\ 0 & 1 & 2\Delta t \\ 0 & 0 & 1 \end{bmatrix} .$$

Although this model is quite adequate when the time span is short, it degrades rapidly as the time span grows. When combining the estimates from different mini-batches, some allowance must be made for the errors in the secular model (e.g., third and higher order derivatives). In other words the secular model can be better written as

$$\underline{x}(t) = \Phi(t-t_0)\ \underline{x}(t_0) + \underline{g}(t-t_0)$$

where $\underline{g}$ is assumed to be an unknown, random disturbance vector.

We now change the notation so that time is not explicitly shown:

$$\underline{x}_{i+1} = \Phi_i\ \underline{x}_i + \underline{g}_i \ .$$

Here, the subscript refers to the epoch of each mini-batch. Since each mini-batch will have a different epoch (at the middle of the data span), an equation of this type must be used to relate the coefficients (state vector) for different mini-batches. However, since q_i is unknown (to us), our best estimate of $\underline{x}_{i+1}$ based upon the measurements included in mini-batch i is

$$\hat{\underline{x}}_{i+1/i} = \Phi_i\ \hat{\underline{x}}_{i/i}$$

where $\hat{\underline{x}}_{i/j}$ means the estimate of $\underline{x}_i$ at mini-batch i based upon measurements up to mini-batch j. $\hat{\underline{x}}_{i+1/i}$ is called the a priori estimate at time i+1 and $\hat{\underline{x}}_{i/i}$ is called the a posteriori estimate at time i.

The a priori error covariance matrix for $\hat{\underline{x}}_{i+1/i}$ is easily shown to be

$$P_{i+1/i} = \Phi_i P_{i/i} \Phi_i^T + Q_i$$

where $Q_i = E(\underline{q}_i \, \underline{q}_i^T)$. For the moment, we will ignore how Q_i is obtained.

After mini-batch i+1 is processed, we can obtain an a posteriori estimate for $\hat{x}_{i+1}$ which optimally combines the results of the new mini-batch and the results of previous mini-batches,

$$P_{i+1/i+1} = [P^{-1}_{i+1/i} + T(M^T W^{-1} M)_{i+1} T^T]^{-1}$$

$$\hat{x}_{i+1/i+1} = P_{i+1/i+1}[P^{-1}_{i+1/i}\hat{x}_{i+1/i} + T(M^T W^{-1} M)_{i+1}\hat{x}_{b,i+1}] \, .$$

where T is a matrix consisting of zeroes and ones which shifts the elements of $\hat{x}_{b,i+1}$ to match those of $\hat{x}_{i+1}$ ($\hat{x}_b$ does not contain quadratic time terms). This is called an information filter (rather than a Kalman filter) because the result is obtained by combining information matrices. For this particular problem, it is more efficient than a Kalman filter. At each step, the inversion of two, positive-definite symmetric matrices is required. This is best done by Cholesky factorization which takes a total of $n^3/2$ operations. For the dimension of the problem discussed previously, this requires a relatively small amount of computer time.

There are two aspects of this procedure which deserve further discussion. First, it was not necessary that all of the coefficient sets be the same size for all mini-batches. For example, it was not desirable (because of the sparseness of data) to solve for all high degree coefficients and derivatives for periods prior to 1960. This simply means that the partitions of the information matrix $(M^T W^{-1} M)$ corresponding to these coefficients contained zeroes. Secondly, notice that new data can be easily incorporated into the solution without rerunning the entire procedure. As additional satellite data is obtained, it can be used to improve the field model.

The final output from this procedure is a state vector (coefficients) and error covariance matrix which are evaluated at the epoch of the last data span. These can then be used to predict the coefficients and error covariance for the next few years. This estimate should be better than the estimate obtained from the last mini-batch because it uses more data going back further in time. However, notice that old data is given less weight in the final solution than new data. The inclusion of Q tells the filter that the state vector is subject to random changes and, thus, it gives the most weight to recent data.

The ability to estimate the error in the predicted coefficients is an important output of this procedure. Although all batch estimation procedures produce an error covariance matrix as a by-product, the usefulness of this covariance has not been widely appreciated. Since the batch procedures do not include a Q term, their error covariance matrices cannot be used to accurately predict the field errors for times outside of the data span. However, the procedure proposed here can do this. By a simple transformation on the covariance matrix, it is also possible to compute the error in the estimated magnetic field at various points on the earth's surface. This could be used to produce a contour map of the earth showing the accuracy of the estimated field.

The accuracy of the proposed estimation procedure depends upon the accuracy of the Q which is used. Past experience has shown that, for most problems where Q is small, the final estimate is not very sensitive to Q. If Q is known within an order of magnitude, the output will probably be satisfactory.

The next section derives the mathematical equations used to compute Q while section 2.3 shows how the likelihood function can be computed in the Kalman filter and used to help refine the estimate of Q.

2.3.3 State Noise Covariance Matrix

The state noise covariance matrix, Q, is defined as the covariance matrix of the unmodeled dynamics in a discrete system. Q_i can be calculated from the continuous system if the spectral density of the random input is known. In other words, if the continuous system is defined as

$$\dot{\underline{x}}(t) = F\underline{x}(t) + \underline{u}(t)$$

where u(t) is white noise, then Q_i can be computed from $E(u(t)u^T(t))$. Using this equation for the continuous system, the corresponding equation for the discrete system is:

$$\underline{x}(t) = \Phi(t-t_0)\underline{x}(t_0) + \int_{t_0}^{t} \Phi(t-\lambda)\underline{u}(\lambda)d\lambda$$

where the second term is equal to q_i as described in section 2.2.2. Thus

$$Q_i = E\left[\int_{t_{i-1}}^{t_i} \Phi(t_i-\lambda)\underline{u}(\lambda)d\lambda \int_{t_{i-1}}^{t_i} \underline{u}^T(\lambda)\Phi^T(t_i-\lambda)d\lambda\right]$$

$$= E\left[\int_{t_{i-1}}^{t_i} \Phi(t_i-\lambda)\underline{u}(\lambda)\underline{u}^T(\lambda)\Phi^T(t_i-\lambda)d\lambda\right]$$

$$= \int_{t_{i-1}}^{t_i} \Phi(t_i-\lambda)E[\underline{u}(\lambda)\underline{u}^T(\lambda)]\,\Phi^T(t_i-\lambda)d\lambda \quad .$$

It is assumed that $E[\underline{u}(\lambda)\underline{u}^T(\lambda)]$ is a constant (Q_s). For the polynomial representation of the spherical harmonic coefficients, the Φ and Q_s matrices take one of two forms:

quadratic terms:
$$\Phi(\Delta t) = \begin{bmatrix} 1 & \Delta t & \Delta t^2 \\ 0 & 1 & 2\Delta t \\ 0 & 0 & 1 \end{bmatrix}, \quad Q_s = \begin{bmatrix} 0 & 0 & 0 \\ 0 & 0 & 0 \\ 0 & 0 & Q_{s2} \end{bmatrix}$$

linear terms:
$$\Phi(\Delta t) = \begin{bmatrix} 1 & \Delta t \\ 0 & 1 \end{bmatrix}, \quad Q_s = \begin{bmatrix} 0 & 0 \\ 0 & Q_{s1} \end{bmatrix}$$

When these expressions are substituted in the expression for Q_i and integrated, the following results are obtained:

quadratic terms:
$$Q_i = Q_{s2} \begin{bmatrix} \frac{\Delta t^5}{5} & \frac{\Delta t^4}{2} & \frac{\Delta t^3}{3} \\ \frac{\Delta t^4}{2} & \frac{4\Delta t^3}{3} & \Delta t^2 \\ \frac{\Delta t^3}{3} & \Delta t^2 & \Delta t \end{bmatrix}$$

linear terms:
$$Q_i = Q_{s1} \begin{bmatrix} \frac{\Delta t^3}{3} & \frac{\Delta t^2}{2} \\ \frac{\Delta t^2}{2} & \Delta t \end{bmatrix}$$

We have implicitly assumed that the process noises for coefficients of different degree and order are uncorrelated. This seems to be a reasonable assumption considering the orthogonality of the spherical harmonic coefficients.

2.4 Computation of the Likelihood Function

In any estimation problem where the measurement and dynamic models are not known with certainty, it is generally useful to compute the log likelihood function within the Kalman filter. This likelihood function can then be used to aid in defining the model. When filter runs using different model parameters are compared, the run which has the highest likelihood function can usually be selected as having the "best" model.

In an ordinary Kalman filter, the extra burden required to compute the log likelihood is trivial since the required quantities are already computed by the filter. However, in our information form of the Kalman filter, the computational burden is quite significant. The total procedure for the information filter and computation of the likelihood is given below:

Step	Filter	Computation of log likelihood
1	Read t_i, $(M^T W^{-1} M)_i$ and $\hat{x}_{b,i}$	
2	$\hat{x}_{i/i-1} = \Phi\ \hat{x}_{i-1/i-1}$	
	$P_{i/i-1} = \Phi\ P_{i-1/i-1}\ \Phi + Q_i$	
3		$\tilde{x}_i = T_2 \hat{x}_{i/i-1} - \hat{x}_{b,i}$
4		$C = T_2 P_{i/i-1} T_2^T + (M^T W^{-1} M)_i^{-1}$
		$L = L + \tilde{x}_i^T C^{-1} \tilde{x}_i + \ln(\det(C))$
5	$P_{i/i} = (P_{i/i-1}^{-1} + T_1 (M^T W^{-1} M)_i T_1^T)^{-1}$	
	$\hat{x}_{i/i} = P_{i/i}(P_{i/i-1} \hat{x}_{i/i-1} + T_1 (M^T W^{-1} M)_i \hat{x}_{b,i})$	

where: T_1 and T_2 are transformation matrices consisting of zeroes and ones which change the dimension of the filter state and the mini-batch state to match. T_1 is used to increase the dimension of $\hat{x}_b$ to match $\hat{x}$ and T_2 is used to decrease the dimension of $\hat{x}$ to match $\hat{x}_b$. In the computer program, this transformation is performed by shifting operations (no matrix multiplications are involved).

L is equal to -2 log likelihood (plus a constant bias).

The inversion of $(M^T W^{-1} M)_i$ in step 3 and the inversion of C in step 4 are the most costly operations in computing the log likelihood. In fact, these operations almost double the running time of the program. However, the information obtained from the likelihood function is so valuable that the extra burden is well worth the price.

Since the combined operation of an information filter and some computations of the Kalman filter (steps 3 and 4) appears to be somewhat redundant, the question arises as to whether everything could be done more efficiently using just a Kalman filter or an information filter. The answer is no. In fact, if a Kalman filter were used to compute everything, the running time of the program would double. (This statement is not generally true for most filtering applications).

For more information on the properties of the log likelihood function, see Edwards, 1972 and Gupta, 1974.

3.0 RESULTS

3.1 Pre-MAGSAT Model PMAG (7/80)

The models used as a basis of comparison for prediction accuracy include the AWC 75 (Peddie & Fabiano), the WC 80 (Barker & Barraclough) and the Goddard Space Flight Center Model, PMAG (7/80) (Estes). Because the PMAG (7/80) model is not fully documented in the literature and because the techniques utilized in the development are also used in deriving the mini-batch models of Section 3.2, a brief description of the modeling method will be presented in this section.

The basic core field data set consisted of POGO satellite scalar data, selected observatory vector data, and selected repeat station data and marine survey data over the years 1960-1977. Magnetic potential spherical harmonic coefficients were simultaneously least squares fit to the data set to mathematical degree and order 13 for the constant terms, 13 for the first time derivative terms, 6 for the second derivative terms, and 4 for the third derivative terms. While the satellite data provided a good uniform spatial distribution, vector component data was desired to reduce the Backus effect and observatory annual means data was needed to provide accurate secular variation information. The surface data, however, is the result of contributions from both the core field, $\bar{B}(t)$, and the anomalous crustal field, $\bar{B}_c$, which can contribute several hundred nT to the measurement but is assumed not to vary with time. To properly account for the crustal influence in the data, different approaches were taken for satellite and for surface observatory, marine, and repeat station data.

The basic 49,000 measurement POGO data set used in developing the POGO 2/72 model (Langel, et al) was extended in time to include approximately 25,000 additional OGO-6 quiet measurements over the

interval 1970-1971. This quiet time data set exhibits good uniform spatial distribution. The crustal field influnece is greatly attenuated at the spacecraft altitude of over 500 km and is assumed negligible for processing satellite data in the model.

The observatory data was accomodated in the solution by solving for an independent constant anomaly bias magnetic field vector at the site of each observatory simultaneously with the spherical harmonic coefficients. A global set of 148 observatories was selected for the data set based on continuity of operation over the desired interval, data accuracy and spatial uniformity. The time series of annual means were examined for each observatory and jumps in the data caused by station relocation, equipment modification, etc. were identified and the intervals treated as independent stations with respect to the crustal biases. This resulted in a total set of 167 independent observatory vector biases from the 148 selected observatories.

The repeat station data was selected based on data accuracy, spatial distribution and number of site occupations. At least three site occupations were required to qualify as acceptable. As the data set was generally sparse (and most often did not contain all three vector components), vector anomaly biases were not estimated for this data type. Instead, quadratic polynomial fits were made to the component time series and time derivatives (which are assumed to be independent of the crustal field) taken to be used as data for the main field model. Approximately 500 $\dot{D}$, $\dot{H}$, and $\dot{Z}$ measurements from areas of Africa, South America and Australia were utilized.

Marine survey data also contains contributions due to magnetic crustal anomalies. To obtain data for vast areas of the Atlantic, Pacific and Indian Oceans, forty-one long, straight tracks of surface marine scalar magnetic data (length greater than 1200 km) were selected and low pass filtered to remove wavelengths shorter than 500 km. This

filtered track of data was then sampled to provide marine data for he model data set.

The weighting of the measurements in the least squares fit was based on the assumed accuracy of the data types. The satellite data was assigned a measurement noise sigma of 10 nT., while the sigma for individual magnetic observatories was determined from the scatter about a quadratic polynomial fit of the time series data. The invariant noise sigmas for the 167 observatory vector components varied from approximately 5 to 40 nT. The sigmas used for the repeat station derivative data were also determined from polynomial fits, while that for the marine data (100 nT) was obtained by comparing filtered values of the long tracks at intersecting points.

The PMAG (7/80) model has proven to be the best predictor of MAGSAT data among the available pre-MAGSAT models in the literature. The strength of the model is due to the extremely good POGO satellite coverage over the years 1965-1971 and the solution for observatory anomaly biases together with the inclusion of the third derivative spherical harmonic coefficients. It has been shown that the marine data and repeat station data has added no improvement to the predictive capability of the model.

3.2 Mini-Batch Models

The derivation of batch least squares main magnetic field models over approximatlely five year intervals from 1950-1976 was accomplished using the techniques described in Section 3.1 for PMAG (7/80) using the same POGO satellite data set and the same set of 167 magnetic observatories extending back to 1950. However, the filtered marine data and differentiated repeat station data from PMAG (7/80) was not used in the mini-batches. Instead, a selection of surface and airborne survey data was utilized to improve the data distribution within each mini-batch interval. No attempt was made to model the crustal anomaly influence in

the survey data. The measurement noise sigma given this data in the estimation was set to reflect the crustal uncertainty.

Because of differences in the distribution of the data and different data types, the processing of the five mini-batches was not identical. Table 3.1 shows the number of measurements for each data type, the weighting used for each data type and the maximum degree of the field coefficients and first derivatives for each of the mini-batches. The first satellite data was taken in 1965 (OGO-2) and thus the time intervals for the third and fourth mini-batches were adjusted so that this data was included in the third. Without the global satellite data, the distribution of the remaining data is sparse in some areas and thus the accurate recovery of all spherical harmonic coefficients and first derivatives is difficult. For this reason, the mini-batches from 1950 to 1960 did not solve for all coefficients and derivatives. It is believed that the aliasing caused by truncation of the field model was small.

The end time of the last batch was extended to include the latest observatory data available to us. The satellite data during this interval was taken in 1970-71 so that the solution is heavily weighted toward the beginning of the interval.

The weighting sigmas used for the different data types were selected based upon the fit of the data to the field model. Although this is not a rigorous procedure for determining the data accuracy, it is a reasonable approximation to it. The weighting sigmas for the observatory data were determined by the deviation of the data from a polynomial fit for each observatory. Thus the weighting varied from one observatory to the next.

In each of these mini-batches, no corrections were made for the external field. The bias due to the external field should be accounted for as part of the main field while the high frequency variations of the external field will be treated as noise.

Table 3.1 Summary of Mini-Batch Field Models

Time Span	Number of observatories	Number of Observations					Maximum Degree and Order of Field Model	
		Observatory (vector components)	Survey/ airborne	Satellite	Total accepted	Number edited	constant	linear
1950-1955	67	849	6776	0	7625	153	9	6
1955-1960	111	1335	12658	0	13993	194	10	7
1960-1966	142	2145	58075	3559	63779	468	13	13
1966-1970	148	1578	13545	52016	67139	127	13	13
1970-1976	139	2292	9596	15916	27804	189	13	13

Data Type		Data Weighting	Data Editing Threshhold
Observatory:	X,Y,Z	5-45 nT*	5000 nT
Survey/Airborne:	B, H, Z	300 nT	5000 nT
	D	1.0°	5°
	I	0.5°	5°
Satellite:	B	10 nT	5000 nT

*σ determined by polynomial fit to observatory data.

3.3 Computation of State Noise Covariance and Mini-Batch Weighting

Figures 3.1 are line printer plots of the field model coefficients for the five mini-batchs. There is one plot for all coefficients of the same degree. The code used to identify the coefficient order is:

$$
\begin{aligned}
0 &= g^{i,0} \\
A &= g^{i,1} \\
B &= h^{i,1} \\
C &= g^{i,2} \\
&\vdots \quad\quad \vdots \\
Z &= h^{i,13} \qquad .
\end{aligned}
$$

Also shown on each plot is the range of the standard deviations for the coeficients (evaluated at the beginning of the interval) as computed from the least squares covariance matrix (inverse of information matrix). In general it may be stated that only the two or four coefficients of the highest order (for each degree) had large sigmas; most of the coefficients had sigmas which were closer to the smaller of the two numbers. The number in parentheses is an "eyeball" average of the standard deviations where the sigmas of the high order coefficients were excluded. This is the number which was used to determine the scaling of the information matrix (to be explained shortly).

These plots were made for two purposes: to determine whether or not the computed standard deviation was a realistic approximation of the coefficient accuracy and to aid in estimating the state noise variances. In examining these plots, we discovered that it was generally possible to fit a smooth curve through the five (or less) separate lines for each low degree coefficient. However, the deviation of coefficients from that curve was considerably larger than the computed uncertainty of the coefficient (i.e. computed sigma). This was disturbing because it suggests that either the sigmas which were used in weighting the data were wrong or that aliasing (because of the truncated field model or

Figure 3.1 Plots of Mini-Batch Field Model Coefficients
Degree 1.

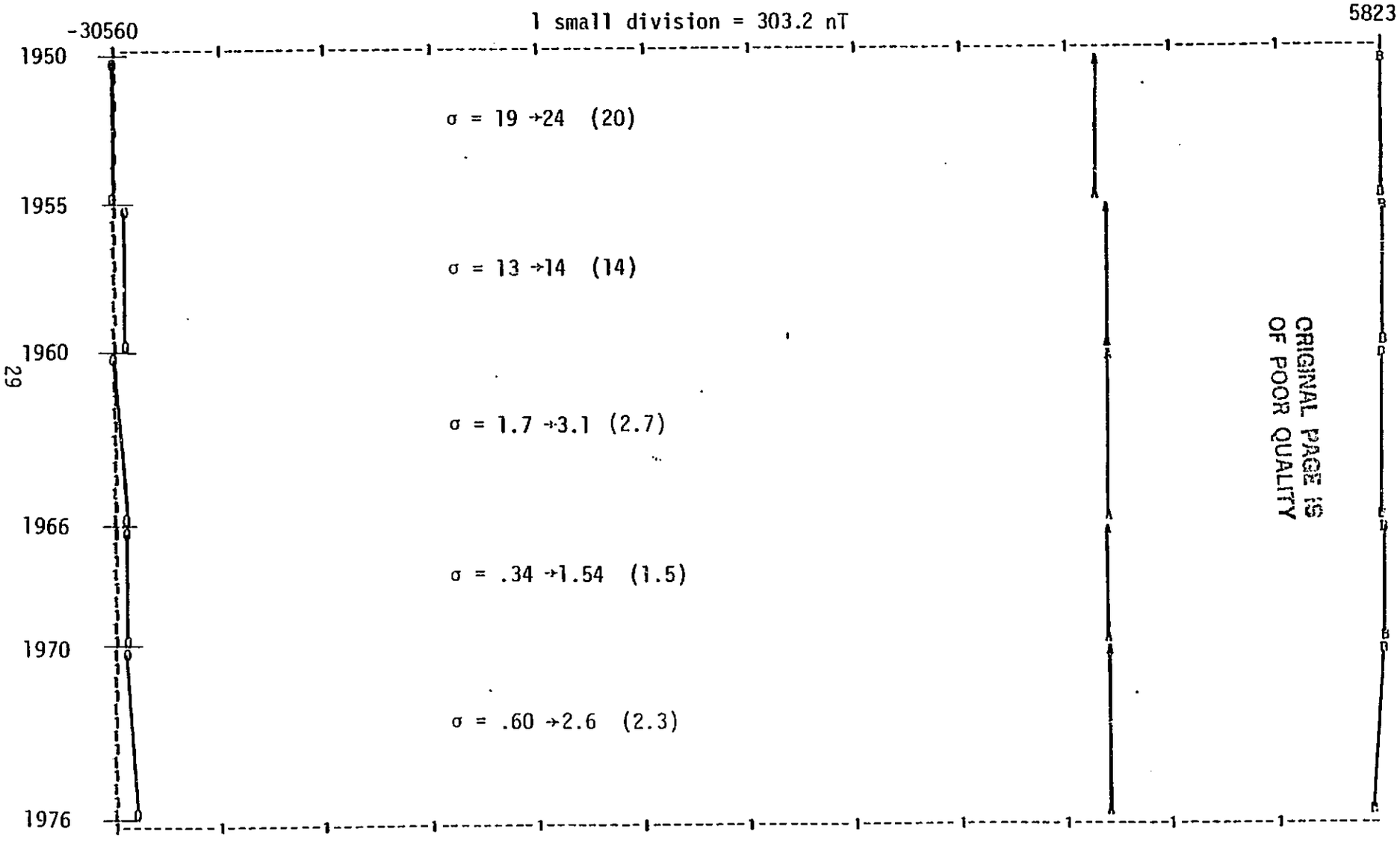

Figure 3.1 (continued), Degree 2

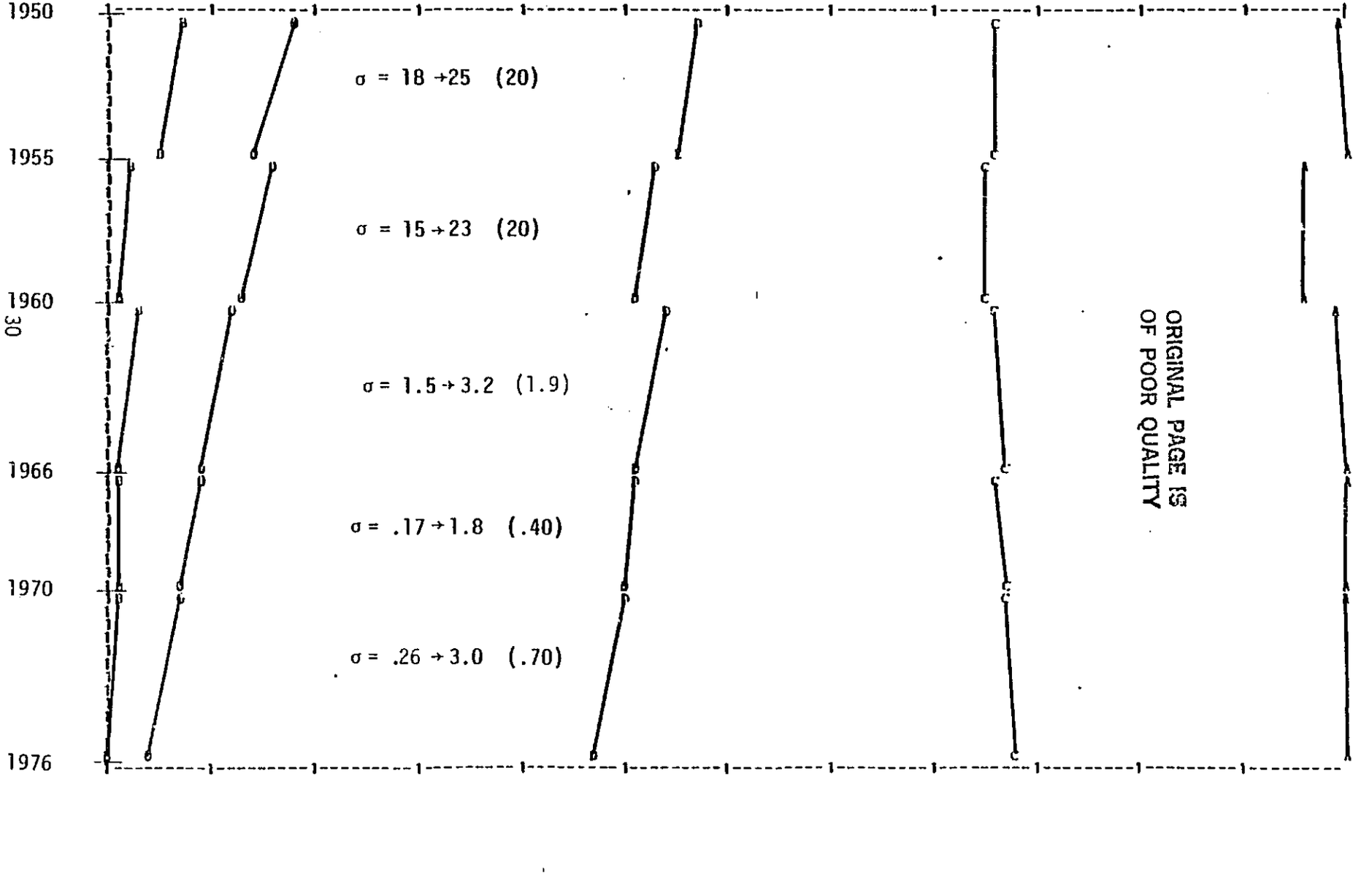

Figure 3.1 (continued), Degree 3

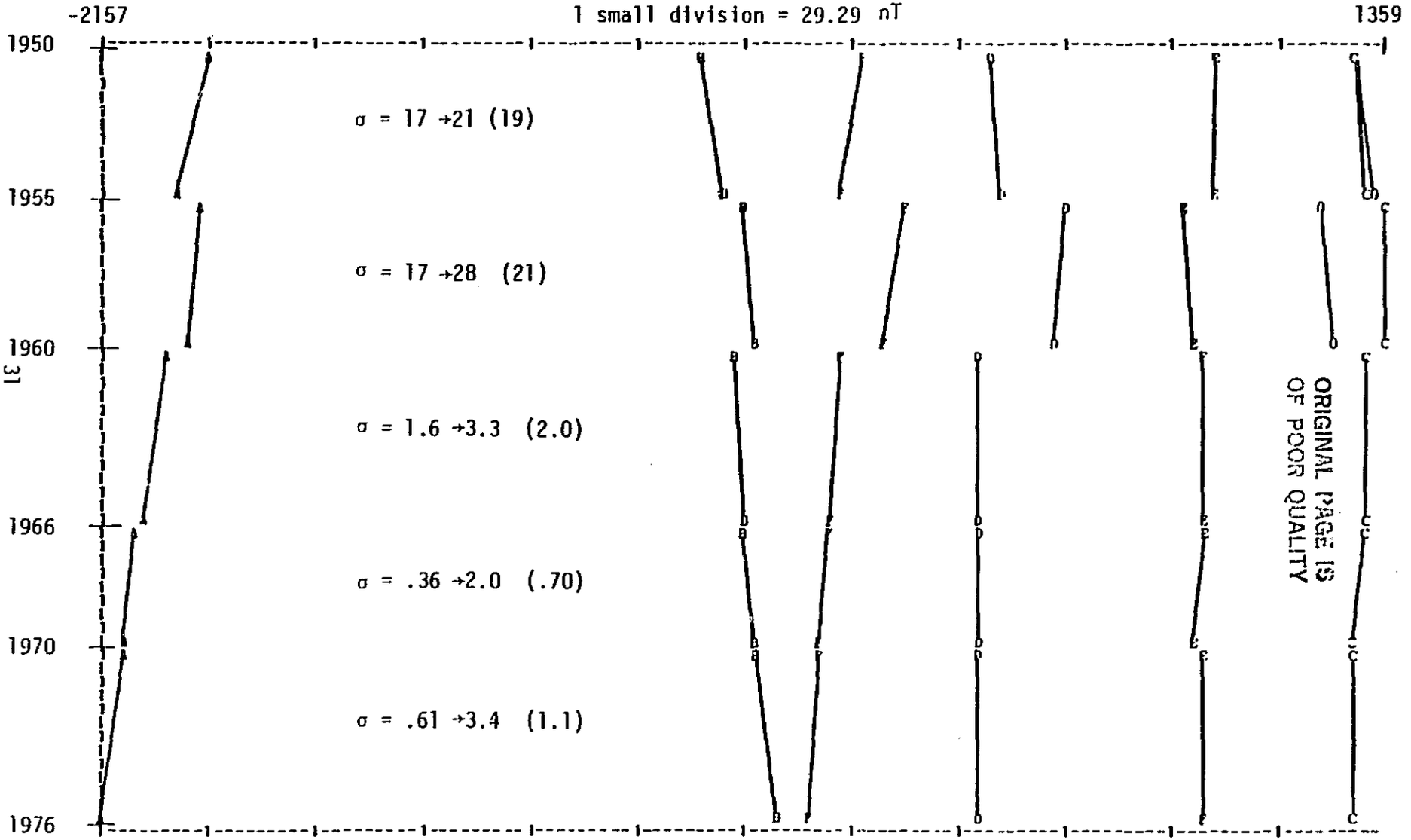

Figure 3.1 (continued), Degree 4

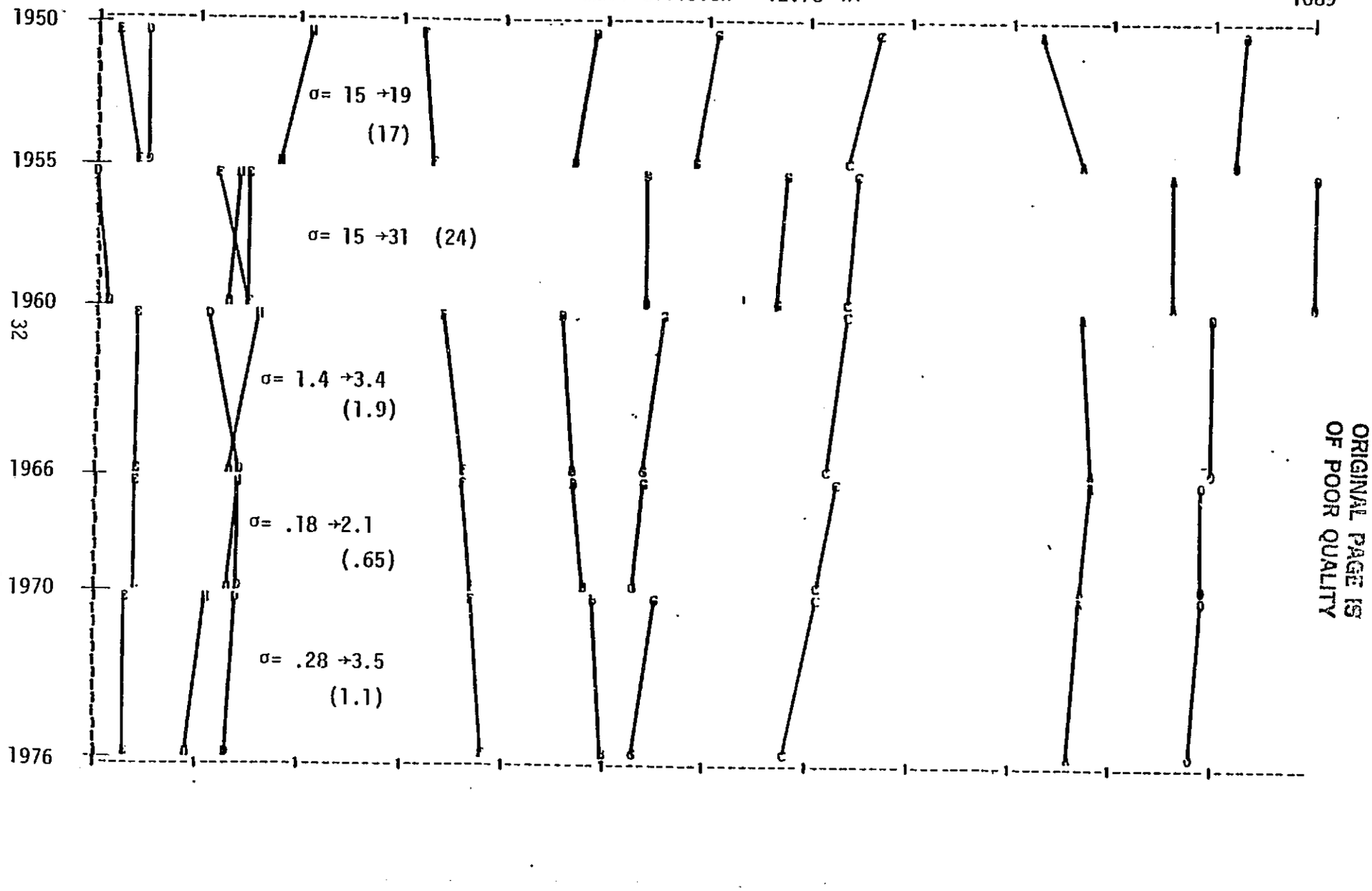

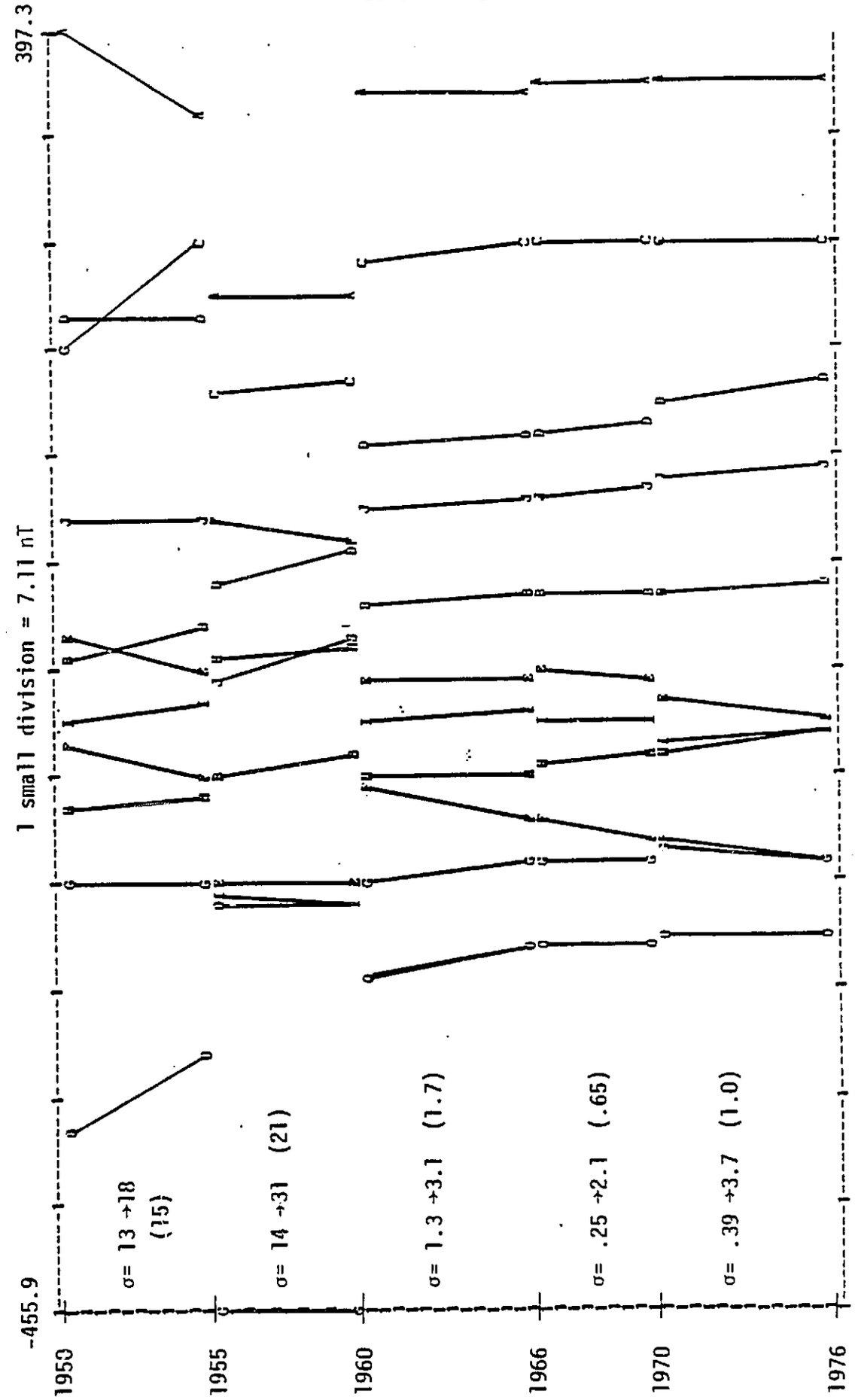

Figure 3.1 (continued), Degree 5

Figure 3.1 (continued), Degree 6

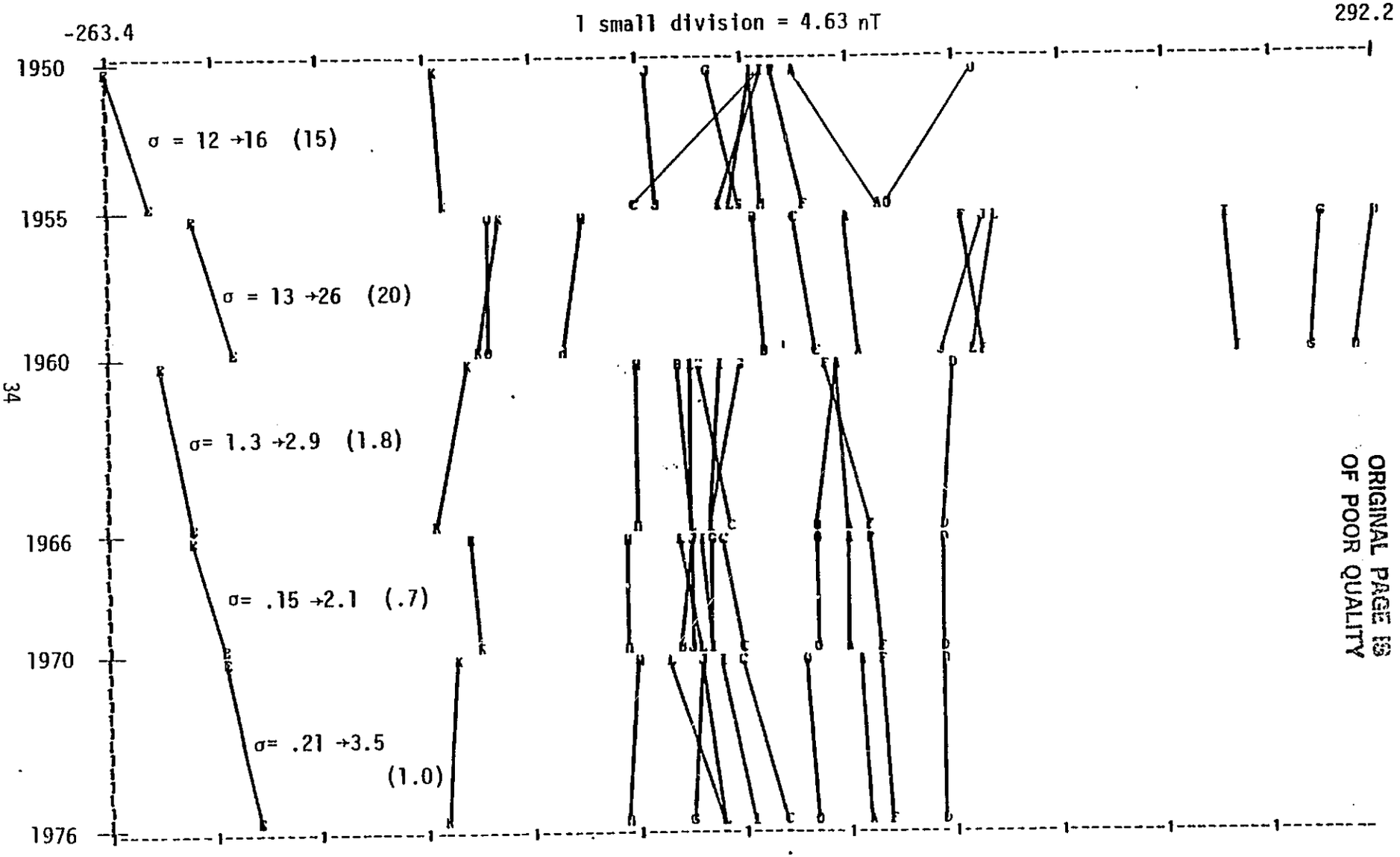

Figure 3.1 (continued), Degree 7

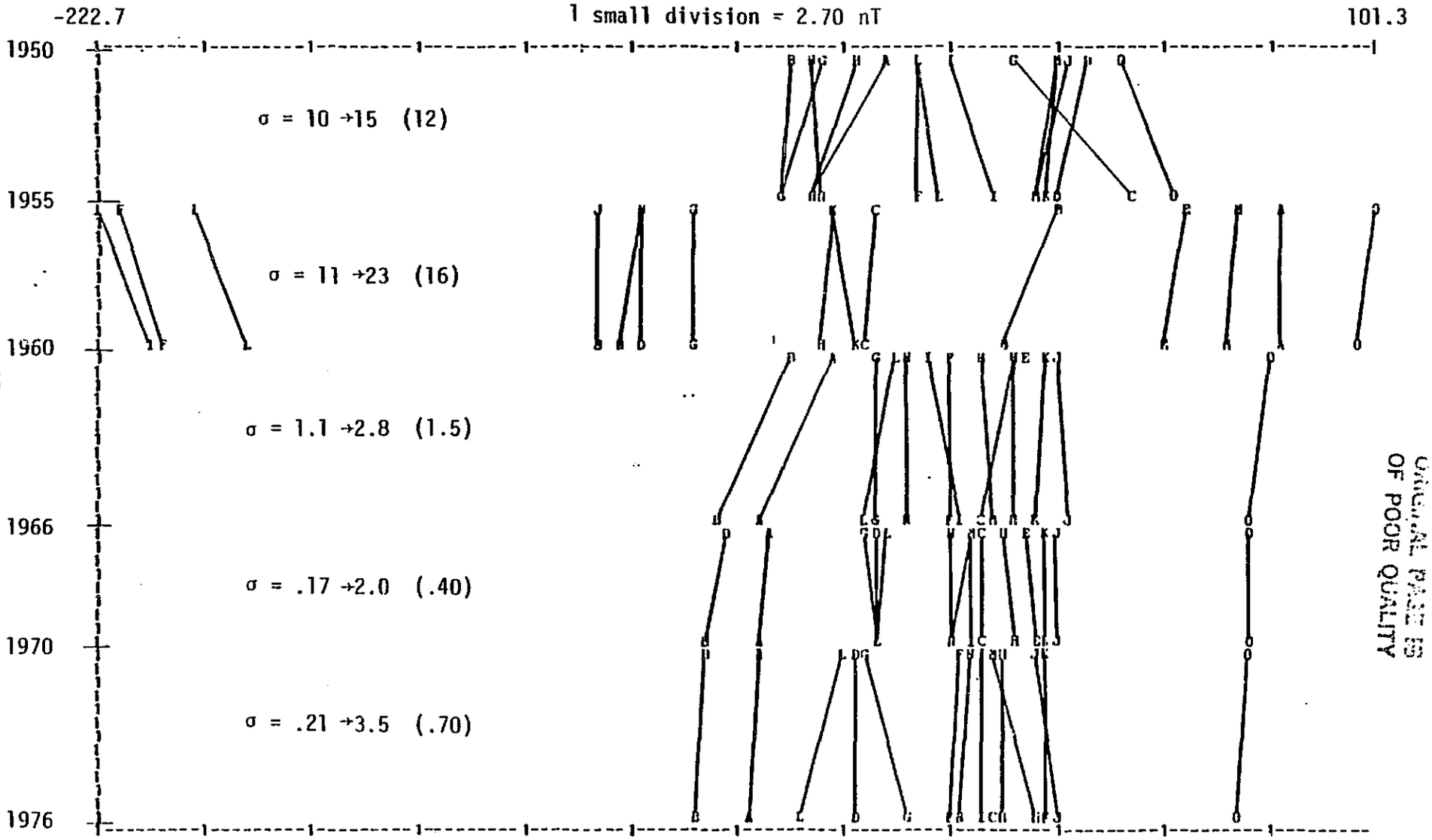

Figure 3.1 (continued), Degree 8

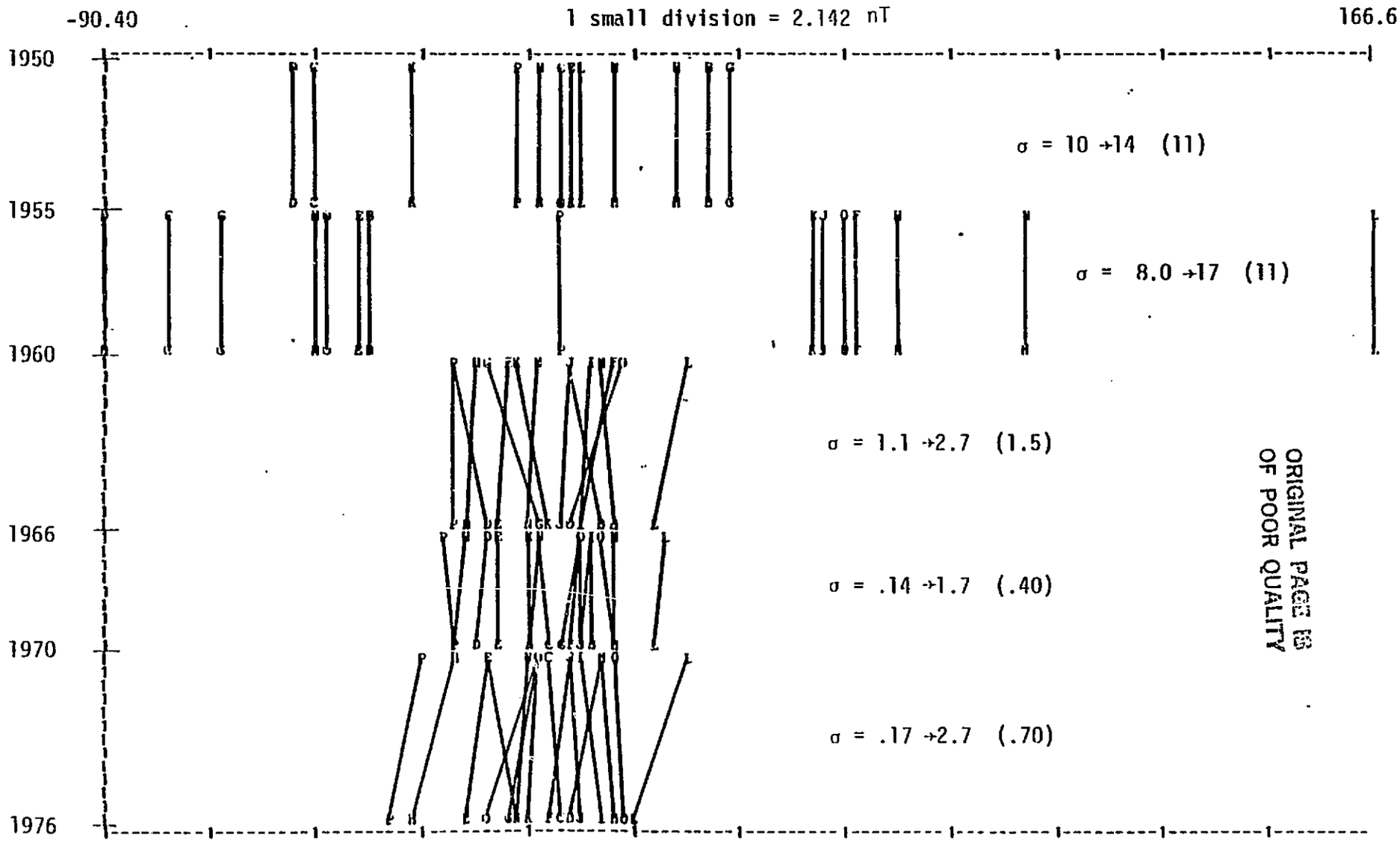

Figure 3.1 (continued), Degree 9

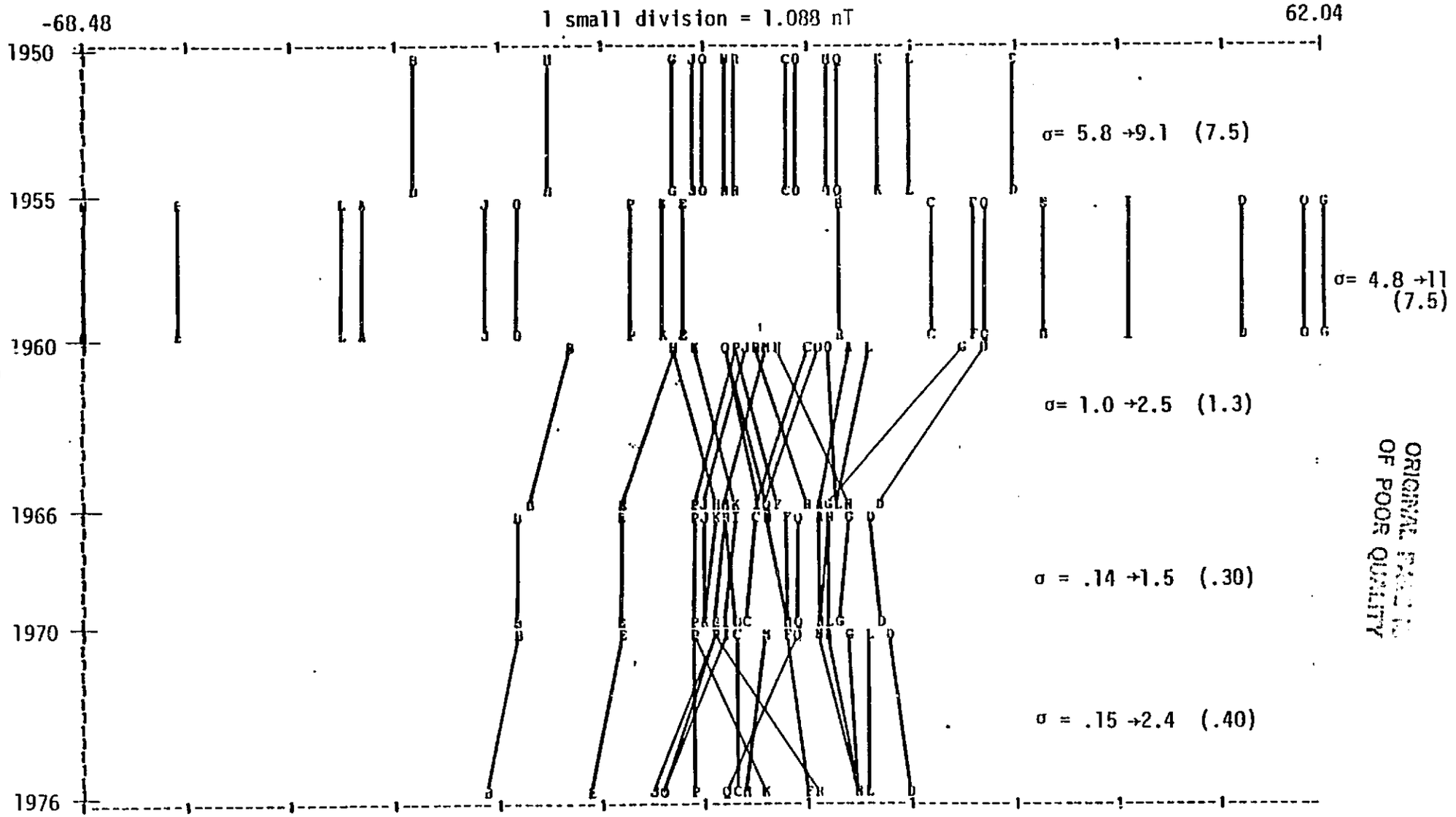

Figure 3.1 (continued), Degree 10

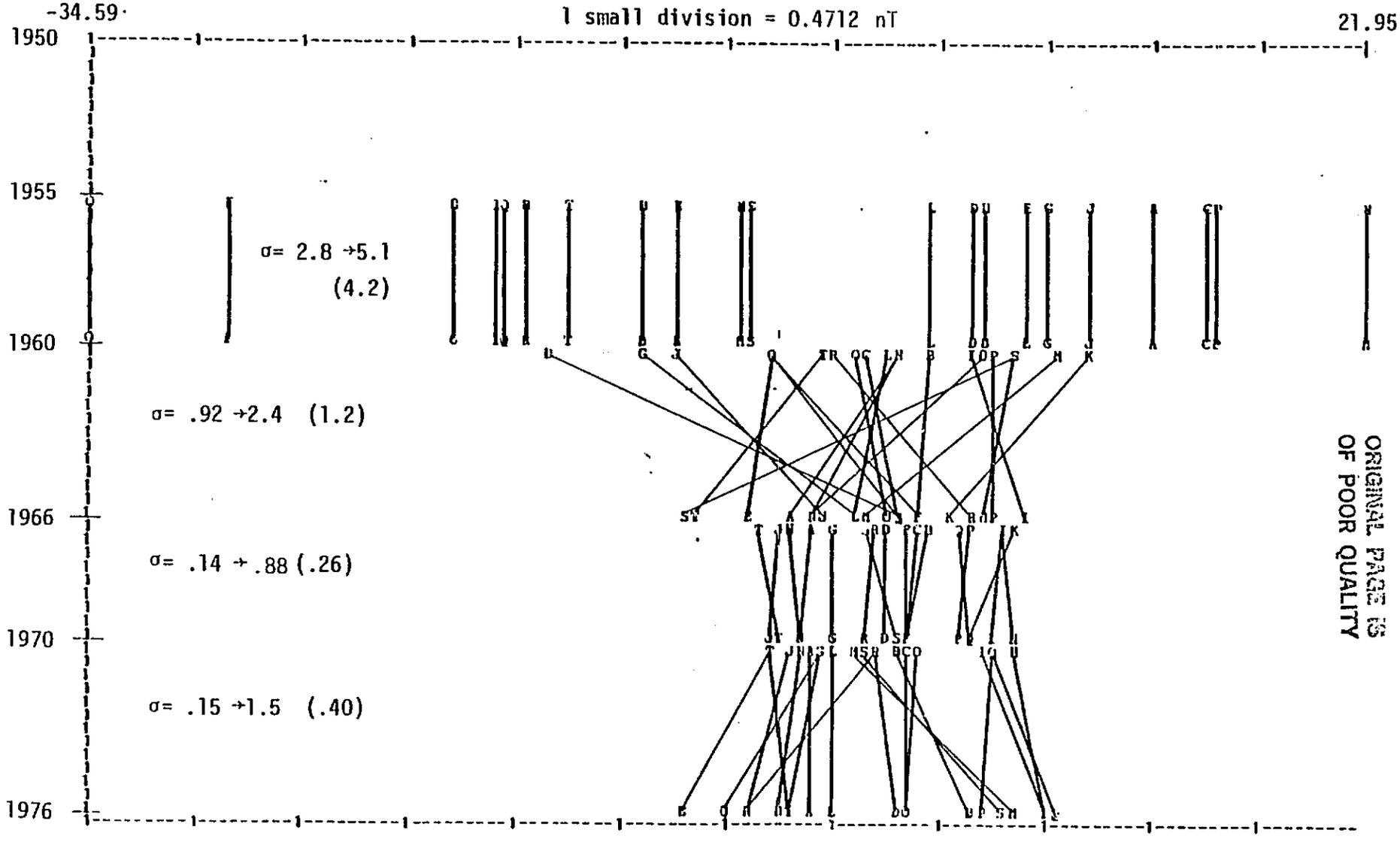

Figure 3.1 (continued), Degree 11

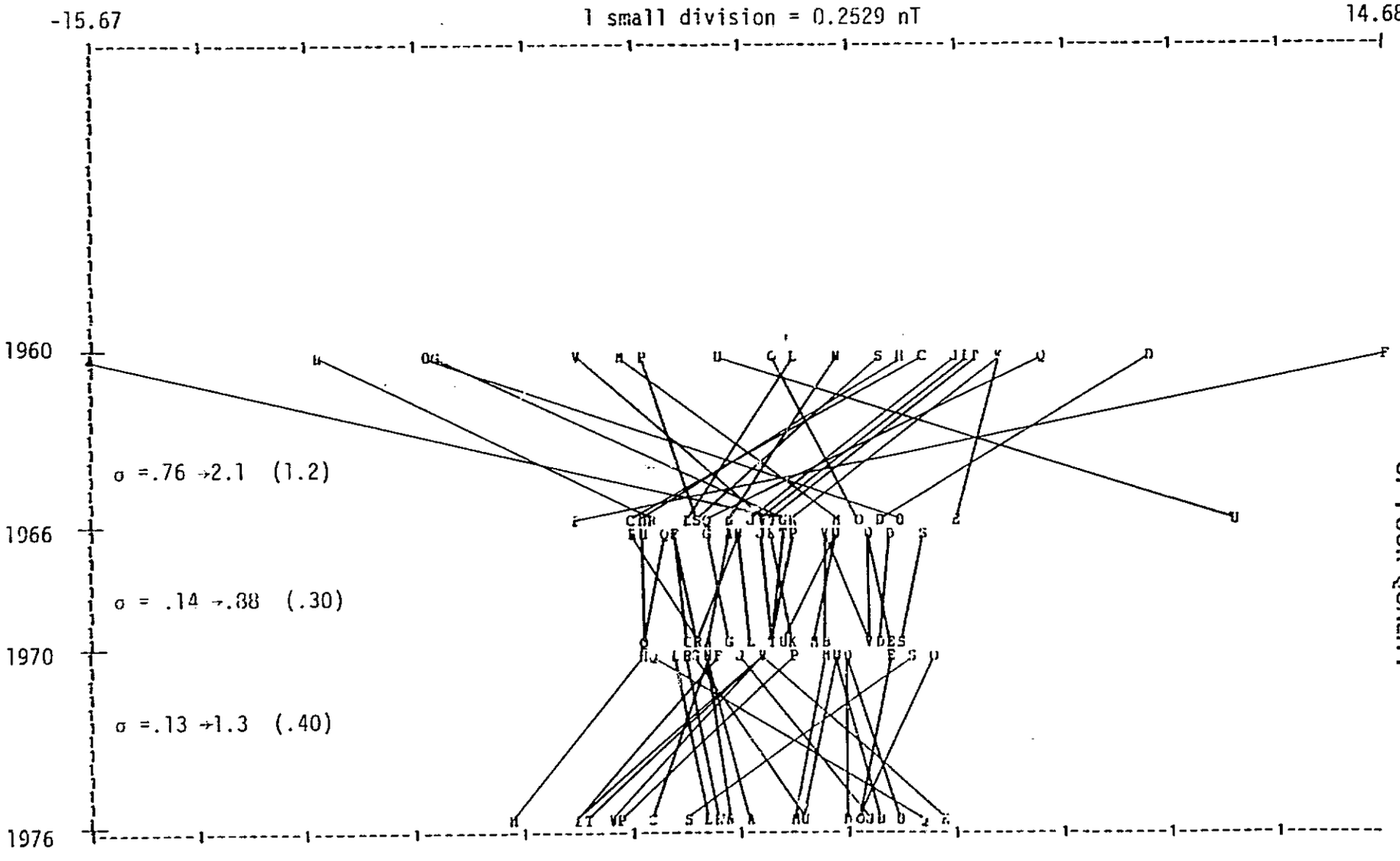

Figure 3.1 (continued) Degree 12

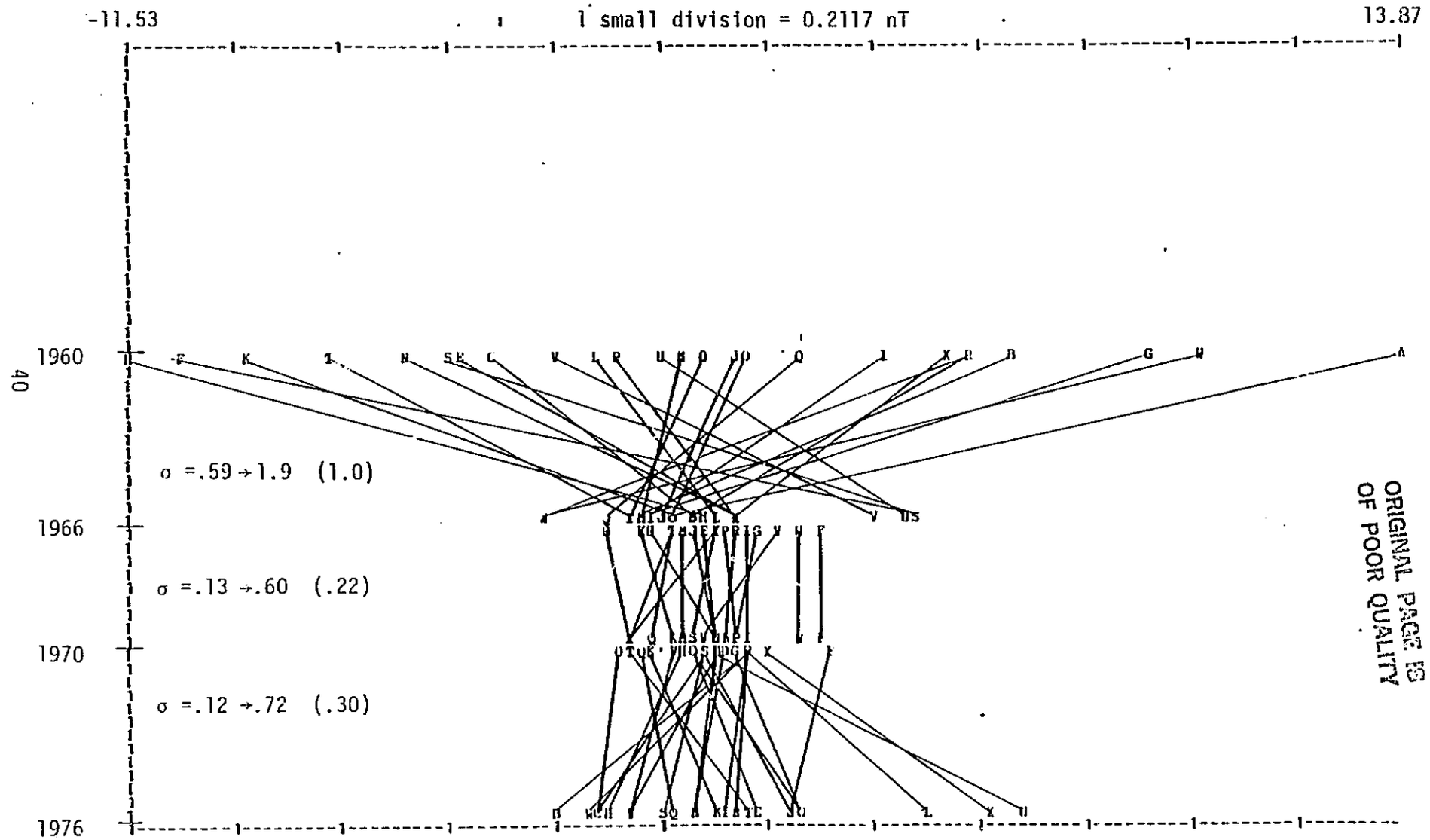

Figure 3.1 (continued), Degree 13

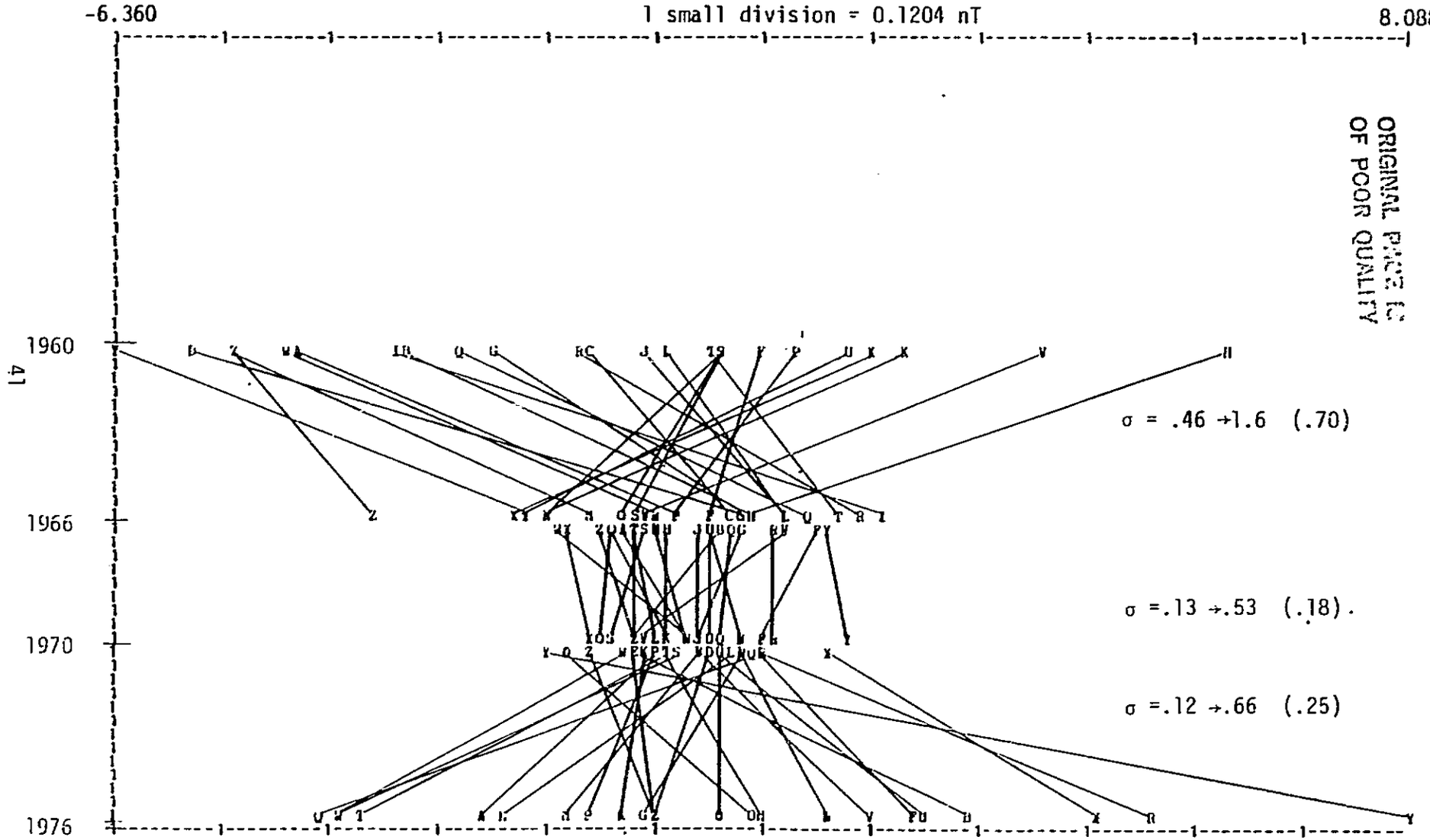

other modeling errors) was significant. At this time, it is not known which explanation is more probable. The possibility of an error in the software has been investigated and it does not seem likely.

In any case, it was obvious that the covariance matrix computed for each mini-batch had to be scaled to account for these modeling errors. Scaling the entire covariance matrix by a constant may not generate a matrix with the same structure as the true error covariance but it is certainly better than no scaling at all. The scaling factors for each mini-batch were determined by using the plots to estimate the true error sigma for all coefficients of the same degree. In other words, the deviation of the plots from a smooth curve (and from plots of other field models) was assumed to be a measure of the true accuracy. This number was divided by the average computed sigma (listed in parentheses) to compute a scale factor for each coefficient degree and then these scale factors for the different degrees were averaged to compute an overall scale factor for each mini-batch (Table 3.2). In general, the scale factors for coefficients of different degrees within the same mini-batch were quite consistent and thus there is some confidence in the method. However, this procedure for estimating the scale factors is subject to rather large uncertainty.

Table 3.2 Estimated Scale Factors

Mini-Batch				
1950-55	1955-60	1960-66	1966-70	1970-76
1.0	4.0	2.9	2.0	2.4

The second problem, determining the spectral density of the state noise, is somewhat more difficult to solve in a systematic manner. The deviation of the plots from a quadratic (or linear) curve should be a good indication of the state noise but since the uncertainty of the coefficients is so large, this deviation cannot be estimated accurately. Rather, a procedure which was based more upon the value of coefficients was used. For the coefficients which were assumed to obey a quadratic law (degrees 1 to 7), the standard deviation of the coefficient will grow as $\sqrt{Q_S \Delta t^5/5}$. Therefore, the expected deviation of the coefficient from the quadratic curve after a period of 20 years was chosen for coefficients of each degree and Q_S was computed from this. Likewise, the same procedure was used for coefficients which obey a linear trend where the coefficient uncertainty grows as $\sqrt{Q_S \Delta t^3/3}$. Table 3.3 lists the assumed coefficient uncertainty after 20 years for each degree and the resulting spectral density (Q_S).

Table 3.3 Estimated State Noise

Coefficient Degree	Estimated Coefficient Deviation after 20 years	Time Model	Spectral Density of White Noise Input
1	120nT	quadratic	$.0224nT^2/sec^5$
2	80nT	quadratic	$.0100nT^2/sec^5$
3	60nT	quadratic	$.0056nT^2/sec^5$
4	40nT	quadratic	$.0025nT^2/sec^5$
5	30nT	quadratic	$.0014nT^2/sec^5$
6	20nT	quadratic	$.0006nT^2/sec^5$
7	14nT	quadratic	$.0003nT^2/sec^5$
8	10nT	linear	$.0376nT^2/sec^3$
9	8nT	linear	$.0240nT^2/sec^3$
10	6nT	linear	$.0136nT^2/sec^3$
11	4nT	linear	$.0060nT^2/sec^3$
12	2nT	linear	$.0016nT^2/sec^3$
13	1.5nT	linear	$.0008nT^2/sec^3$

3.4 Filtering Results

Table 3.4 lists the statistics on the measurement residuals (difference between observed measurement and computed measurement) using MAGSAT data taken on March 15, 1980 and predictions from various field models. March 15 data was selected because this was a magnetically "quiet" day. The data was corrected for MAGSAT attitude errors and the effects of external magnetic fields and the vector data was limited to ±45° in latitude. A brief description of the various field models is given below.

AWC75 - Developed by Peddie and Fabiano using data from 1965 to 1975. Uses constant coefficients to degree 12 and linear time terms to degree 12.

WMC80 - World Magnetic Chart 1980. Developed by Barker and Barracough using data from 1950 to 1977. Uses constant coefficients to degree 12 and linear time terms to degree 8.

PMAG (7/80) - Developed by GSFC using data from 1960 to 1977. Uses cubic time coefficients to degree 4, quadratic time coefficients to degree 6, linear and constant terms to degree 13.

Mini-Batch (1970-1977) - last mini-batch as described in section 3.1.

GSFC (9/80) - Developed by GSFC combining MAGSAT Nov. 5 and 6 data with the PMAG (7/80) data set. Same form of time model as PMAG.

GSFC (2/81) - Developed by GSFC using MAGSAT (Nov. 5 and 6, 1979 plus March 15, 1980), POGO (1965-1971) and observatory data over the period 1950 to 1977. Same form of time model as PMAG.

Best filter model - field model from filter computer run which had highest likelihood function.

Table 3.4 Residual Statistics (nt) of March 15, 1980 MAGSAT Data for Various Field Models (corrected for attitude and external field)

Component		Geomagnetic Field Model							
		AWC75	WC80	PMAG(7/80)	Mini-Batch 1970-1976	GSFC(9/80)	GSFC(2/81)	Best Filter Model (Pre-MAGSAT)	Best Filter Model (Including MAGSAT)
B	mean	67	-14	-20	5	-3	-1	19	-1
	RMS	148	117	92	101	11	9	78	10
X	mean	48	-14	-9	9	-3	-2	11	-3
	RMS	115	91	70	110	10	8	67	10
Y	mean	6	2	2	0	1	1	2	0
	RMS	90	73	77	119	13	12	73	9
Z	mean	25	23	9	8	-1	-2	-4	-2
	RMS	163	128	109	186	13	9	108	11
RMS		135	107	89	127	12	9	82	10

The mean and root-mean-square residual for the scalar and vector data are listed for each field model. The RMS value listed at the bottom is an RMS for all the measurements (approximately twice as many scalar measurements were used compared to vector measurements).

Our filtered model is substantially better (8 to 39%) than any of the tested pre-MAGSAT models for prediction time intervals of 4 to 5 years. (The date of the last data used in the WMC80 model is not precisely known). This demonstrates that the filtering method is clearly superior to the methods which have traditionally been used in the past to develop field models.

The two GSFC models which used MAGSAT data were included in the table simply to show the limits of batch field modeling when little or no prediction is involved. (The GSFC (9/80) model was predicted 4 months). The final column lists the residual statistics for the filtered model which has been updated with MAGSAT data taken on November 5 and 6. Notice that this model is somewhat better than the GSFC (9/80) model and comparable to the GSFC (2/81) model (which used March 15 data).

Table 3.5 lists the results of six filtering runs in which various inputs were perturbed to determine the optimum field model. Run #6 has the highest likelihood function and nearly the best fit to the data. The following list summarizes the results.

1) The use of likelihood function in conjunction with the sum of weighted residuals was a reliable indicator of the field model which produced the best fit to the MAGSAT data. This is a significant result because it demonstrates that the filter model which is best supported by the data is also the best predictor of future data.

(2) The best results were obtained when the nominal mini-batch scale factors were increased by 65%. See runs 1, 2, 5 and 6.

Table 3.5 Summary of Field Models Produced by Kalman Filtering

Run #	Scaling	State Noise	Residual Statistics (MAGSAT, March 15, 1980)									$\sum \tilde{x}_i^T P_{\tilde{x}_i}^{-1} \tilde{x}_i$	log likelihood
			Mean (nT)				RMS (nT)				RMS (nT)		
			B	X	Y	Z	B	X	Y	Z			
1	note 1a	note 2a	19	10	2	-4	79	64	72	105	81	3548	-2767
2	note 1a	note 2b	19	10	2	-3	79	77	82	122	89	2197	-2226
3	note 1a	note 2c	19	7	3	-2	85	93	92	144	102	1339	-1985
4	note 1a	note 2d	19	3	2	-4	94	108	101	172	117	836	-1976
5	note 1b	note 2a	20	10	3	-3	84	62	70	109	83	1785	-2082
6	note 1b	note 2b	19	11	2	-4	78	67	73	108	82	1156	-1867

Notes:

(1) Scaling of mini-batches

a) Nominal scaling (1.0, 4.0, 2.9, 2.0, 2.4)

b) 1.65 x nominal scaling (1.7, 6.6, 4.7, 3.4, 4.0)

(2) State Noise Spectral Density

a) $Q_S = Q_{S,nom}$

b) $Q_S = 4\ Q_{S,nom}$ (sigma multiplied by 2)

c) $Q_S = 16\ Q_{S,nom}$ (sigma multiplied by 4)

d) $Q_S = 64\ Q_{S,nom}$ (sigma multiplied by 8)

(3) The best results were obtained when the state noise spectral density listed in Table 3.2 was increased by a factor of 4 (the standard deviation multiplied by 2). See runs 5 and 6. Attempts to vary the scaling of Q_S between the linear and quadratic terms did not improve the results (early runs not listed).

(4) The use of a mini-batch epoch time other than at the middle of the data span will degrade the results. This is supported by the results of runs not listed and runs made on simulated data. Presumably this is the result of aliasing errors (caused by the use of a linear time model in the mini-batch) which are a minimum at the center of the data span.

In addition to the use of the log likelihood function to determine the optimum run, the sum of weighted residuals,

$$\sum_{i}^{m} \tilde{x}_i^T P_{\tilde{x}_i}^{-1} \tilde{x}_i \ ,$$

can also be useful as an indicator of modeling errors. If all models are correct, this sum should be Chi-squared distributed with degrees of freedom equal to the number of measurements, i.e. it should be approximately equal to the number of measurements. Since our measurements are actually the mini-batch field model coefficients, m should be equal to the sum of the number of coefficients for the five mini-batches, i.e.

$$m = 147+183+390+390+390 = 1500.$$

In reality the sum of weighted residual should be slightly less than 1500 because the a priori sigmas we used were considerably larger than the actual errors in the a priori estimate of the field model. It is difficult to determine exactly what this sum should equal but a value of 1200 seems reasonable. Notice that run #6 has the highest likelihood function and the sum of weighted residuals for this run is close to 1200. We found this sum to be quite useful in deciding how to scale the individual mini-batch covariance matrices and the state noise spectral density.

The use of only the likelihood function to select the optimum model parameters can sometimes be misleading if the true measurement noise standard deviation is not known. This is demonstrated in Figure 3.2 where the likelihood function and the RMS fit to the MAGSAT data is plotted for the six runs listed in Table 3.5. Using the nominal scaling of the mini-batches, the likelihood function is maximized when the state noise variances are multiplied by a number between 16 and 64. However, the sum of weighted residuals for these runs is much larger than 1200 and the prediction of the MAGSAT data is poor. When the scaling of the mini-batch variances is increased, a smaller scaling of the state noise variances will produce a higher value of the likelihood function (run 6). Furthermore, the sum of residuals is closer to 1200 and the prediction of the MAGSAT data is improved. Because of the expense of making these computer runs, we did not attempt to find the optimum scaling parameters but run 6 is probably quite close to optimum.

Table 3.6 lists the predicted set of field model coefficients at 1980.0 for run 6. This model is called Geomagnetic Recursive Information Model 1977 (GRIM77). The degree and order listed in the table have been increased by 1 because Fortran will not allow zero subscripts. The field model listed in Table 3.7 (GRIM80) is similar but the results of run 6 have been optimally combined with a field model based only upon November 5 and 6, 1979 MAGSAT data. Thus Table 3.7 represents our best estimate of the geomagnetic field and its secular variation at epoch 1980.0.

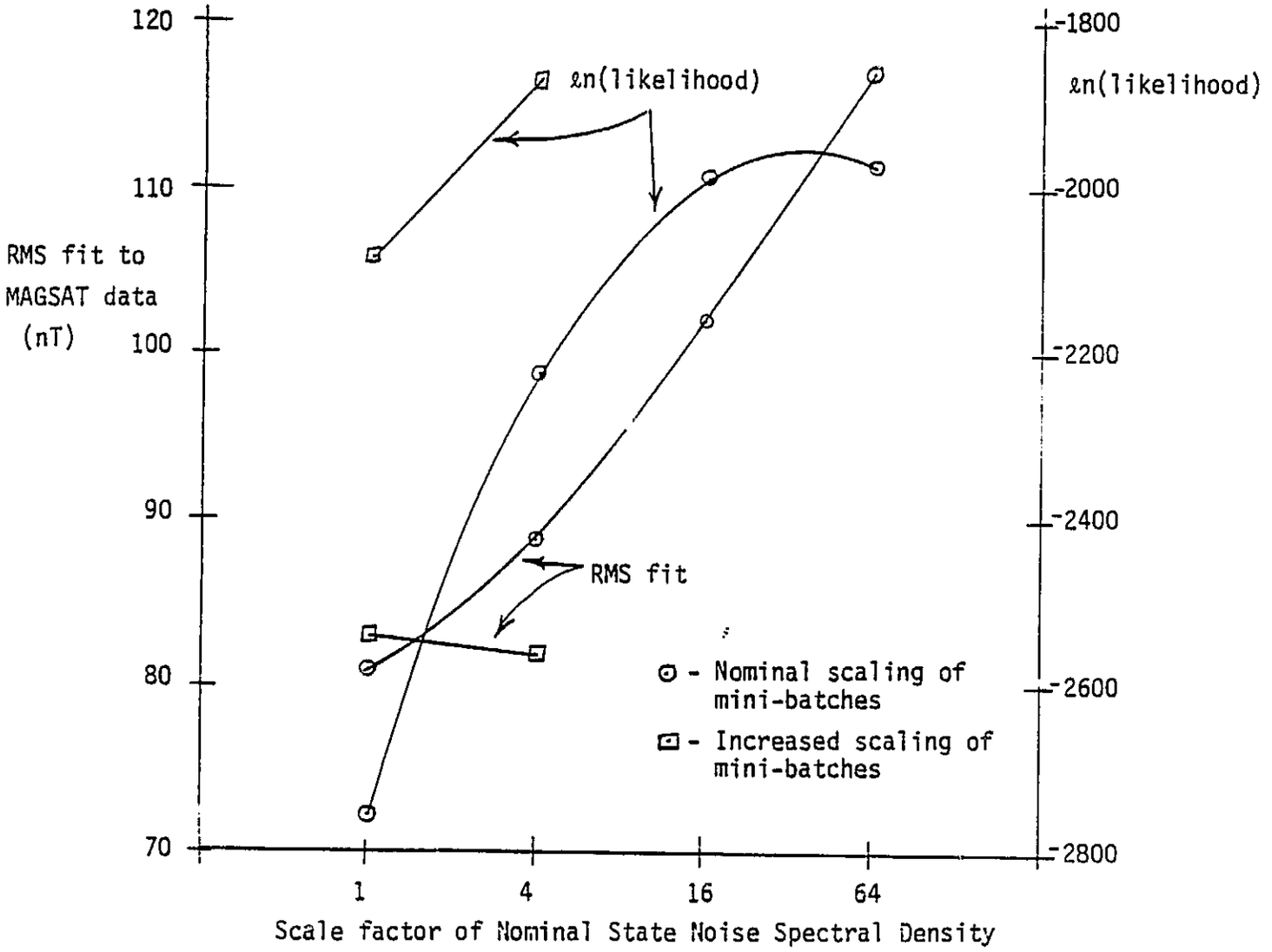

Figure 3.2 Plot of Likelihood Function and Residual Fit of MAGSAT Data

Table 3.6 GRIM77 Field Model at Epoch 1980.0 (Run #6)

n+1	m+1	g	h	ġ	ḣ	g̈/2	ḧ/2
2	1	-29976.1	0.0	24.78	0.0	0.103	0.0
2	2	-1945.5	5583.6	12.79	-16.36	0.094	-0.158
3	1	-1987.9	0.0	-16.70	0.0	0.429	0.0
3	2	3021.2	-2089.2	2.07	-5.97	0.014	-0.104
3	3	1645.1	-193.3	5.69	-25.35	0.121	-0.361
4	1	1271.5	0.0	1.35	0.0	0.266	0.0
4	2	-2167.1	-331.9	-3.56	-1.18	0.350	-0.424
4	3	1242.9	277.1	-4.53	3.57	-0.076	0.067
4	4	846.7	-238.8	3.06	-3.61	0.274	0.036
5	1	927.6	0.0	-3.28	0.0	-0.090	0.0
5	2	767.9	193.3	-4.24	0.29	-0.115	-0.205
5	3	395.6	-282.9	-9.23	-3.41	-0.228	-0.192
5	4	-418.1	47.1	-2.15	2.39	-0.004	0.062
5	5	206.1	-312.9	-3.27	-2.28	0.003	0.016
6	1	-216.9	0.0	-1.09	0.0	-0.071	0.0
6	2	359.7	95.9	-0.35	1.97	-0.026	0.045
6	3	258.5	162.3	-1.28	2.24	-0.122	-0.009
6	4	-79.7	-151.8	-5.39	-0.23	-0.156	0.111
6	5	-164.9	-65.0	-1.63	2.56	-0.078	0.021
6	6	-57.9	111.4	0.13	1.83	-0.042	0.016
7	1	58.7	0.0	2.33	0.0	0.099	0.0
7	2	59.0	-6.6	-1.12	1.76	-0.074	0.117
7	3	45.6	87.3	4.02	-2.32	0.094	-0.086
7	4	-183.6	73.7	2.90	-0.02	-0.001	-0.008
7	5	4.7	-41.7	0.65	-0.20	0.023	0.031
7	6	25.2	9.7	2.97	2.69	0.075	0.103
7	7	-93.6	28.4	1.68	3.98	0.045	0.088
8	1	71.1	0.0	0.44	0.0	0.028	0.0
8	2	-56.4	-73.3	-0.25	0.28	-0.004	0.075
8	3	5.9	-16.6	1.04	1.82	0.051	0.080
8	4	15.5	-3.1	-0.46	0.37	-0.044	0.006
8	5	-15.1	13.3	1.29	0.49	0.027	0.008
8	6	-3.5	20.0	-0.74	0.65	-0.045	0.052
8	7	12.9	-31.0	-0.26	-0.66	-0.007	-0.018
8	8	-1.1	-11.3	0.49	-0.17	0.053	-0.002
9	1	14.7	0.0	0.17	0.0	0.0	0.0
9	2	7.3	4.3	0.14	-0.34	0.0	0.0
9	3	5.9	-20.9	0.65	-0.62	0.0	0.0
9	4	-5.5	2.2	0.69	-0.18	0.0	0.0
9	5	-9.7	-27.5	-0.55	-0.32	0.0	0.0
9	6	5.9	3.2	0.04	0.21	0.0	0.0
9	7	-2.3	18.3	-0.00	-0.31	0.0	0.0
9	8	9.5	-7.9	-0.16	-0.23	0.0	0.0
9	9	-10.5	-18.0	-1.10	0.17	0.0	0.0
10	1	6.8	0.0	-0.16	0.0	0.0	0.0
10	2	9.9	-24.3	0.06	-0.17	0.0	0.0
10	3	1.2	19.5	0.01	0.43	0.0	0.0
10	4	-18.4	6.3	-0.67	0.02	0.0	0.0
10	5	11.9	-4.4	0.04	-0.15	0.0	0.0
10	6	-7.3	-6.2	-0.60	-0.21	0.0	0.0
10	7	-0.1	6.6	0.21	-0.42	0.0	0.0
10	8	10.4	10.8	0.64	0.07	0.0	0.0
10	9	1.9	-4.1	0.10	-0.09	0.0	0.0
10	10	4.1	3.6	0.04	0.27	0.0	0.0
11	1	-3.3	0.0	-0.14	0.0	0.0	0.0
11	2	-3.0	2.1	0.01	0.03	0.0	0.0
11	3	-0.7	-0.5	-0.26	-0.13	0.0	0.0
11	4	-5.8	5.4	-0.14	0.34	0.0	0.0
11	5	-2.3	7.0	-0.03	0.07	0.0	0.0
11	6	4.2	-5.4	-0.14	-0.12	0.0	0.0
11	7	0.5	2.3	-0.40	0.25	0.0	0.0
11	8	3.2	-2.6	0.34	0.08	0.0	0.0
11	9	2.3	3.2	0.07	-0.07	0.0	0.0
11	10	5.0	-3.4	0.06	-0.33	0.0	0.0
11	11	5.0	-5.6	0.31	-0.13	0.0	0.0
12	1	2.6	0.0	0.01	0.0	0.0	0.0
12	2	-0.0	2.4	0.10	0.09	0.0	0.0
12	3	-3.5	2.1	-0.17	-0.05	0.0	0.0
12	4	1.2	-3.0	-0.20	-0.14	0.0	0.0
12	5	0.8	-4.5	0.16	-0.17	0.0	0.0
12	6	-0.7	1.1	-0.09	0.08	0.0	0.0
12	7	2.1	1.3	0.22	0.18	0.0	0.0
12	8	-1.6	-3.0	-0.30	-0.16	0.0	0.0
12	9	2.2	-2.4	-0.05	-0.22	0.0	0.0
12	10	-3.8	-0.6	-0.17	0.18	0.0	0.0
12	11	2.5	-1.8	-0.05	-0.19	0.0	0.0
12	12	-2.5	2.2	-0.31	0.09	0.0	0.0
13	1	-4.3	0.0	-0.25	0.0	0.0	0.0
13	2	-0.8	-1.0	-0.09	-0.11	0.0	0.0
13	3	0.9	0.6	0.13	0.01	0.0	0.0
13	4	1.4	3.7	0.15	0.14	0.0	0.0
13	5	0.0	-0.8	-0.05	-0.04	0.0	0.0
13	6	-0.2	0.8	-0.07	0.08	0.0	0.0
13	7	2.0	0.7	0.26	0.02	0.0	0.0
13	8	-1.4	2.6	-0.09	0.23	0.0	0.0
13	9	2.3	-1.7	0.20	-0.20	0.0	0.0
13	10	-2.4	0.4	-0.15	-0.01	0.0	0.0
13	11	-2.1	-0.3	-0.16	0.06	0.0	0.0
13	12	2.4	-3.6	0.24	-0.36	0.0	0.0
13	13	1.4	0.6	-0.04	0.09	0.0	0.0
14	1	0.6	0.0	0.02	0.0	0.0	0.0
14	2	-0.7	1.7	-0.01	0.18	0.0	0.0
14	3	0.9	-1.0	0.03	-0.12	0.0	0.0
14	4	-1.0	1.1	-0.04	0.00	0.0	0.0
14	5	1.1	-1.5	0.07	-0.11	0.0	0.0
14	6	1.5	0.1	0.08	0.00	0.0	0.0
14	7	-1.0	-0.1	-0.07	0.01	0.0	0.0
14	8	0.3	1.4	0.02	0.08	0.0	0.0
14	9	1.4	-2.1	0.19	-0.17	0.0	0.0
14	10	-0.9	3.4	-0.13	0.22	0.0	0.0
14	11	-3.2	-1.8	-0.26	-0.11	0.0	0.0
14	12	1.6	-2.0	0.11	-0.20	0.0	0.0
14	13	-0.2	1.4	0.02	0.17	0.0	0.0
14	14	4.4	-3.7	0.33	-0.25	0.0	0.0

Table 3.7 GRIM80 Field Model at Epoch 1980.0 (Includes MAGSAT Data)

n+1	m+1	g	h	$\dot{g}$	$\dot{h}$	$\ddot{g}/2$	$\ddot{h}/2$
2	1	-29987.5	0.0	21.79	0.0	-0.152	0.0
2	2	-1956.7	5605.4	9.50	-12.60	-0.159	0.029
3	1	-1997.1	0.0	-19.33	0.0	0.224	0.0
3	2	3027.4	-2130.1	2.39	-17.10	0.031	-0.942
3	3	1663.7	-201.0	9.89	-26.73	0.197	-0.354
4	1	1291.9	0.0	-5.46	0.0	0.581	0.0
4	2	-2180.9	-335.5	-24.24	-0.05	0.205	-0.233
4	3	1251.3	271.4	-1.81	1.70	0.151	-0.064
4	4	833.6	-251.8	-0.36	-5.49	0.158	-0.020
5	1	-937.9	0.0	-0.36	0.0	0.069	0.0
5	2	782.9	212.8	-0.44	4.47	0.133	0.043
5	3	398.9	-256.2	-4.94	2.89	-0.217	0.224
5	4	-420.0	32.9	-2.69	4.48	-0.040	0.173
5	5	198.0	-297.4	-5.67	-0.19	-0.186	0.091
6	1	-217.5	0.0	-1.20	0.0	-0.070	0.0
6	2	357.3	35.9	-0.33	4.09	-0.053	0.175
6	3	260.9	149.1	-0.74	-0.64	-0.086	-0.189
6	4	-74.4	-150.4	-4.39	-0.20	-0.099	0.100
6	5	-160.2	-78.1	-0.01	-0.23	-0.027	-0.146
6	6	-48.9	91.8	1.01	-1.35	0.040	-0.210
7	1	49.3	0.0	-0.02	0.0	-0.049	0.0
7	2	45.3	-14.6	0.22	-0.10	0.006	-0.005
7	3	41.9	93.5	3.19	-0.34	0.044	0.014
7	4	-172.1	70.9	1.05	-0.61	-0.115	-0.042
7	5	3.3	-43.3	0.48	-0.59	0.023	-0.007
7	6	14.6	-2.6	0.97	-0.27	-0.016	-0.091
7	7	-107.4	16.9	-0.53	2.20	-0.066	0.022
8	1	72.0	0.0	0.64	0.0	0.038	0.0
8	2	-39.5	-42.6	-1.14	-1.64	-0.072	-0.035
8	3	1.7	-27.4	-0.02	-0.73	-0.024	-0.085
8	4	20.7	-3.0	0.66	0.36	0.013	0.027
8	5	-12.1	16.1	1.73	0.66	-0.049	-0.008
8	6	0.4	18.0	0.25	-0.01	0.019	0.008
8	7	10.3	-23.0	-0.36	0.30	-0.048	0.051
8	8	-21.3	-4.3	0.44	0.08	0.060	-0.015
9	1	13.7	0.0	0.64	0.0	0.0	0.0
9	2	-7.1	6.7	0.12	-0.05	0.0	0.0
9	3	-10.1	-17.6	-0.49	-0.21	0.0	0.0
9	4	-10.1	1.7	-0.08	-0.03	0.0	0.0
9	5	-2.2	-22.0	-0.11	-0.11	0.0	0.0
9	6	4.4	9.2	-0.11	-0.43	0.0	0.0
9	7	2.3	14.2	-0.49	-0.62	0.0	0.0
9	8	-5.2	-14.0	-0.71	-0.30	0.0	0.0
9	9	-1.2	-14.3	-0.17	0.39	0.0	0.0
10	1	8.7	0.0	-0.31	0.0	0.0	0.0
10	2	10.1	-20.9	-0.95	0.46	0.0	0.0
10	3	1.3	13.4	0.05	-0.37	0.0	0.0
10	4	-12.2	9.1	0.23	0.31	0.0	0.0
10	5	9.1	-5.0	-0.46	-0.30	0.0	0.0
10	6	-3.6	-4.6	0.02	-0.05	0.0	0.0
10	7	-1.0	8.9	-0.00	-0.20	0.0	0.0
10	8	7.0	10.2	0.25	0.02	0.0	0.0
10	9	0.9	-4.2	-0.03	-0.55	0.0	0.0
10	10	-5.3	2.1	-0.83	0.26	0.0	0.0
11	1	-5.3	0.0	-0.07	0.0	0.0	0.0
11	2	-5.9	1.3	-0.05	-0.08	0.0	0.0
11	3	2.4	0.8	0.23	0.16	0.0	0.0
11	4	-5.8	2.7	-0.09	-0.16	0.0	0.0
11	5	-1.8	5.6	0.12	0.03	0.0	0.0
11	6	4.7	-4.8	0.01	-0.11	0.0	0.0
11	7	3.4	-0.2	0.02	-0.09	0.0	0.0
11	8	0.6	-1.1	-0.01	0.13	0.0	0.0
11	9	2.1	3.3	0.13	-0.01	0.0	0.0
11	10	0.9	-0.2	-0.17	0.05	0.0	0.0
11	11	-0.1	-4.4	-0.14	-0.19	0.0	0.0
12	1	2.7	0.0	0.03	0.0	0.0	0.0
12	2	-1.6	0.7	-0.14	-0.22	0.0	0.0
12	3	-1.3	1.7	0.17	-0.14	0.0	0.0
12	4	2.4	-1.3	-0.01	0.18	0.0	0.0
12	5	-0.1	-2.9	0.00	0.04	0.0	0.0
12	6	-0.9	0.7	-0.10	-0.05	0.0	0.0
12	7	-0.4	0.1	-0.13	0.00	0.0	0.0
12	8	1.4	-2.3	0.11	-0.09	0.0	0.0
12	9	-1.8	-0.0	-0.16	0.24	0.0	0.0
12	10	-0.7	-1.8	0.22	-0.02	0.0	0.0
12	11	-1.8	-1.6	-0.03	-0.07	0.0	0.0
12	12	3.9	1.3	0.28	0.09	0.0	0.0
13	1	-1.4	0.0	0.12	0.0	0.0	0.0
13	2	0.4	0.3	0.08	0.03	0.0	0.0
13	3	-0.4	1.2	-0.02	0.12	0.0	0.0
13	4	-0.2	2.4	-0.05	-0.04	0.0	0.0
13	5	0.9	-1.6	0.05	-0.08	0.0	0.0
13	6	1.0	0.4	0.04	0.01	0.0	0.0
13	7	-0.5	0.1	-0.02	-0.05	0.0	0.0
13	8	-0.2	-0.3	0.04	-0.09	0.0	0.0
13	9	-0.2	0.0	-0.12	0.03	0.0	0.0
13	10	-0.4	-0.2	0.09	-0.06	0.0	0.0
13	11	-0.0	-1.3	0.05	-0.01	0.0	0.0
13	12	0.6	0.4	0.07	0.06	0.0	0.0
13	13	-0.2	0.7	-0.13	0.13	0.0	0.0
14	1	0.0	0.0	-0.04	0.0	0.0	0.0
14	2	-0.2	-0.2	0.04	-0.03	0.0	0.0
14	3	0.6	-0.3	-0.00	-0.04	0.0	0.0
14	4	-0.4	1.5	-0.03	0.05	0.0	0.0
14	5	-0.1	-0.1	-0.04	0.01	0.0	0.0
14	6	0.3	-0.6	0.01	-0.06	0.0	0.0
14	7	-0.2	-0.2	-0.04	0.01	0.0	0.0
14	8	0.3	1.1	0.04	0.04	0.0	0.0
14	9	-0.7	0.1	-0.06	0.03	0.0	0.0
14	10	0.3	0.3	0.03	-0.02	0.0	0.0
14	11	0.1	0.2	0.07	0.07	0.0	0.0
14	12	0.6	0.2	0.03	0.03	0.0	0.0
14	13	-0.7	-0.3	-0.04	-0.08	0.0	0.0
14	14	-0.3	-1.3	-0.11	-0.05	0.0	0.0

4.0 DISCUSSION

The results of the preliminary study show that recursive estimation has great potential for geomagnetic field modeling but more needs to be done to realize that potential. There are several problems in modeling that need to be addressed in order to achieve optimal estimation.

First there is the question of the scaling of the covariance matrices produced in the mini-batches. When comparing the field estimates produced for different time spans, it is obvious that the actual errors in the field coefficients are larger than the computed standard deviations. The cause of this modeling error is not known but it may be the result of incorrect weighting of the various measurement types. For example, it is possible that nonlinear weighting of the angular survey data as a function of the local field strength may be more appropriate. Other possiblities include aliasing caused by truncation of the spherical harmonic expansion (and secular variation terms) and program errors. These explanations and others must be examined until the cause of the discrepancy between the actual errors and the covariance matrix are resolved. It should not be necessary to scale the output of any mini-batches. This scaling is a crude attempt to account for modeling errors which should not be present.

The determination of the optimum state noise variances is another problem which should be addressed in future work. Although we tried using different factors to scale the linear and quadratic state noise variances, the individual variances for each degree should be determined by a more systematic procedure than the eyeball estimate. In fact, it would be desireable to determine the variances for each degree and order separately, but this is probabaly an unrealistic goal (because of the computational burden). In our proposal, we suggested using maximum likelihood estimation (MLE) to determine the state noise variances. However, more study is required to find computationally efficient methods of performing MLE.

Other factors which should be examined in attempting to improve the field model include the use of marine and repeat survey data and the handling of observatory biases. It is questionable whether the use of marine and repeat survey data will improve the field prediction but it should be included in the mini-batches. A more significant factor is the handling of observatory biases. In the PMAG solution, one set of biases was estimated for the period 1960 to 1977 but a different set of biases was estimated for each mini-batch. Since the estimated biases were not entirely consistent from one mini-batch to the next (the estimated biases for the first two mini-batches were wildly inconsistent), the field estimates were likewise not consistent. An attempt was made to constrain the biases used in the mini-batches to the PMAG estimates but the estimate of the field model was further degraded and the covariance matrix was too small. Apparently there is some inconsistency between the PMAG bias estimates and the data in the individual mini-batches. It would be preferable to combine the mini-batch bias estimates using the filter to produce an estimate of the biases for the entire period. Unfortunately this would greatly increase the computational burden, both in the mini-batches and in the filtering.

Finally, the lack of consistency in the field coefficient estimates for the 1955 to 1960 mini-batch compared to the other mini-batches may have degraded the final filtered estimate. The inconsistency of this mini-batch may have resulted from over-parameterization of the field model (use of a maximum coefficient degree which is too high) for the available data. Thus minor modeling errors such as incorrect weighting of the measurements could have caused highly erroneous bias and field model estimates. This explanation can be tested easily and should be investigated in future studies.

5.0 CONCLUSIONS AND RECOMMENDATIONS

5.1 Conclusions

(1) The feasibility of using Kalman filtering for geomagnetic field modeling has been clearly demonstrated. The prediction of the MAGSAT data using the filtered field model was significantly better than the prediction of other tested pre-MAGSAT field models. This was accomplished even though some modeling errors existed in the mini-batch field models.

(2) The use of the likelihood function in conjunction with the sum of weighted residuals to determine the optimum models has been validated. There was a strong positive correlation between the value of the likelihood function and the ability of the field model to predict the MAGSAT data.

(3) It is believed that the dominant error source in performing the mini-batch data reduction was incorrect weighting of the survey measurements.

5.2 Recommendations

(1) The source of the modeling errors in the mini-batch data reduction should be determined and eliminated. This is a necessary step for further filtering work and for any type of geomagnetic field modeling.

(2) Marine and repeat survey data should be included in the mini-batch data reduction.

(3) It would be desireable to solve for a common set of observatory biases for all the mini-batches using the Kalman filter. This should eliminate some of the inconsistency between field estimates for different mini-batches.

(4) After the modeling errors have been eliminated, optimum values of the state noise variances should be determined. Ideally this should be performed using maximum likelihood estimation and may require the use of data back to 1900.

(5) Field models for times in the past should be obtained using an optimal smoother based upon the results of the filter.

(6) Contour maps showing the accuracy of the field model can be produced using the error covariance matrix computed by the filter.

6.0 References

(1) Barker, F. S. and D. R. Barraclough, "World Magnetic Chart Model for 1980", EOS, Transactions of A. G. U., No. 61, P. 453, 1980.

(2) Barraclough, D. R., J. M. Harwood, B. R. Leaton and S. R. C. Malin, "A Model of the Geomagnetic Field at Epoch 1975", Geophys. J. Royal Astr. Soc., 43, 645-659, 1975.

(3) Barraclough, D. R., "Spherical Harmonic Analysis of the Geomagnetic Secular Variation - A Review of Methods", Physics of the Earth and Planetary Interiors, 12, 1976, pg. 365-382.

(4) Barraclough, D. R., "Spherical Harmonic Models of the Geomagnetic Field", Institute of Geological Sciences, Natural Environment Research Council, Geomagnetic Bulletin 8, Edinburgh, 1978.

(5) Barraclough, D. R., and F. S. Barker, "Word Magnetic Chart Model for 1980", EOS, Vol. 61, No. 19, 1980.

(6) Cain, J. C., S. J. Hendricks, R. A. Langel, and W. V. Hudson, "A Proposed Model for the International Geomagnetic Reference Field - 1965", Journal of Geomagnetism and Geoelectricity, Vol. 19, No. 4, 1967.

(7) Edwards, A. W. F., Likelihood: An Account of the Statistical Concept of Likelihood and its Application to Scientific Inference, Cambridge Univ. Press, London, 1972.

(8) Estes, R. H., "FIT Program Modifications for Geomagnetic Field Model and Magnetometer Parameter Recovery", BTS-FR-79-84B, NASA Contract NAS 5-25047, April 1979.

(9) Estes, R. H., "Modeling of the Earth's Main Field", presented at the NASA Geodynamics Program Review, Goddard Space Flight Center, Greenbelt, MD, February 6-8, 1980.

(10) Estes, R. H., "FIT Program Documentation and User's Guide", BTS-FR-80-120, NASA Contract NAS 5-25047, June 1980.

(11) Gelb, A. (editor), Applied Optimal Estimation, The Analytical Sciences Corporation, MIT Press, 1974.

(12) Gibbs, B. P. and D. W. Porter, "Development and Evaluation of an Adaptive Algorithm for Predicting Tank Motion", IEEE Conference on Decision and Control, December 1980.

(13) Gupta, N. K., and R. K. Mehra, "Computational Aspects of Maximum Likelihood Estimation and Reduction in Sensitivity Function Calculations", IEEE Transactions on Automatic Control, Vol. Ac-19, December 1974.

(14) Langel, R. A., R. H. Estes, G. D. Mead, E. B. Fabiano, and E. R. Lancaster, "Initial Geomagnetic Field Model from MAGSAT", Geophysical Research Letters, Vol. 7, No. 10, October 1980.

(15) Langel, R. A., R. Coles and M. A. Mayhew, "Comparison of Magnetic Anomalies of Lithospheric Origin Measured by Satellite and Airborne Magnetometers over Western Canada", Canadian J. of Earth Science, in press, 1980.

(16) Peddie, N. W. and E. B. Fabiano, "A Model of the Geomagnetic Field for 1975", Journal of Geophysical Research, No. 81, pp. 2539-2542, 1976.

(17) Zmuda, A. J. (editor), World Magnetic Survey 1957-1968, IAGA Bulletin No. 28, 1971.

Appendix A.1

COMPARISON OF KALMAN AND WIENER FILTERING

The review of our proposal for this study requested that the Kalman filtering approach be compared to Wiener filtering. In general, it may be stated that Wiener filtering is a subset of Kalman filtering: Wiener filtering requires certain assumptions that are not required in Kalman filtering. It may appear that Kalman filtering requires knowledge of the system dynamics but, in fact, no more knowledge is required than for Wiener filtering [1].

In this section, an explanation of Wiener filtering, a discussion of how the geomagnetic field problem fits into the framework of Wiener filtering, and a comparison between Wiener and Kalman filtering for this specific problem will be given. Other references which discuss, more generally, the comparisons between the two approaches are [1 ,4].

The basic problem addressed in Kalman and Wiener filtering is one where we have observations $z(t)$ of a signal process $y(t)$ corrupted by additive white noise $v(t)$

$$z(t) = y(t) + v(t) \qquad t_0 \leq t \leq t_f \tag{1}$$

where

$$E(v(t)v^T(\tau)) = V\,\delta(t-\tau) \quad .$$

Although Wiener and Kalman filtering can handle the case where $y(\cdot)$ is correlated with $v(\cdot)$, (e.g. this occurs when feedback is used) we shall only consider the uncorrelated case

$$E(y(t)v^T(\tau)) \equiv 0 \quad .$$

It should be noted that Wiener's original work was limited to the case where z, y and v were scalars, $y(t)$ and $v(t)$ were statistically stationary and the observation interval was infinite, ($t_0 = -\infty$). Although his work has been extended to avoid these restrictions, the following description of Wiener filtering is limited to scalar observations over an infinite interval.

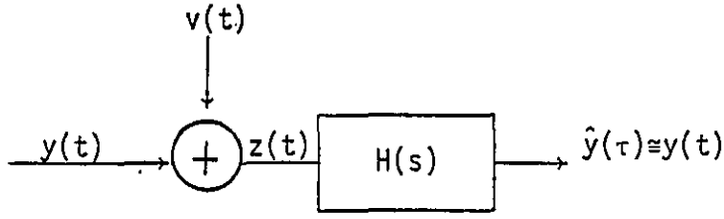

Figure 1 General Filtering/Prediction Problem

Figure 1 shows the general filtering/smoothing/prediction problem. We wish to find a function $h(t,\tau)$ in

$$\hat{y}(t|t_f) = \int_{t_0}^{t_f} h(t,\tau)z(\tau)d\tau \qquad (2)$$

such that $\text{tr } E[y(t)-\hat{y}(t)][y(t)-\hat{y}(t)]^T$ is minimized. The three separate problems are defined as:

$$\begin{aligned} &\text{filtering :} && t = t_f \\ &\text{smoothing :} && t_0 \leq t < t_f \\ &\text{prediction:} && t > t_f \ . \end{aligned}$$

Although we are primarily interested in prediction of the geomagnetic field, we shall confine the present discussion to filtering ($t=t_f$) since the derivation for prediction is similar.

It is well known [3] that the least squares solution to (2) is obtained by the orthogonality property

$$E[(y(t)-\hat{y}(t))z^T(\tau)] = 0 \qquad t_0 \leq \tau \leq t \quad . \tag{3}$$

Using (2) and (3) we find that

$$h(t,\tau)V + \int_{t_0}^{t} h(t,\lambda)E[y(\lambda)y^T(\tau)]d\lambda = E[y(t)y^T(\tau)] \qquad t_0 \leq \tau \leq t \tag{4}$$

We now apply Wiener's assumptions that $t_0 = -\infty$ and $E[y(t)y^T(\tau)]$ is statistically stationary, i.e. depends only on $|t-\tau|$. Then by making a change of variables, equation 4 becomes

$$h(t)V + \int_0^{\infty} h(\lambda)\ \phi_y(t-\lambda)d\lambda = \phi_y(t) \qquad 0 < t < \infty \tag{5}$$

where $\phi_y(t) = E[y(t)y^T(0)] = E[y(-t)y^T(0)]$. Equation (5) is the famous Wiener-Hopf equation. Wiener solved this using spectral factorization (for the scalar case). For the processes with rational spectral densities, $\phi_y(t)$ has the form

$$\phi_y(t) = \phi_y(|t|) = \sum_{i=1}^{n} \alpha_i\ e^{-\beta i|t|} \tag{6}$$

where α_i and β_i are constants (possibly complex). The bilateral Laplace transform of (6)

$$\Phi_y(s) = \int_{-\infty}^{\infty} \phi_y(t)e^{-st}dt \tag{7}$$

is a ratio of polynomials in s^2 whose poles always occur in complex conjugate pairs: every root in the right-half s-plane is accompanied by a root in the left-half plane. Thus, $\Phi(s)$ can be written as

$$\Phi_y(s) = \Phi_y^+(s)\ \Phi_y^+(-s) \tag{8}$$

where Φ_y^+ is a unique factor of $\Phi(s)$. Using this factorization, Wiener showed that the convolution in equation (5) could be written in terms of these spectral factors and the optimum $H(s)$ is found to be

$$H(s) = \frac{\Phi_y^+(s)}{V+\Phi_y^+(s)} \qquad (9)$$

A brief description of the Kalman filter was given in preceding sections of this report. We shall not elaborate further on the details of Kalman filtering since they are generally well known and numerous fine references exist on the subject [for example, see 2 or 3].

In comparing the development of the Wiener filter with the Kalman filter, several differences in assumptions are apparent.

(1) The (original) Wiener filter assumes stationarity of $y(t)$ and $v(t)$ while the Kalman filter makes no such assumption. As we have noted, Wiener filtering has been extended to handle non-stationarity but the procedures tend to be complicated.

(2) The (original) Wiener filter assumed that the signal $z(t)$ was available from time = $-\infty$ while the Kalman filter operates on finite data spans. The Kalman filter can be made equivalent to a Wiener filter by using the steady state Kalman gains but the Wiener filter is not so easily modified to handle finite data spans. This limitation of the Wiener filter is a problem for geomagnetic modeling because the data span is relatively short compared to time constants of the field dynamics.

(3) It would appear that the Kalman filter may only be used when the signal process is the output of a known finite-dimensional system driven by process noise. In contrast, the Wiener filter makes no such assumption. Instead, it requires knowledge of the covariance functions $E(y(t)y^T(\tau)]$ and $E(z(t)z^T(\tau)]$. However, [1] shows that a Kalman filter may be constructed using only the same covariance

functions used in the Weiner filter (although the state error covariances computed by the Kalman filter may not have any physical meaning). Furthermore, the solution of the Wiener-Hopf equation requires that the system be finite-dimensional. Thus, the distinction between the two approaches is not as significant as might be presumed.

The implications of these different assumptions for geomagnetic field modeling are quite significant. Particularly for this problem, the Kalman filter is to be preferred to the Wiener filter. The stationarity assumption used in the Wiener filter is certainly not valid for geomagnetic modeling. The "measurements" input to the filter must be the mini-batch estimates of the geomagnetic field rather than the raw magnetic field measurements obtained at specific points on the earth. (If the thousands of raw measurements were used directly in the filter, the computational burden would be enormous). Thus the covariance of $v(t)$ will vary from one mini-batch to the next. Furthermore, the signal process is not stationary for the limited time period of our data. Since the data span is short compared to the time constants of the geomagnetic field dynamics, we have modeled (in the Kalman filter) the dynamics as free (no feedback) integrators fed by white noise. Obviously the output of these integrators will not be bounded or stationary and thus the model is only approximately valid for relatively short periods of time. This is a reasonable approximation for a Kalman filter, but the lack of stationarity is a serious problem for the Wiener filter.

The extremely short data span (5 time points) is also a serious drawback to the use of the Wiener filter. This has two bad effects: the sample covariance function $E[z(t)z^T(\tau)]$ will be grossly in error (and truncated) and the optimal weighting function $h(t)$ will not have a sufficient amount of data to operate on. The only assumption used in the Kalman filter which may cause problems is the finite dimensional dynamic model. If this model were grossly in error, then the estimates produced by the filter would be erroneous. However, this is not a serious problem for geomagnetic modeling since we are sampling a short time span of a system

with long time constants. As we have already pointed out, the alternative (use of a sample covariance function) is much less attractive.

Although it is possible to eliminate some of the restrictive assumptions imposed upon Wiener filtering, the methods used to overcome the restrictions are not simple (particularly for the non-stationary, multi-dimensional, discrete time, limited data span case). In contrast, Kalman filtering seems ideally suited to the task. We are aware of no advantages (either analytically or computationally) that Wiener filtering enjoys relative to Kalman filtering for this application.

REFERENCES

(1) Anderson, B. D. O. and J. B. Moore, "The Kalman-Bucy Filter as a True Time-Varying Wiener Filter", IEEE Transactions on Systems, Man and Cybernetics, Vol. SMC-1, No. 2, April 1971.

(2) Gelb, A. (editor), Applied Optimal Estimation, MIT Press, 1974, Cambridge, Mass.

(3) Jazwinski, A. H. Stochastic Processes and Filtering Theory, Academic Press, 1970, New York.

(4) Kailath, T., "A View of Three Decades of Linear Filtering Theory", IEEE Transactions on Information Theory, Vol. IT-20, No. 2, March 1974.

Appendix A.2

Discussion of the Predictive Properties of Kalman Filtering Versus Batch Least Squares

In a review of a proposal for geomagnetic modeling by Kalman filtering, one reviewer made the statement that "Kalman filtering is known to be not so good for prediction." Although there are some problems for which the long term predictions of Kalman filters are inferior to those of batch processors, the preceeding statment is generally not true. As evidence of this, numerous applications papers exist demonstrating (successfully) the predictive ability of Kalman filters. It is the purpose of this appendix to discuss the conditions under which the Kalman predictor is inferior or superior.

Consider the case where measurements of a dynamic process are to be input to a Kalman filter and a batch least squares estimator where the same measurement and dynamic models are used in both estimators. The only difference between the two estimators is the inclusion of process (state) noise statistics in the Kalman filter. We also assume that the dynamic model used in the estimators is not a perfect match to the real world model. Thus both estimators will produce state estimates which contain errors due to the modeling errors. We restrict our attention to the state estimate produced at the end of the data span so that both estimators have processed an equal amount of data. Under the assumption that the state noise covariance used in the Kalman filter is a reasonable approximation to the actual modeling errors in the dynamics, the Kalman filter will almost always produce a better estimate of the final state (at the end of the data span) than the batch estimator. In fact, the estimation errors of the batch estimator tend to be largest at the ends of the interval. Thus, the Kalman predictions based upon the final state estimate will usually be better than those of the batch estimator for "short term" predictions. However, under some circumstances, the long term predictions of the batch estimator will be better than those of the Kalman filter. This is particularly true when the modeling errors tend to be cyclic.

As an example of this, consider satellite orbit determination. As with most real world problems, it is almost impossible to model the system perfectly. Typical orbital modeling errors include solar radiation, atmospheric drag, gravity field errors, tracking system biases and refraction effects. When orbit predictions from Kalman filters are compared with those of batch estimators, it is usually found that the error in the Kalman estimate is greater than that of the batch estimator for prediction intervals greater than one quarter orbit. For prediction less than one-quarter orbit, the Kalman filter is usually superior. This can be explained on the basis of the batch processor's global fit to the data: it is attempting to average the modeling errors over the entire data span, whereas, the Kalman filter applies the most weight to data at the end of the interval. In other words, the batch processor behaves somewhat like a low pass filter and treats the dynamic errors as high frequency noise with zero mean. Since the propogation of orbital errors is cyclic (because of orbital dynamics), the prediction of the batch processor usually tends to match the long term behavior of the orbit.

In order to better understand this phenomenon, consider a trivial example which contains large modeling errors. Assume that we have measurements of $z(t) = cos\omega_0 t \qquad (0 \leq t \leq \frac{2\pi}{\omega_0})$ and that we model the process as a constant plus linear term:

$$z = x_1 + v$$

$$\dot{x}_1 = x_2$$

$$\dot{x}_2 = q$$

where v and q are white noise processes. We use this same model in both the Kalman filter and batch least squares estimator (although q is obviously assumed to be zero in the batch estimator). We also assume that the contribution of *a priori* information is negligible so that the state estimates are dominated by the measurement data. It is easy to show that

the estimates of x_1 and x_2 from the batch estimator will be identically equal to zero. However, the estimates from the Kalman filter depend upon the value of $Q_s\delta(t-\tau) = E(q(t)q^T(\tau))$ used. Figure 1 shows typical behavior of the Kalman filter.

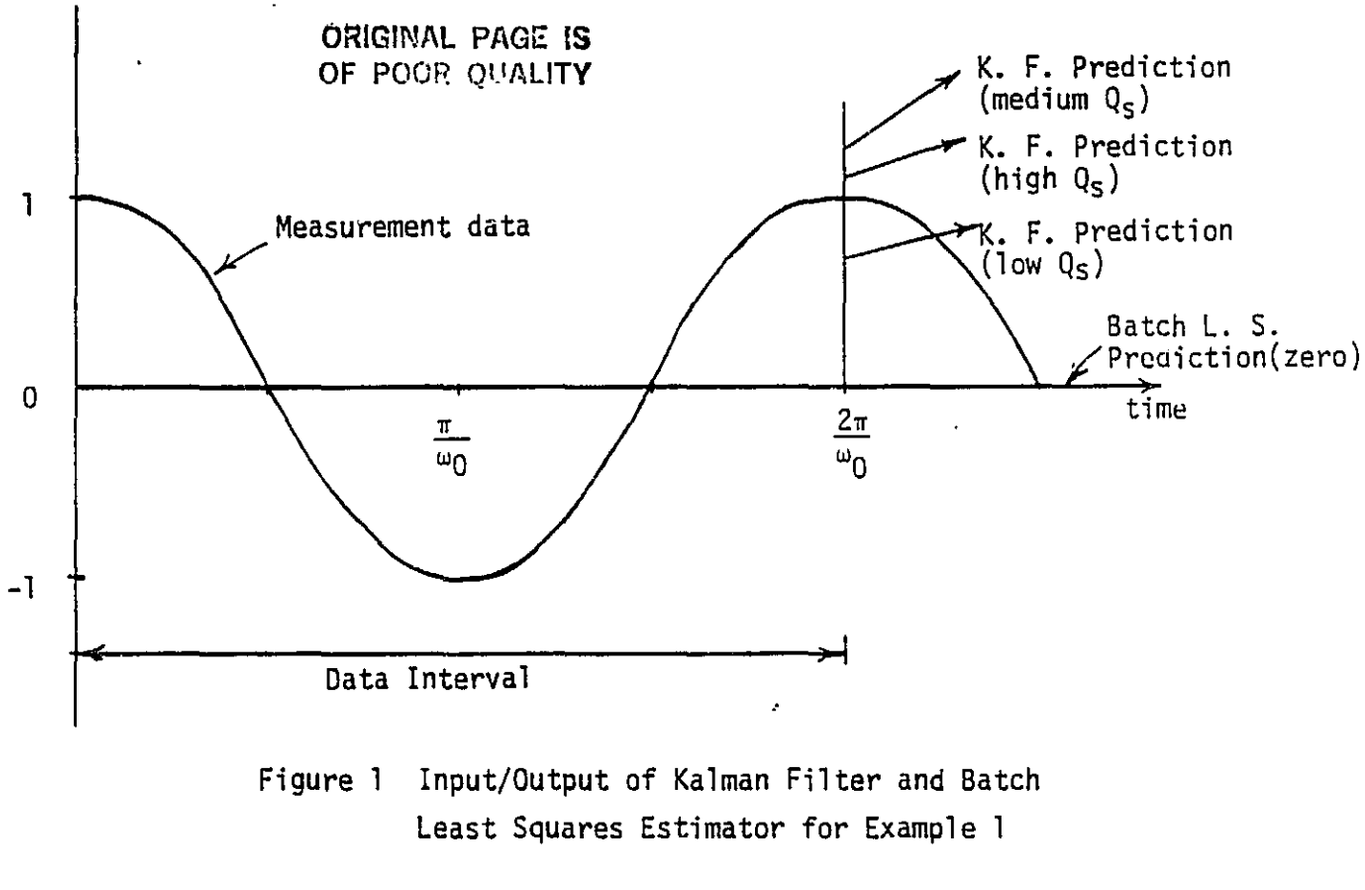

Figure 1 Input/Output of Kalman Filter and Batch Least Squares Estimator for Example 1

Notice that for medium values of Q_s, the Kalman filter estimate of x_1 at $t = \frac{2\pi}{\omega_0}$ is fairly accurate but the prediction rapidly diverges from the true $z(t)$. For higher values of Q_s, both the estimate and the derivative are more accurate. For low values of Q_s, the estimate of x_1 and x_2 are closer to those of the batch estimate (i.e. zero). Notice the batch least squares estimator produces better long term predictions than the Kalman filter.

Now consider a minor modification of this example which is closer to the problem of geomagnetic modeling. Instead of starting at time

$t = 0$, start at $t = \pi/\omega_0$. Then we get the results shown in Figure 2

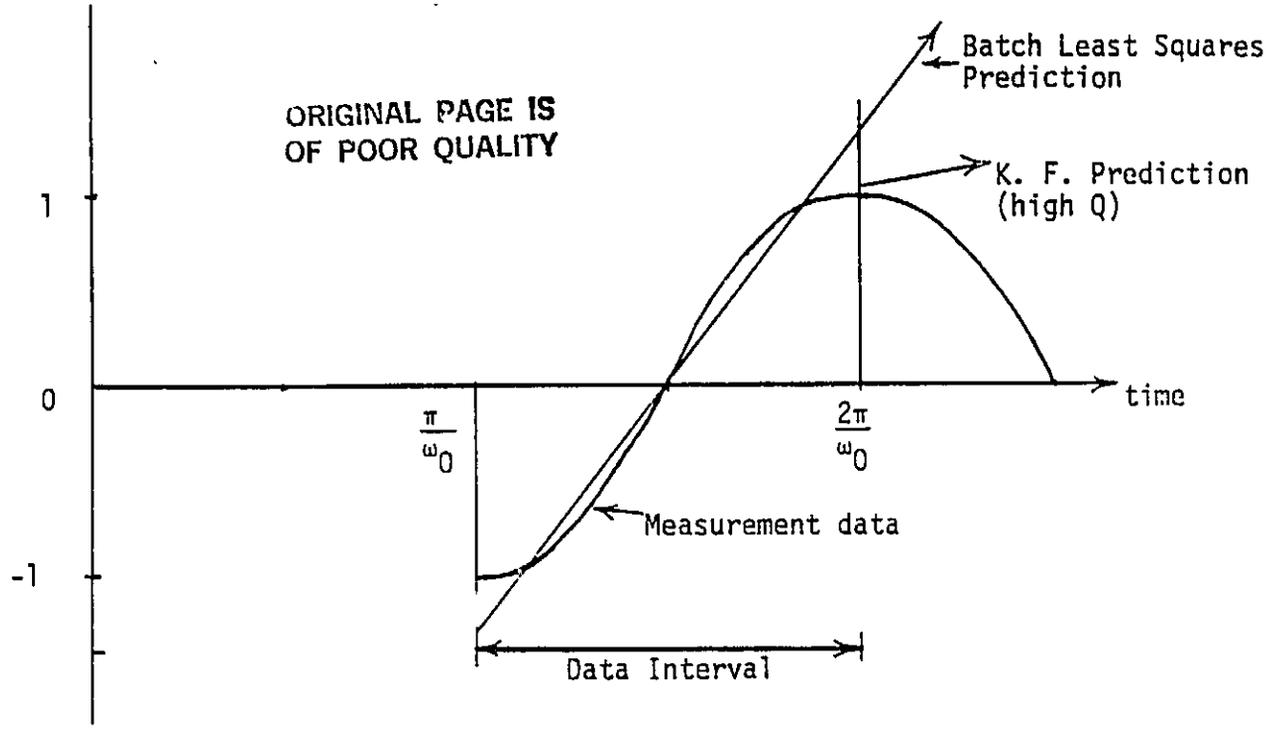

Figure 2 Input/Output of Kalman Filter and Batch Least Squares Estimator for Example 2

Here the prediction of the batch estimator is completely erroneous while the Kalman prediction is much closer to the actual $z(t)$. However, even the Kalman filter cannot accurately predict the signal because of the large modeling errors.

These examples were intentionally chosen to exaggerate the best and worst properties of the Kalman and least squares estimators but, in many respects, these examples are typical of real world problems. As we have noted, the first example is similar to the orbit determination problem (usually one revolution or more of data will be processed) while the second example is somewhat similar to geomagnetic field modeling. The second example is also more typical of problems where the underlying process really is stochastic (or appears to be stochastic) rather than deterministic. When attempts are made to predict the behavior of stochastic signals, then it is important for the

estimator to have the best possible state estimate at the end of the data span. That is exactly what the Kalman filter is intended to do.

Appendix A-3 Plots of WC 80 Field Model Coefficients

The following line printer plots of the WC80 field model were produced using almost the same scale as the plots of the mini-batch coefficients (Figure 3.1). Directly above each plot are four numbers. The first number is the coefficient degree. The second and third numbers are the minimum and maximum values of the plot in nanotesla. The last number is the scale factor in nT per small division (one print position).

The coding of the coefficient order is the same as in Figure 3.1, i.e.

$$0 = g^{i,0}$$

$$A = g^{i,1}$$

$$B = h^{i,1}$$

$$C = g^{i,2}$$

$$\vdots$$

$$Z = h^{i,13}$$

The numbers at the top of each plot are the print positions for each letter (order) for the ten points plotted. This is useful in resolving plotting ambiguities.

WC 80

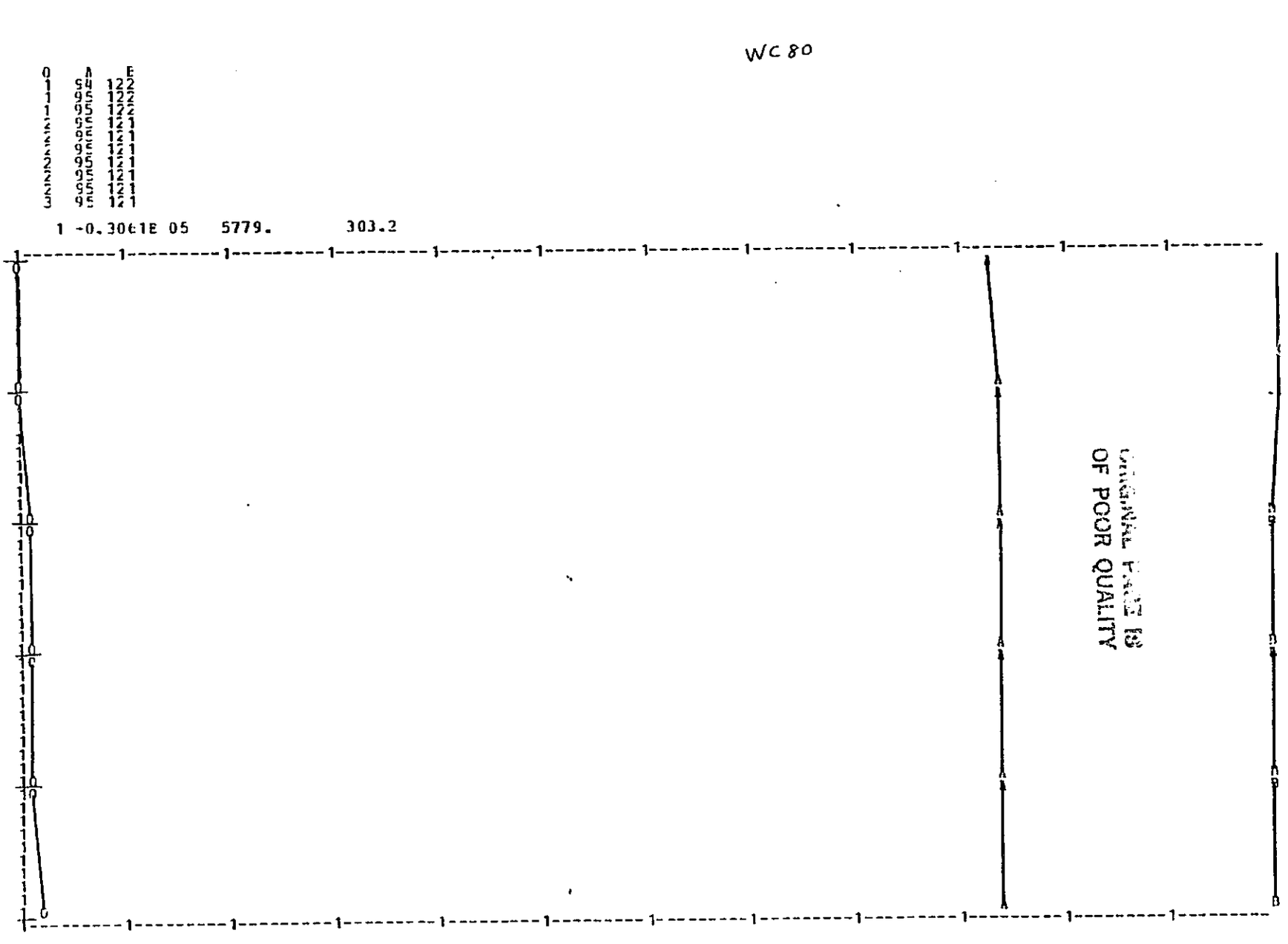

ORIGINAL PAGE IS
OF POOR QUALITY

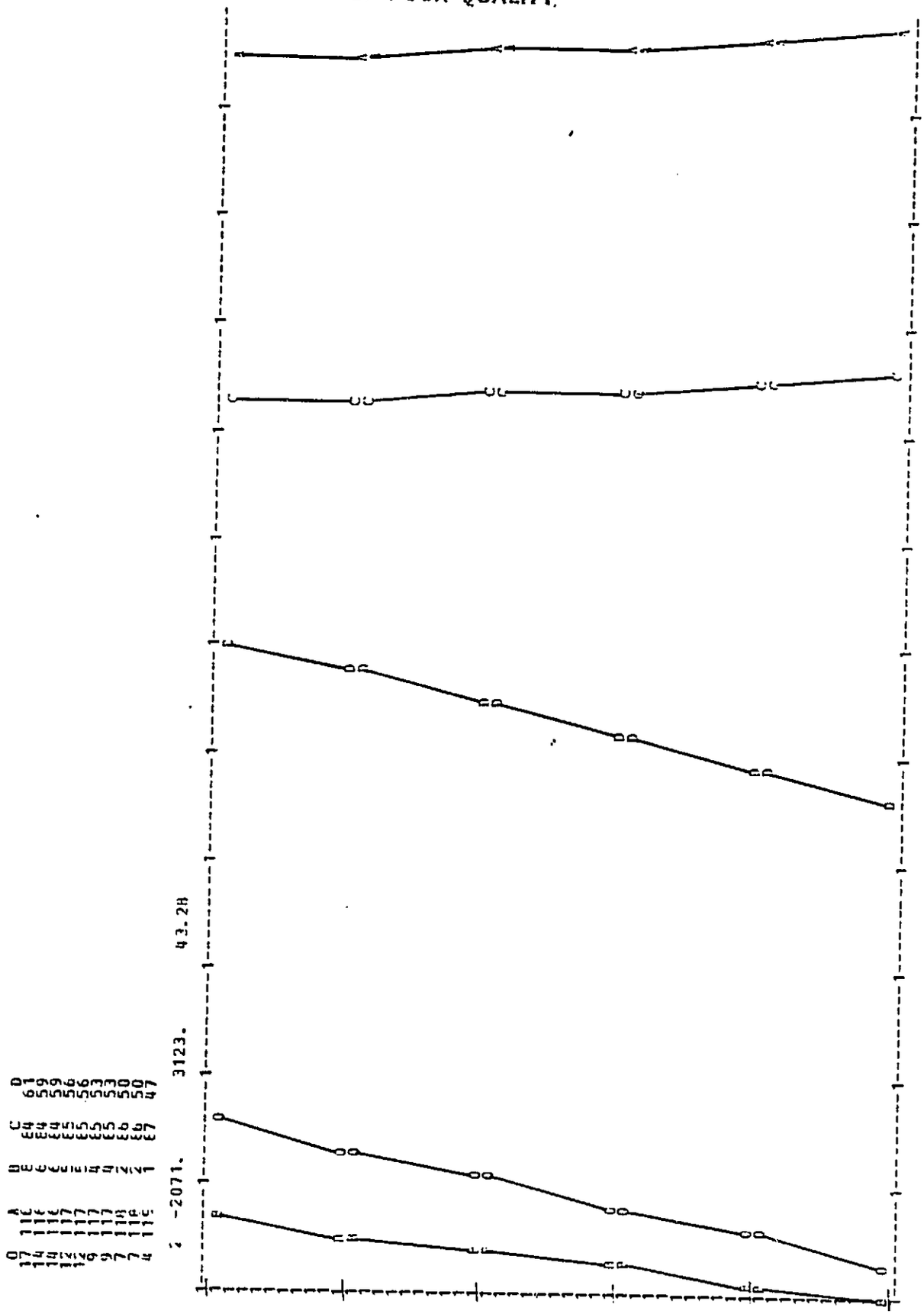

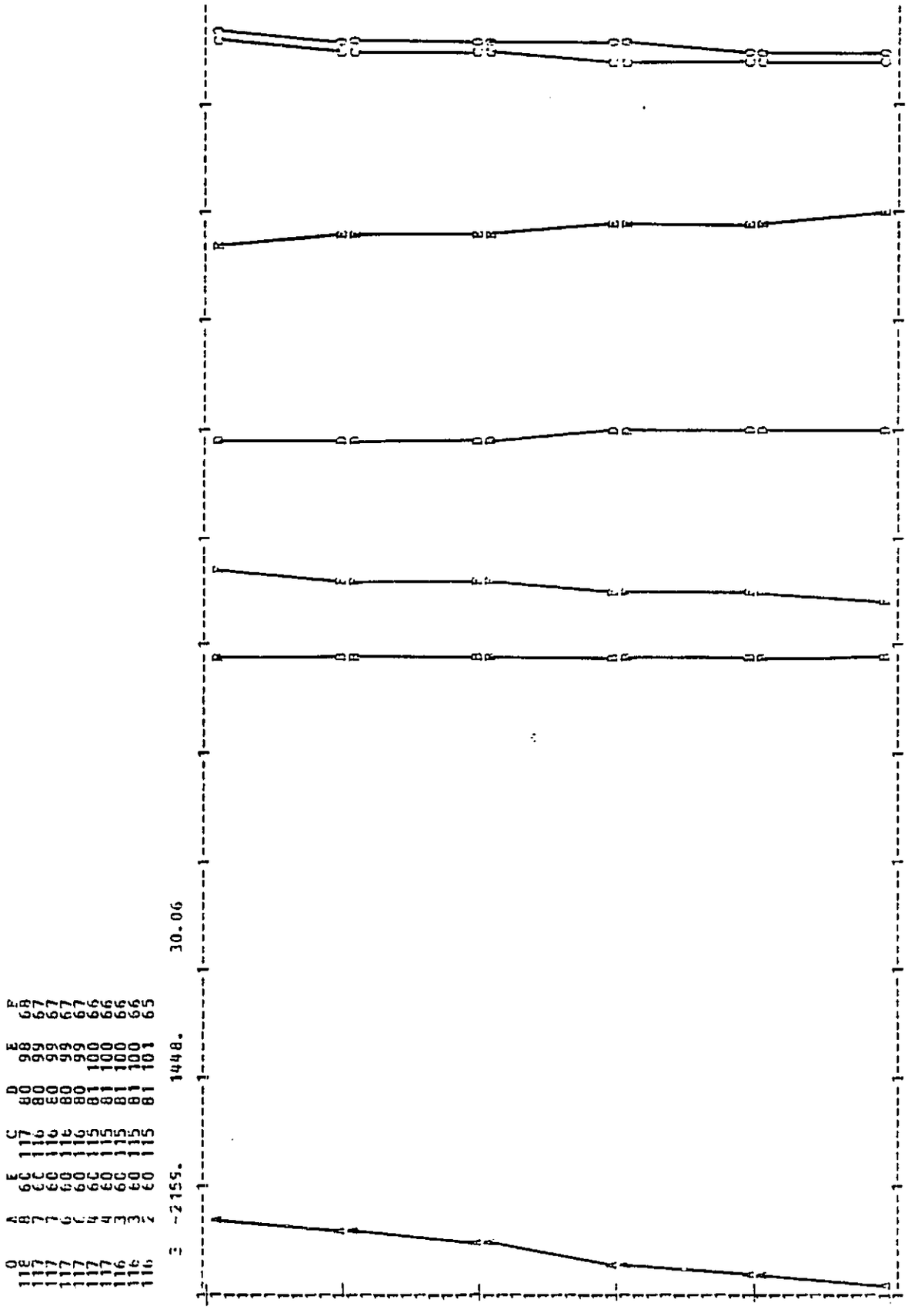

ORIGINAL PAGE IS
OF POOR QUALITY

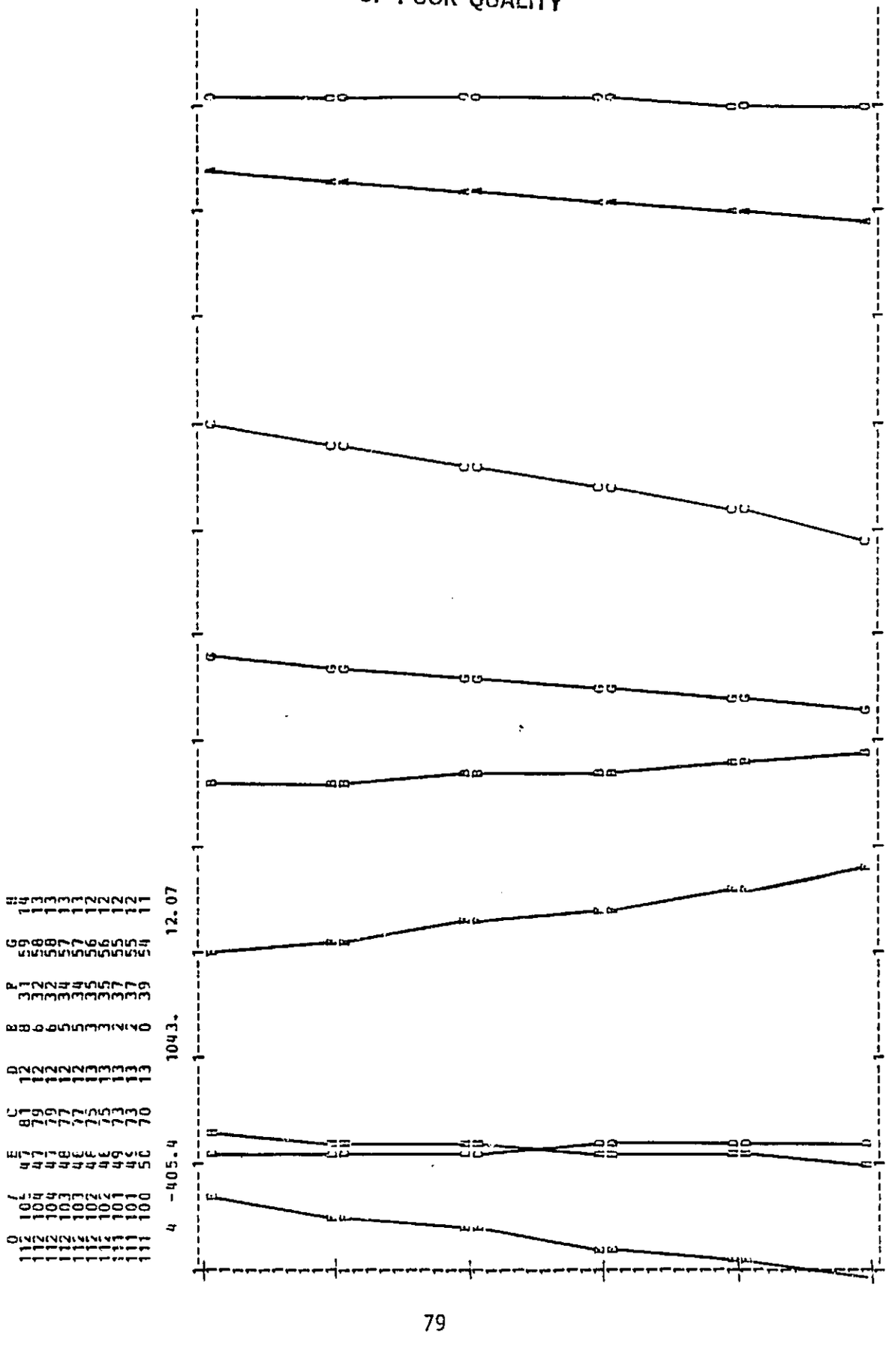

0	A	B	C	D	E	F	G	H	I	J
37	126	56	110	83	71	43	40	42	54	72
35	125	59	109	84	68	42	39	43	54	73
36	125	59	109	84	68	42	39	43	54	73
34	124	62	108	84	64	41	38	45	54	74
34	124	62	108	84	64	41	38	45	54	74
32	122	65	107	84	61	41	37	46	54	75
32	122	65	107	84	61	41	37	46	54	75
30	121	68	106	85	58	40	36	48	54	76
30	121	68	106	85	58	40	36	48	54	76
29	120	72	105	86	54	39	35	50	54	78

5 -379.5 364.4 6.199

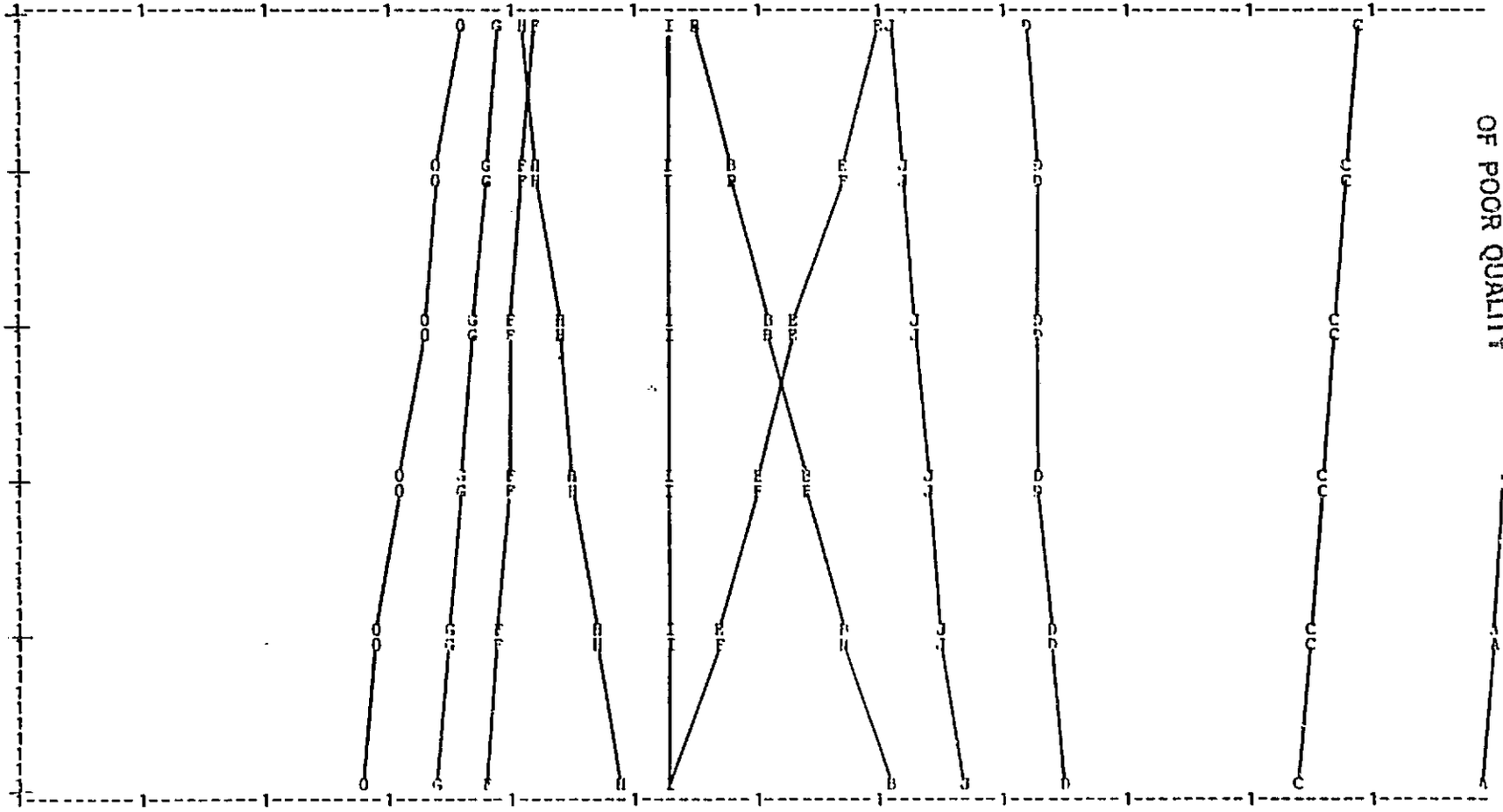

0	A	B	C	D	E	F	G	H	I	J	K	L
71	78	55	56	88	15	85	63	62	65	65	46	61
72	78	55	60	88	17	85	64	62	67	66	46	64
72	78	55	60	88	17	85	64	62	67	66	46	64
74	79	60	63	88	20	84	65	61	68	66	46	66
74	79	60	63	88	20	84	65	61	68	66	46	66
75	79	62	67	88	22	84	67	61	69	67	47	68
75	79	62	67	88	22	84	67	61	69	67	47	68
76	79	63	71	88	25	84	68	61	70	68	47	70
76	79	63	71	88	25	84	68	61	70	68	47	70
78	80	65	75	88	28	84	69	60	71	68	48	72

E -339.9 263.4 5.027

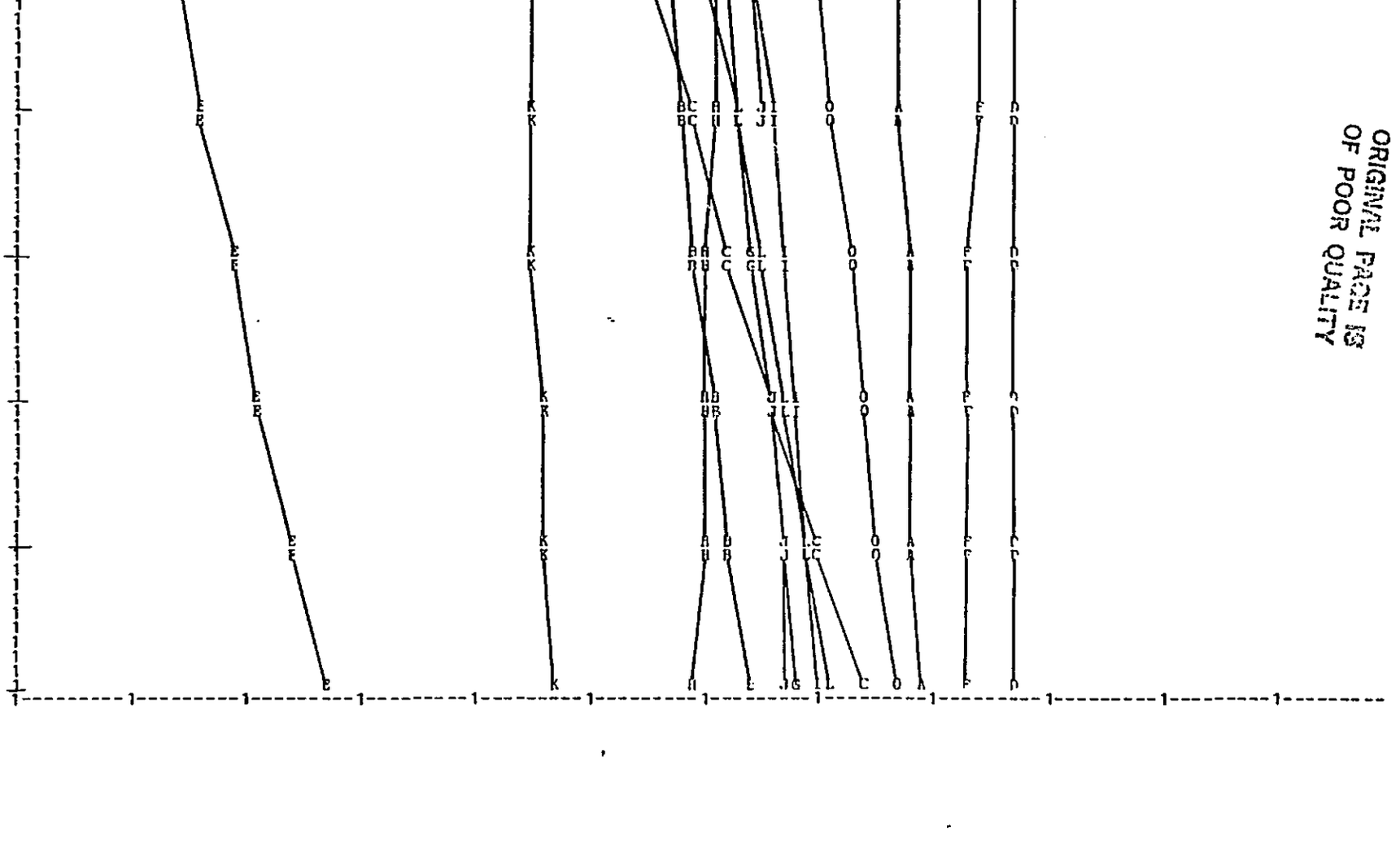

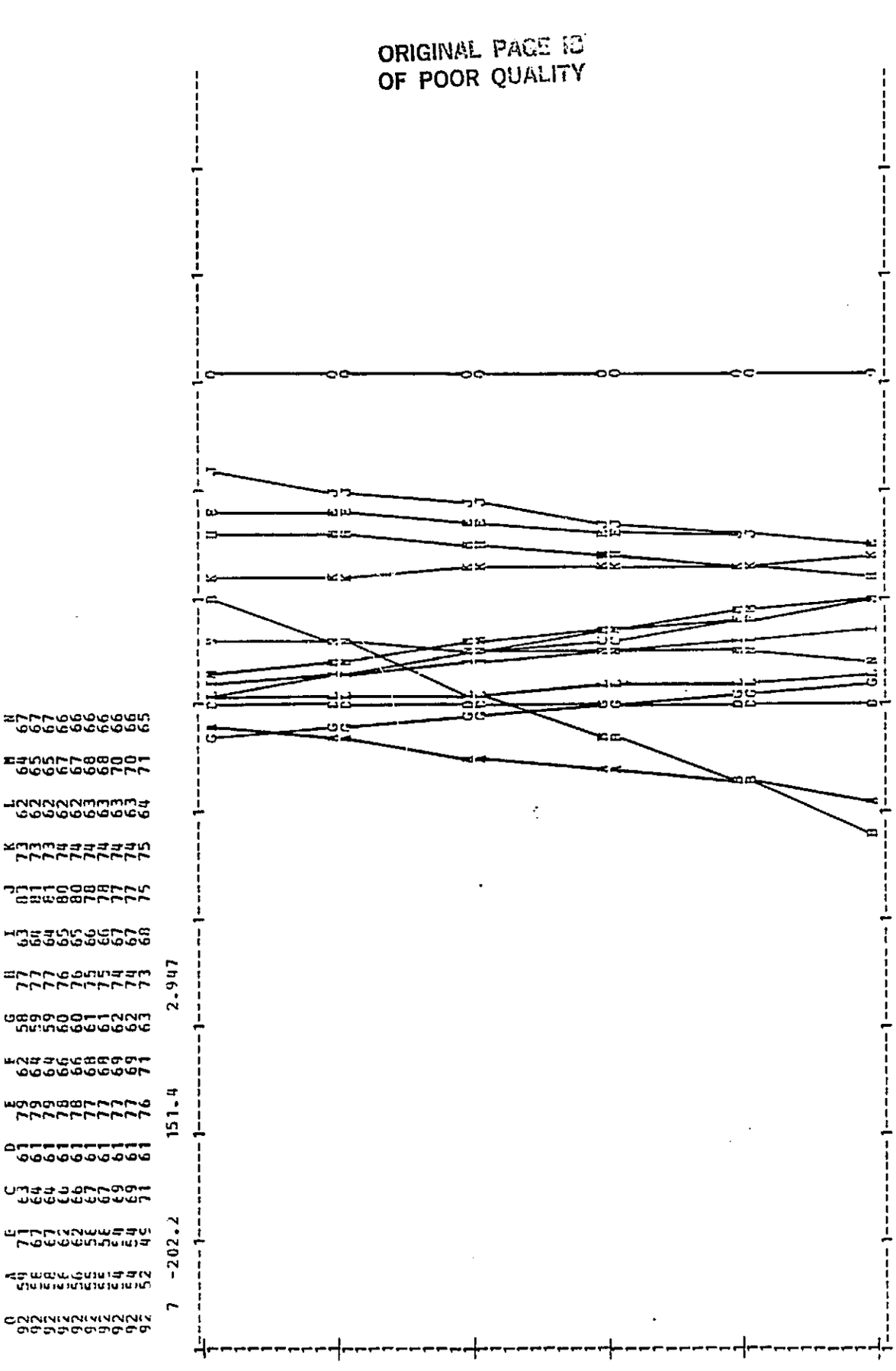

ORIGINAL PAGE IS
OF POOR QUALITY

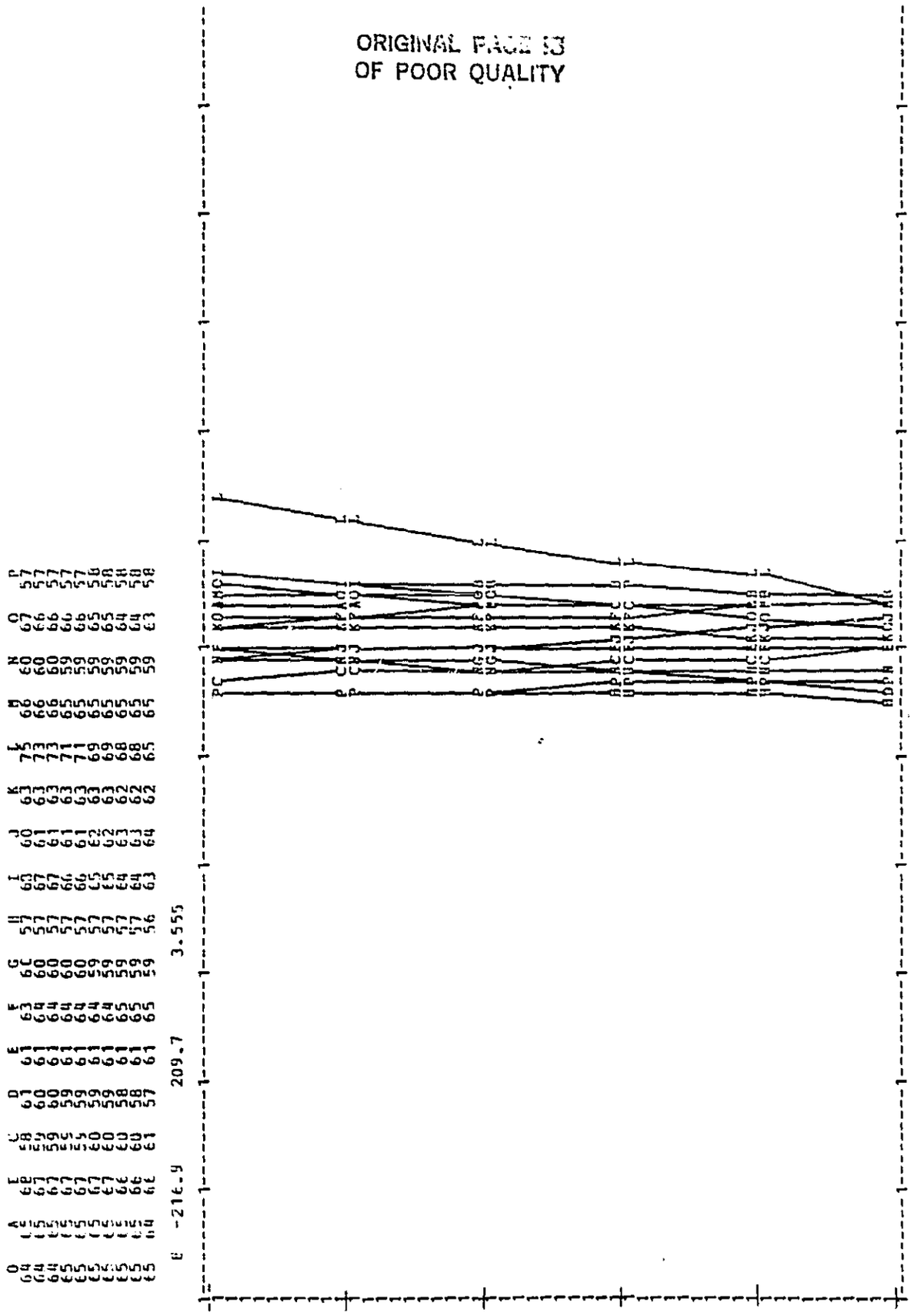

0	A	B	C	D	E	F	G	H	I	J	K	L	M	N	O	P	Q	R
61	60	53	57	67	53	62	61	59	60	57	58	64	60	64	60	59	58	59
61	60	53	57	67	53	62	61	59	60	57	58	64	60	64	60	59	58	59
61	60	53	57	67	53	62	61	59	60	57	58	64	60	64	60	59	58	59
61	60	53	57	67	53	62	61	59	60	57	58	64	60	64	60	59	58	59
61	60	53	57	67	53	62	61	59	60	57	58	64	60	64	60	59	58	59
61	60	53	57	67	53	62	61	59	60	57	58	64	60	64	60	59	58	59
61	60	53	57	67	53	62	61	59	60	57	58	64	60	64	60	59	58	59
61	60	53	57	67	53	62	61	59	60	57	58	64	60	64	60	59	58	59
61	60	53	57	67	53	62	61	59	60	57	58	64	60	64	60	59	58	59
61	60	53	57	67	53	62	61	59	60	57	58	64	60	64	60	59	58	59
61	60	53	57	67	53	62	61	59	60	57	58	64	60	64	60	59	58	59

9 -137.1 146.7 2.365

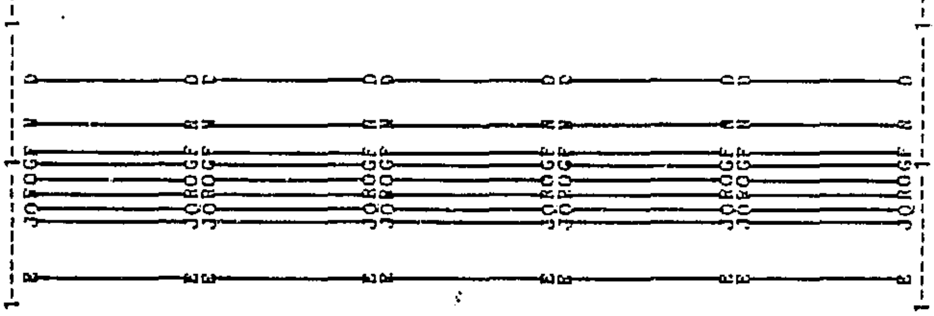

ORIGINAL PAGE IS OF POOR QUALITY

0	A	B	C	D	E	F	G	H	I	J	K	L	M	N	O	P	Q	R	S	T
63	69	70	67	67	69	70	66	70	74	62	74	70	67	66	69	72	71	70	68	64
63	69	70	67	67	69	70	66	70	74	62	74	70	67	66	69	72	71	70	68	64
63	69	70	67	67	69	70	66	70	74	62	74	70	67	66	69	72	71	70	68	64
63	69	70	67	67	69	70	66	70	74	62	74	70	67	66	69	72	71	70	68	64
63	69	70	67	67	69	70	66	70	74	62	74	70	67	66	69	72	71	70	68	64
63	69	70	67	67	69	70	66	70	74	62	74	70	67	66	69	72	71	70	68	64
63	69	70	67	67	69	70	66	70	74	62	74	70	67	66	69	72	71	70	68	64
63	69	70	67	67	69	70	66	70	74	62	74	70	67	66	69	72	71	70	68	64
63	69	70	67	67	69	70	66	70	74	62	74	70	67	66	69	72	71	70	68	64
63	69	70	67	67	69	70	66	70	74	62	74	70	67	66	69	72	71	70	68	64

10 -97.57 76.74 1.453

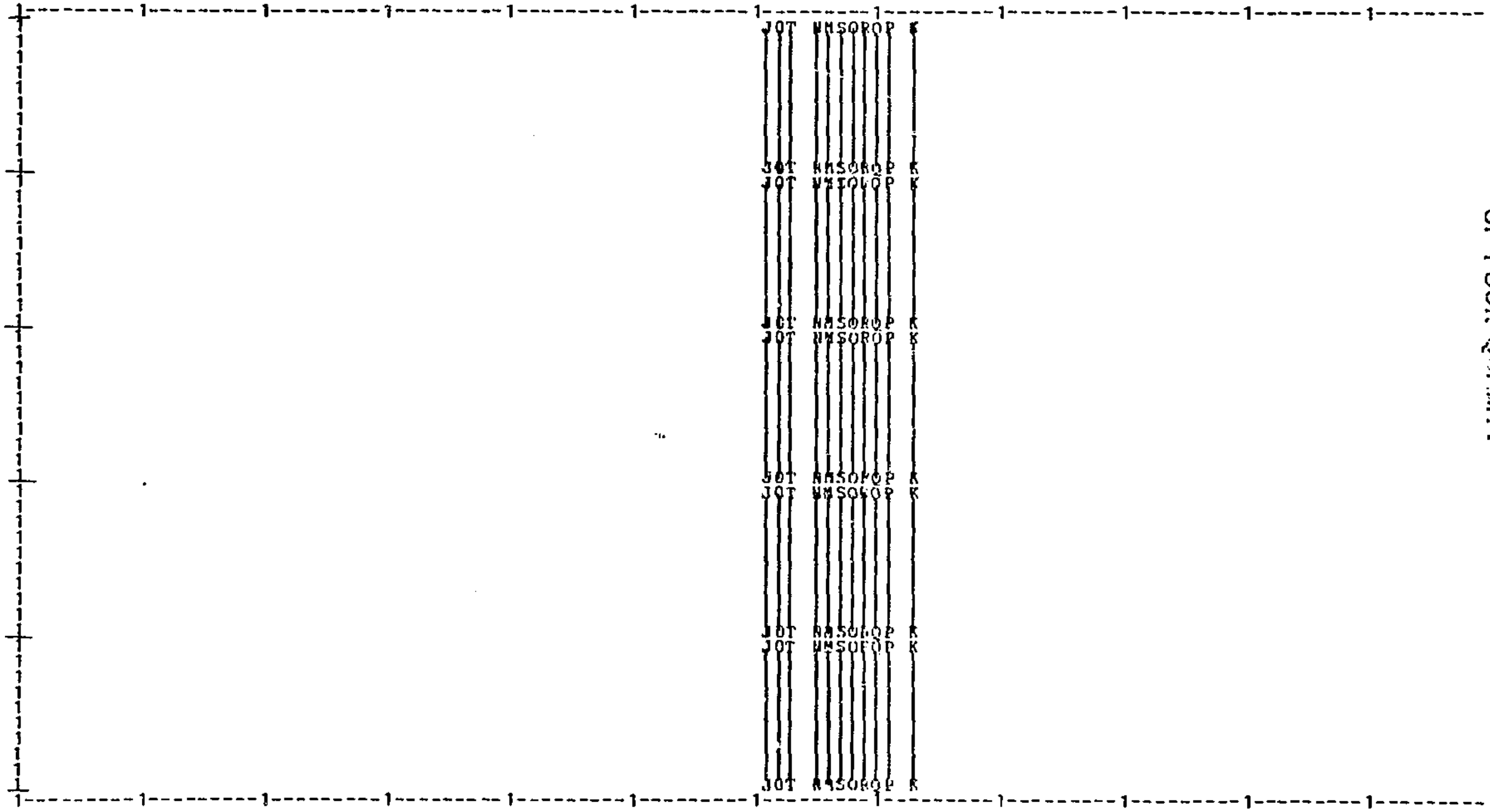

ORIGINAL PAGE IS
OF POOR QUALITY

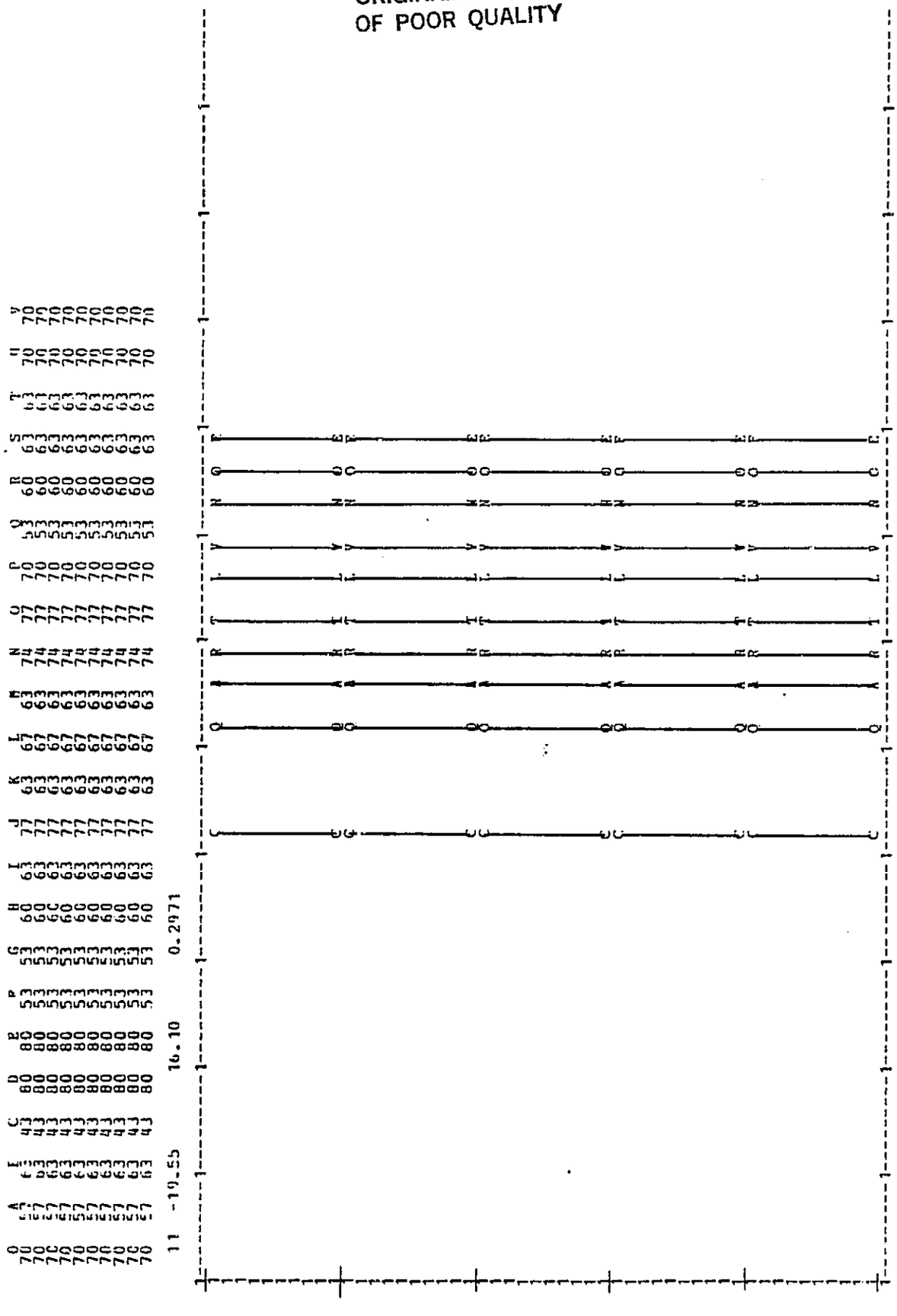

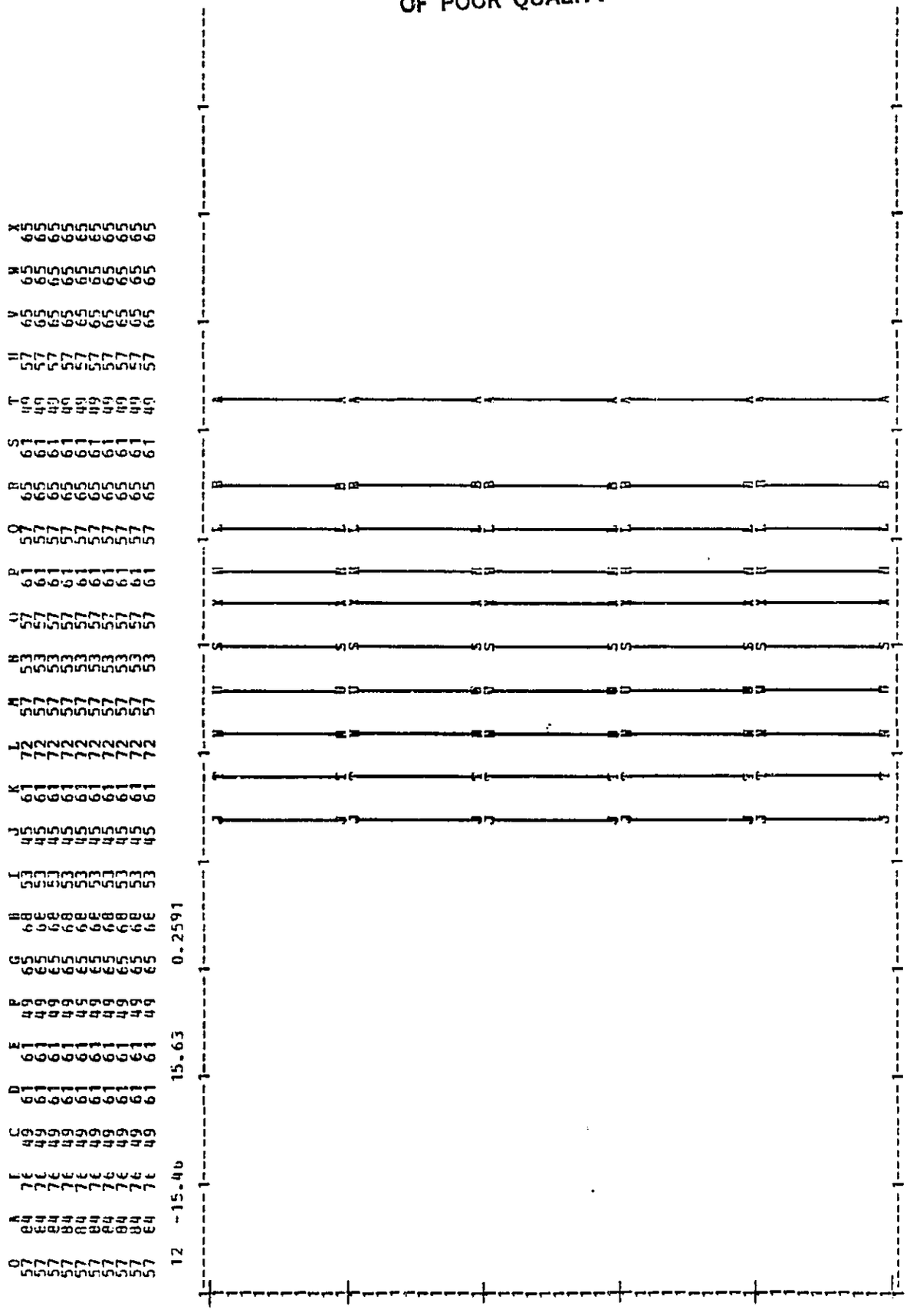

Appendix A-4 Plots of PMAG (7/80) Field Model Coefficients

The following line printer plots of the PMAG (7/80) field model were produced using almost the same scale as the plots of the mini-batch coefficients (Figure 3.1). Directly above each plot are four numbers. The first number is the coefficient degree. The second and third numbers are the minimum and maximum values of the plot in nanotesla. The last number is the scale factor in nT per small division (one print position).

The coding of the coefficient order is the same as in Figure 3.1, i.e.

$$0 = g^{i,0}$$

$$A = g^{i,1}$$

$$B = h^{i,1}$$

$$C = g^{i,2}$$

$$\vdots \quad \vdots$$

$$Z = h^{i,13}$$

The numbers at the top of each plot are the print positions for each letter (order) for the ten points plotted. This is useful in resolving plotting ambiguities.

PMAG (7/90)

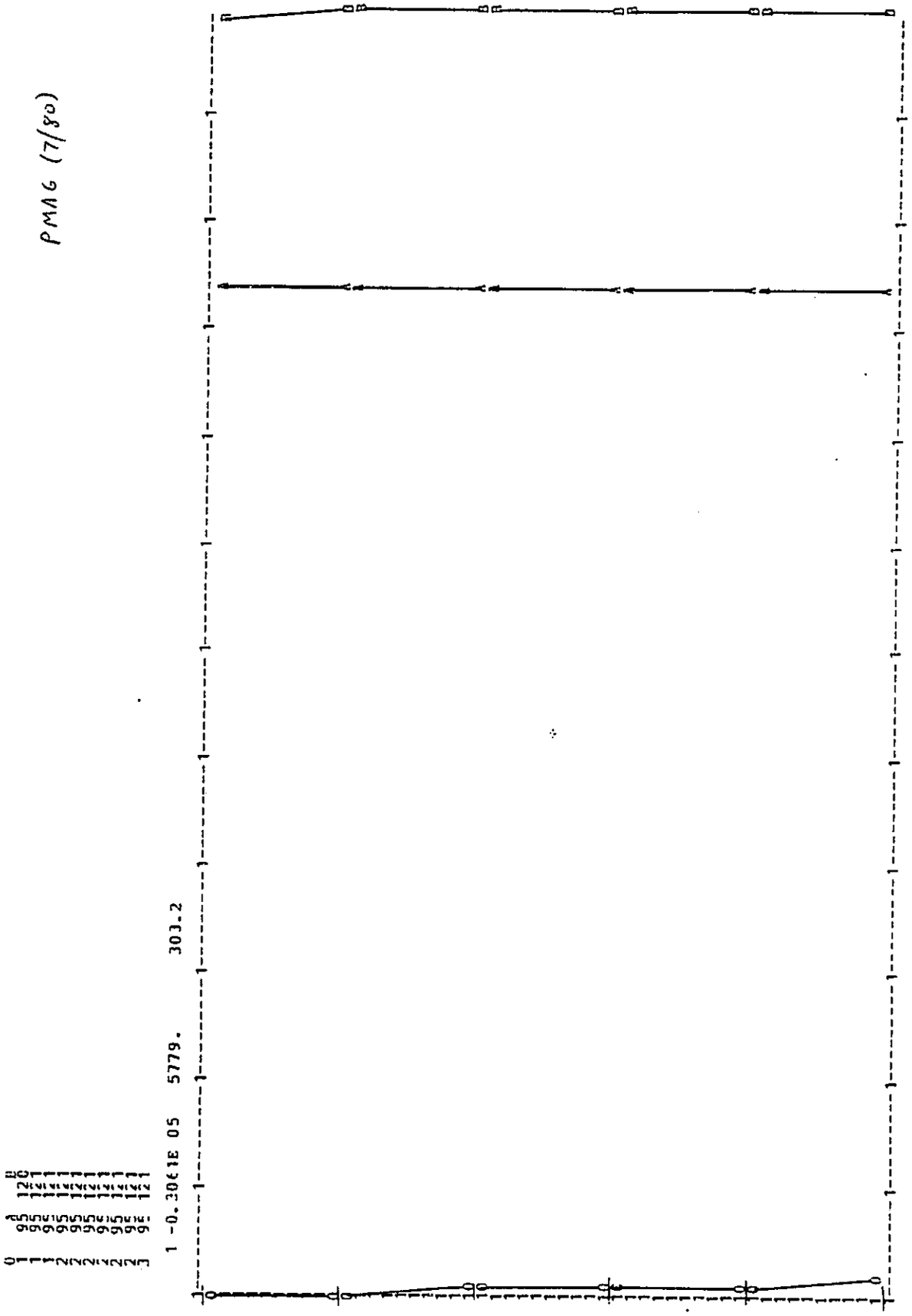

ORIGINAL PAGE IS
OF POOR QUALITY

ORIGINAL PAGE IS
OF POOR QUALITY

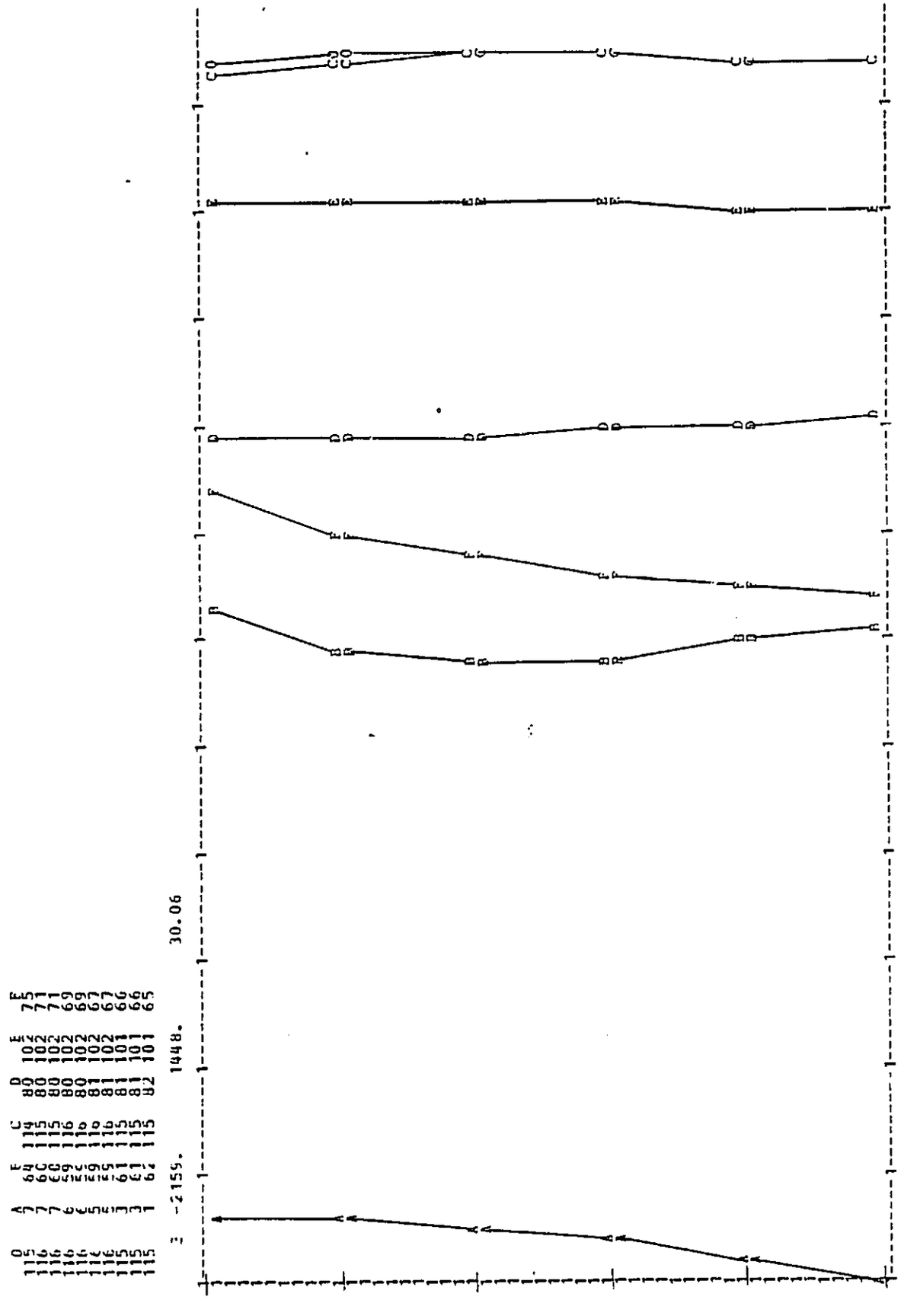

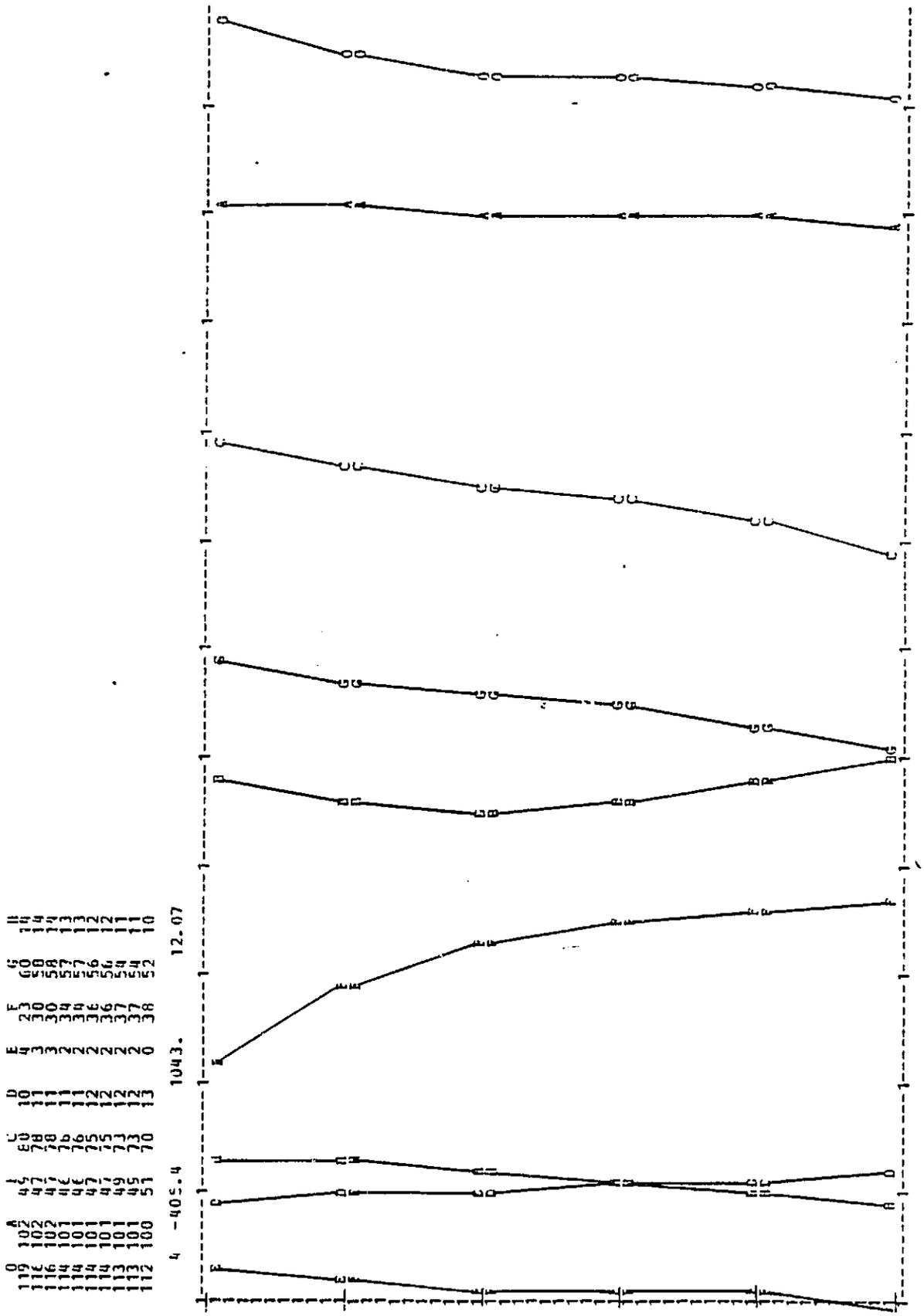

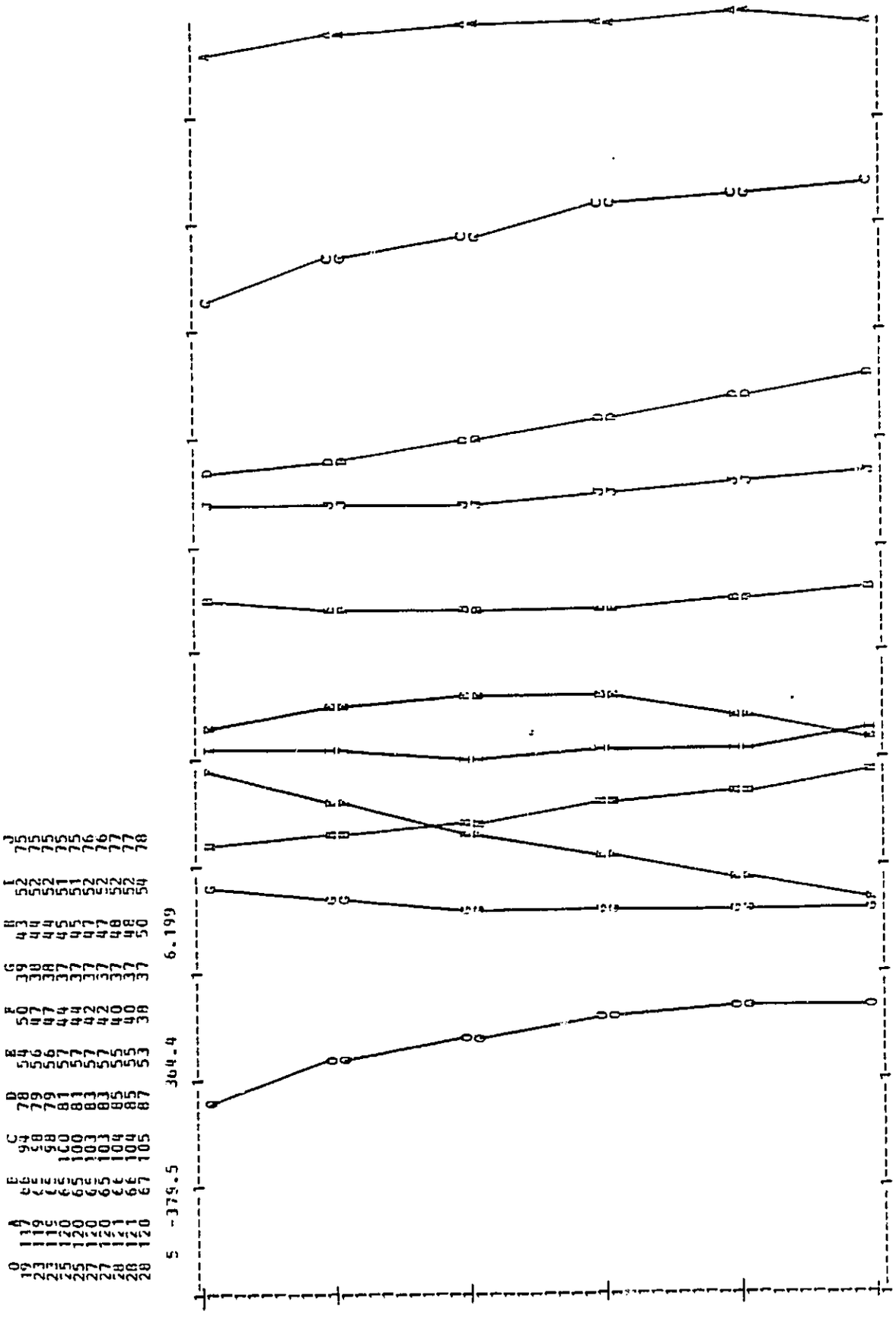

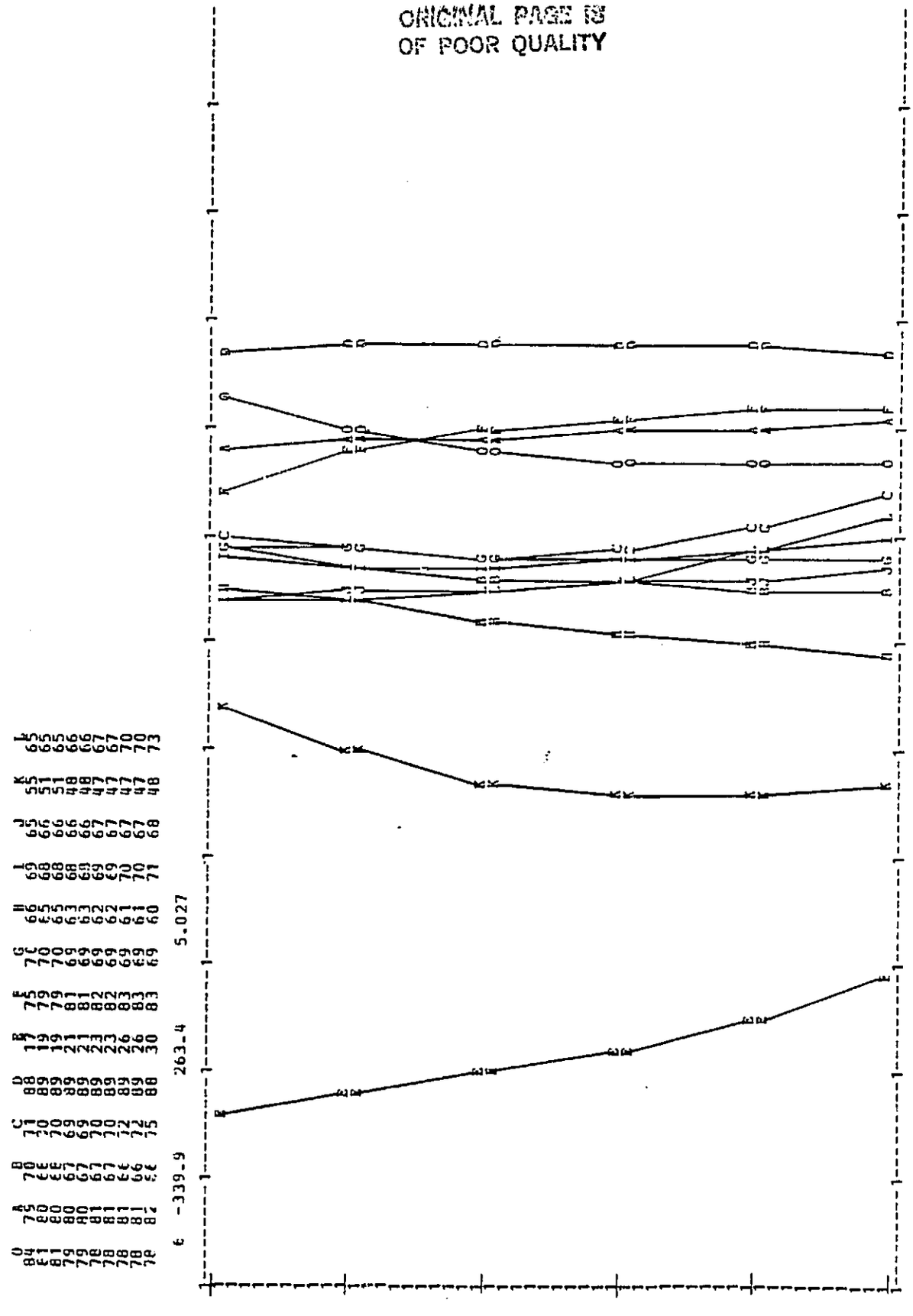

ORIGINAL PAGE IS
OF POOR QUALITY

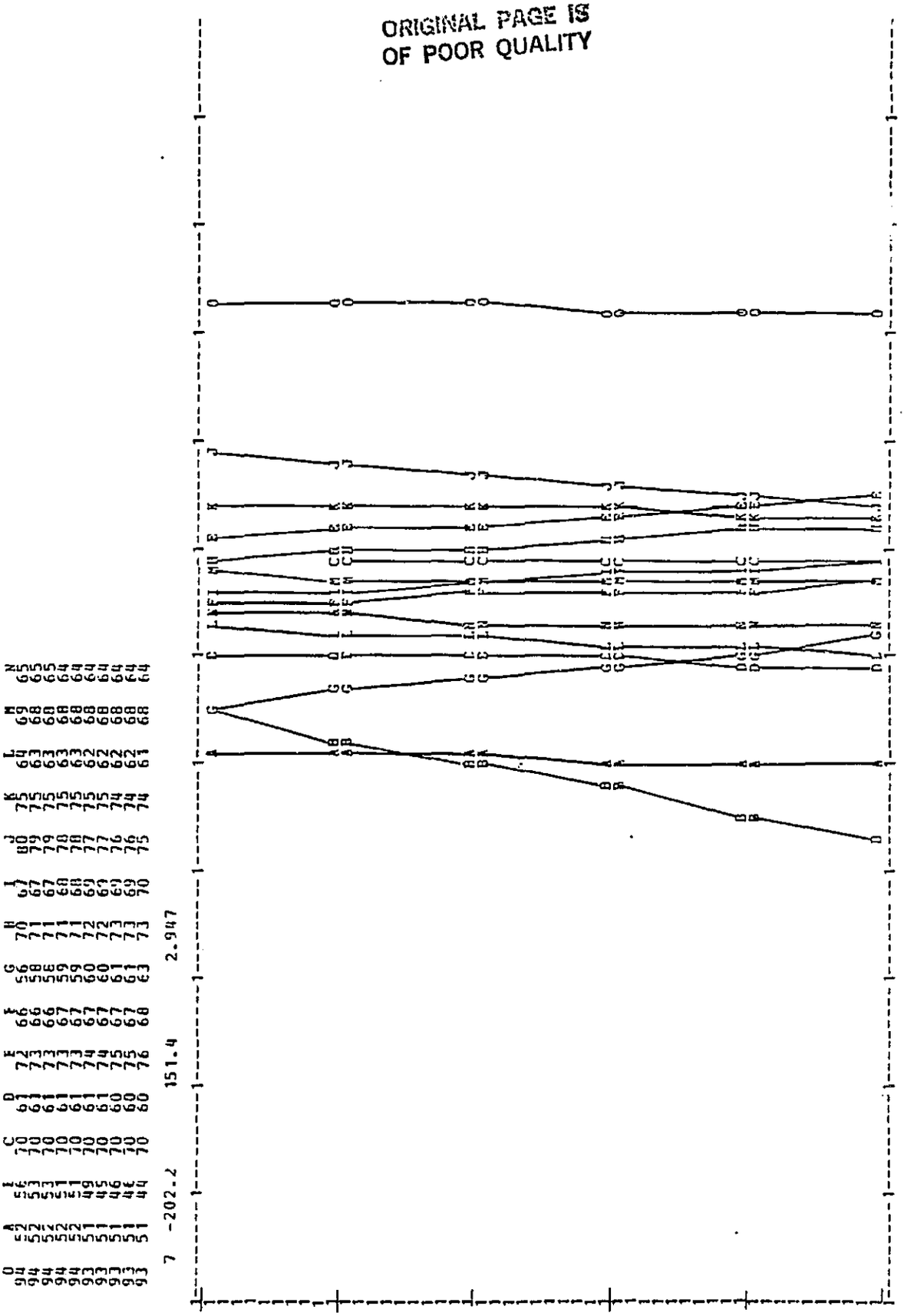

	A	B	C	D	E	F	G	H	I	J	K	L	M	N	O	P
64	63	65	59	59	58	64	62	55	66	62	58	70	66	63	69	56
64	63	65	60	59	58	64	61	58	65	63	59	70	66	62	67	56
64	63	64	61	58	58	64	61	58	65	63	60	69	65	61	66	57
64	63	64	61	58	56	64	61	58	65	63	60	69	65	61	66	57
65	63	64	61	58	55	63	61	57	64	63	61	68	65	61	64	57
65	63	64	61	58	59	63	61	57	64	63	61	68	65	61	64	57
66	64	64	62	58	59	63	61	57	63	64	61	67	65	60	63	57
66	64	64	63	58	59	63	61	56	63	64	63	67	65	59	61	57

E -216.9 209.7 3.555

ORIGINAL PAGE IS
OF POOR QUALITY

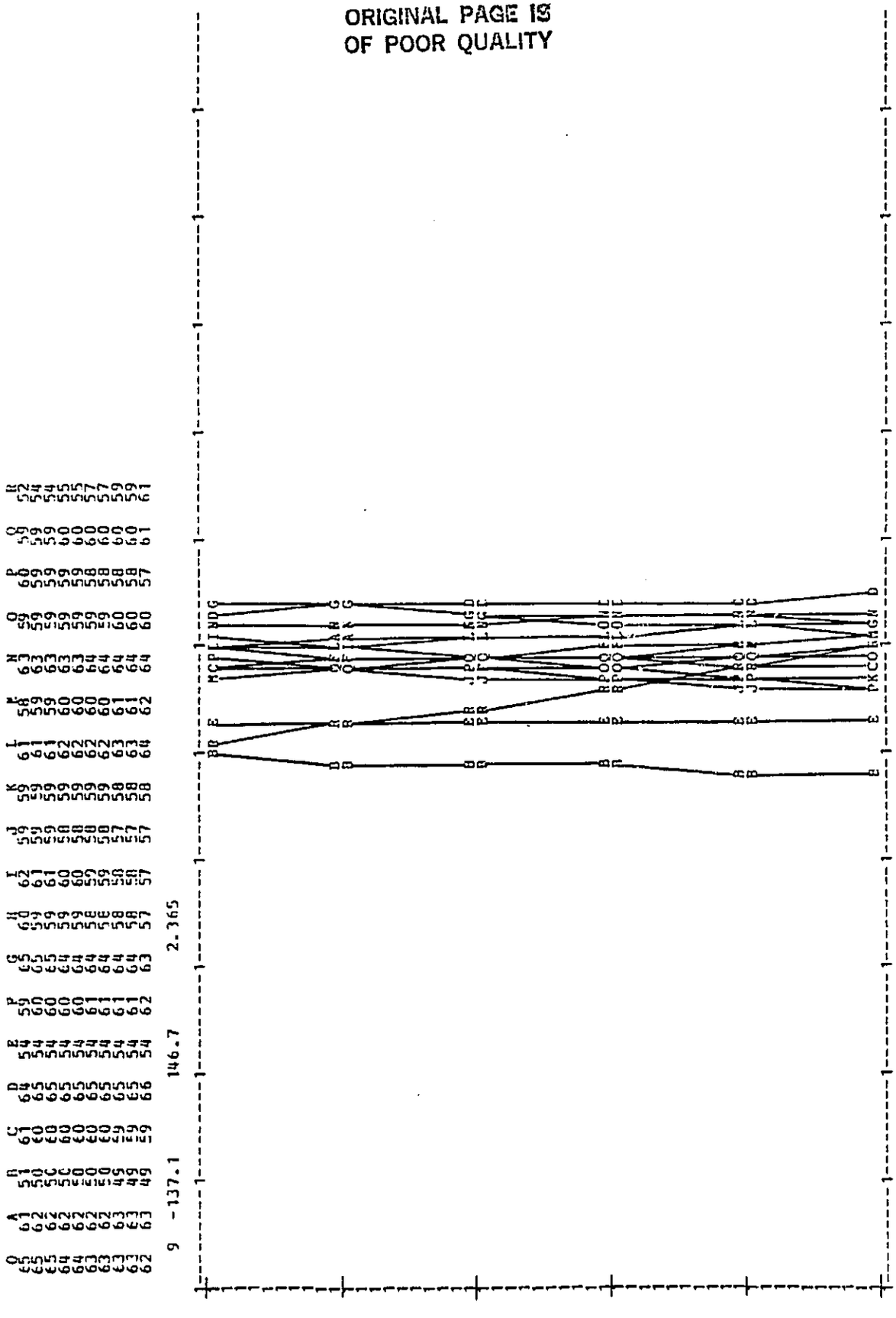

O	A	B	C	D	E	F	G	H	I	J	K	L	M	N	O	P	Q	R	S	T
68	68	72	69	70	68	68	67	72	73	65	76	70	67	67	66	67	72	71	65	71
68	67	71	69	70	67	69	67	72	73	65	75	69	68	67	67	68	71	71	66	69
68	67	71	69	70	67	69	67	72	73	65	75	69	68	67	67	68	71	71	66	69
67	67	70	69	69	67	69	67	72	72	65	74	69	68	67	68	69	71	70	67	68
67	67	70	69	69	67	69	67	72	72	65	74	69	68	67	68	69	71	70	67	68
67	67	70	69	69	66	69	67	72	72	65	72	69	68	67	68	70	71	69	68	66
67	67	70	69	69	66	69	67	72	72	65	72	69	68	67	68	70	71	69	68	66
67	66	69	70	69	65	70	67	72	72	65	71	68	68	67	69	71	71	68	69	65
67	66	69	70	69	65	70	67	72	72	65	71	68	68	67	69	71	71	68	69	65
66	66	69	70	68	64	70	67	72	72	65	70	68	69	67	70	72	70	67	71	63

10 -97.57 76.74 1.453

C-2

O	A	I	C	D	E	F	G	H	I	J	K	L	M	N	O	P	Q	R	S	T	U	V
80	63	67	65	73	84	66	59	54	59	73	62	70	77	79	75	61	68	62	83	71	96	84
79	63	68	64	74	83	65	60	55	61	72	63	69	75	75	75	62	66	62	82	69	90	82
79	63	68	64	74	83	65	60	55	61	72	63	69	75	75	75	62	66	62	82	69	90	82
77	63	70	62	75	81	63	61	56	63	71	64	68	74	70	75	64	64	61	81	68	84	80
77	63	70	62	75	81	63	61	56	63	71	64	68	74	70	75	64	64	61	81	68	84	80
76	64	71	61	76	80	62	63	56	66	70	65	67	73	65	76	65	61	60	80	67	77	78
76	64	71	61	76	80	62	63	56	66	70	65	67	73	65	76	65	61	60	80	67	77	78
75	64	72	60	76	78	61	64	57	68	68	66	67	71	60	76	66	59	60	79	65	71	75
75	64	72	60	76	78	61	64	57	68	68	66	67	71	60	76	66	59	60	79	65	71	75
73	64	74	59	77	76	59	66	58	70	67	67	66	70	54	76	68	57	59	78	64	64	71

11 -19.55 16.10 0.2971

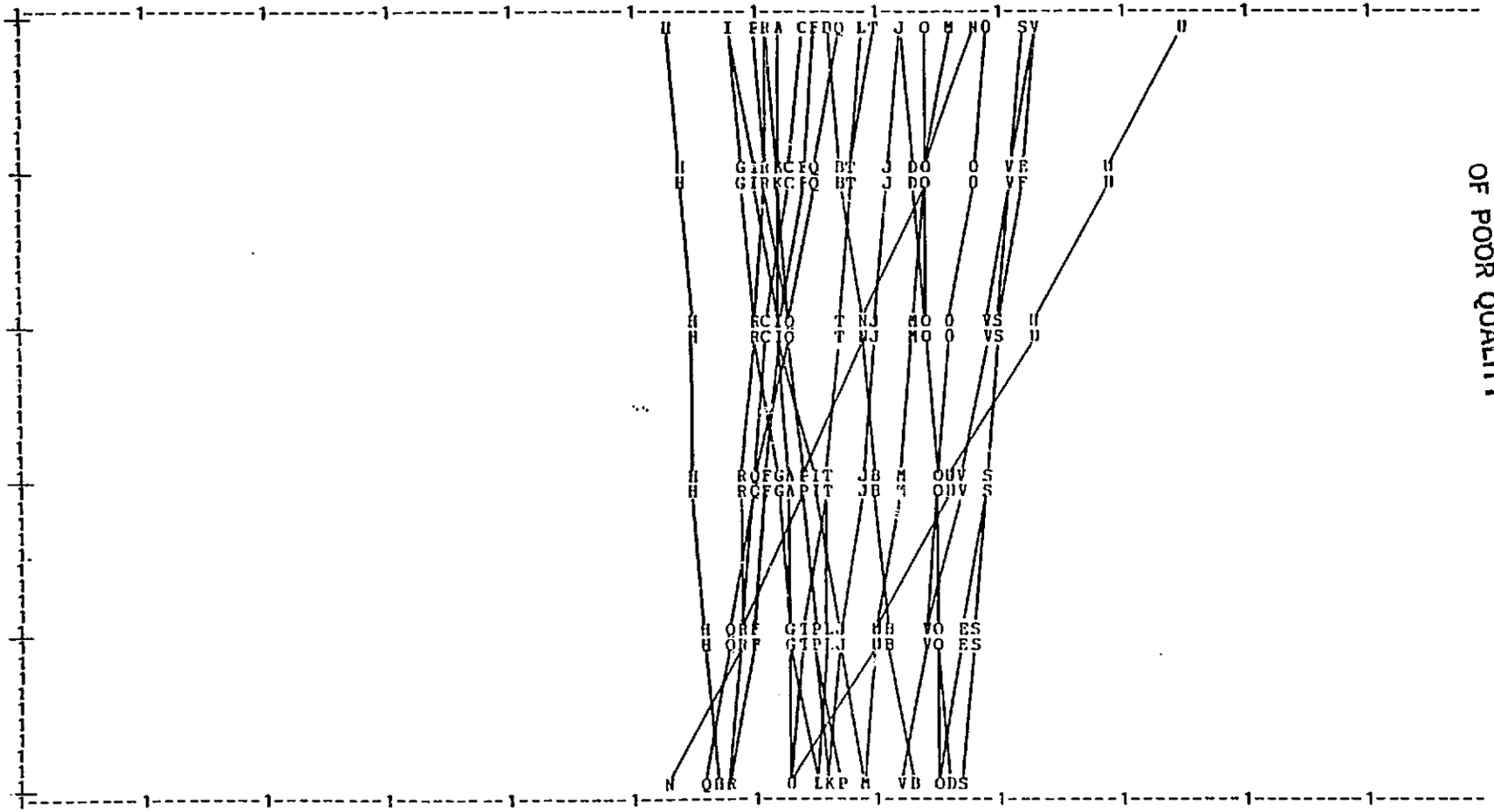

ORIGINAL PAGE IS
OF POOR QUALITY

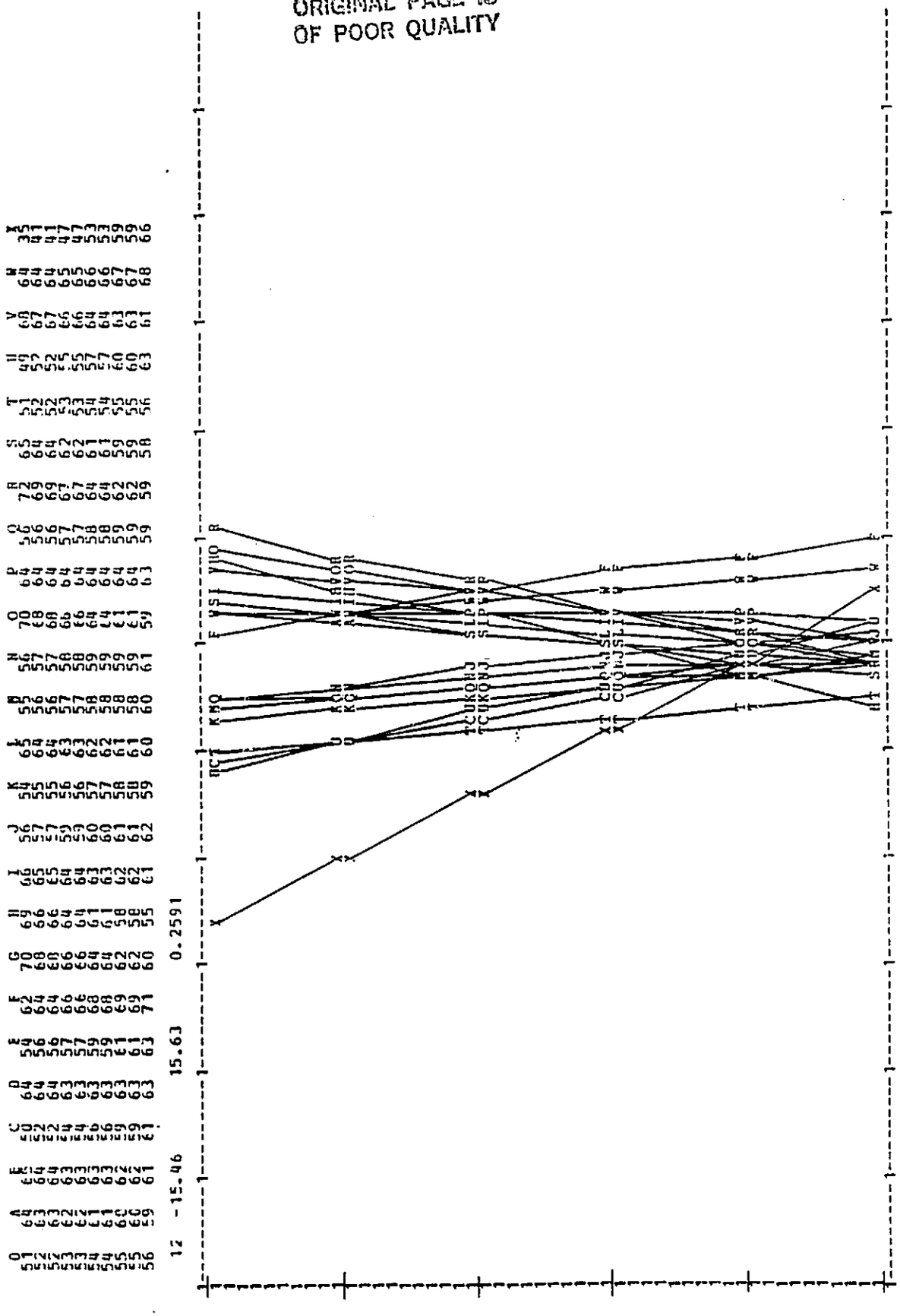

ORIGINAL PAGE IS
OF POOR QUALITY.

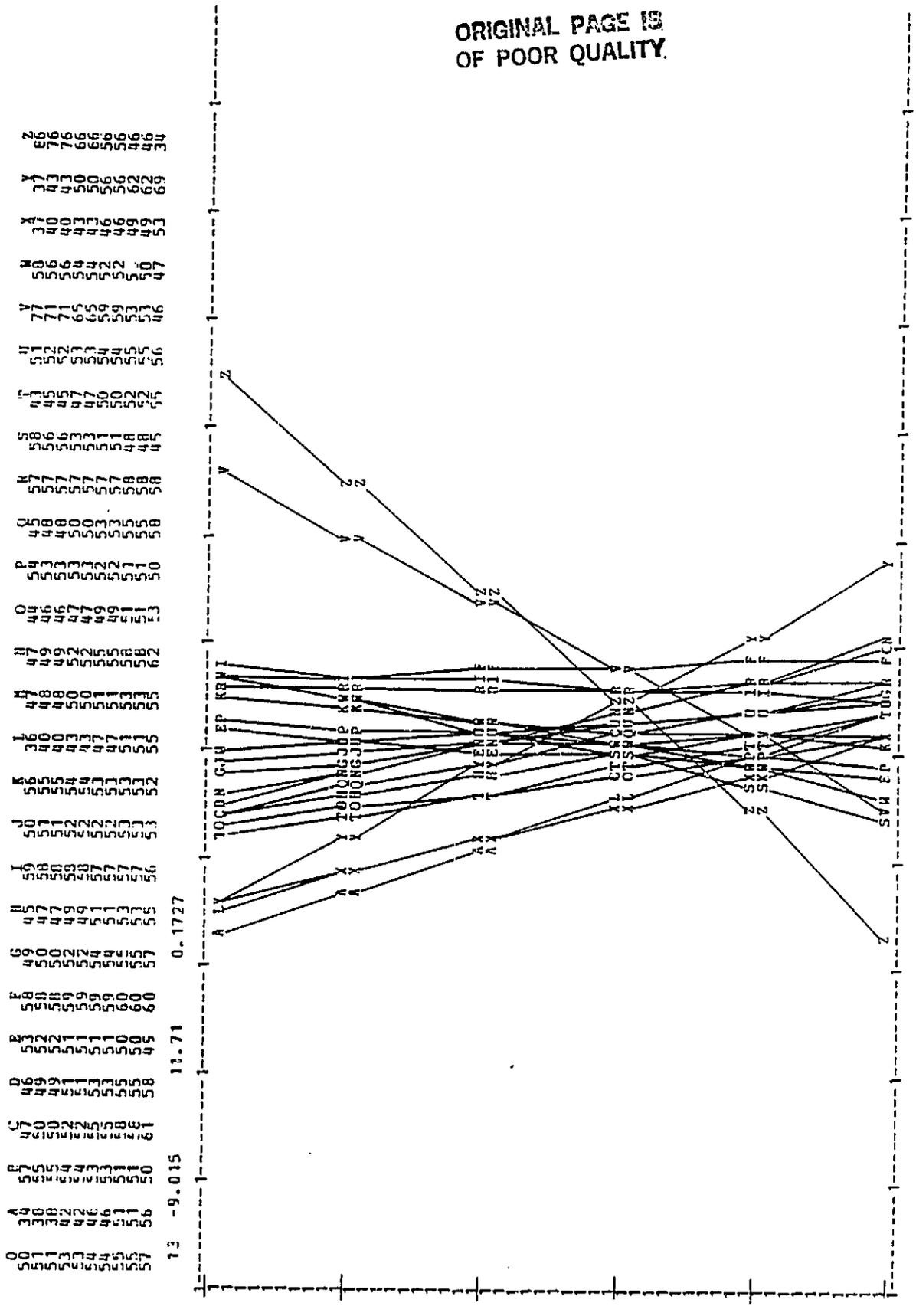

Appendix A-5 Plots of GSFC (2/81) Field Model Coefficients

The following line printer plots of the GSFC (2/81) field model were produced using almost the same scale as the plots of the mini-batch coefficients (Figure 3.1). Directly above each plot are four numbers. The first number is the coefficient degree. The second and third numbers are the minimum and maximum values of the plot in nanotesla. The last number is the scale factor in nT per small division (one print position).

The coding of the coefficient order is the same as in Figure 3.1, i.e.

$$0 = g^{i,0}$$

$$A = g^{i,1}$$

$$B = h^{i,1}$$

$$C = g^{i,2}$$

$$\vdots \quad \vdots$$

$$Z = h^{i,13}$$

The numbers at the top of each plot are the print positions for each letter (order) for the ten points plotted. This is useful in resolving plotting ambiguities.

GSFC (2/81)

POGO + Nov 5,6 + Mar 15 + 168 obs (1950-80)

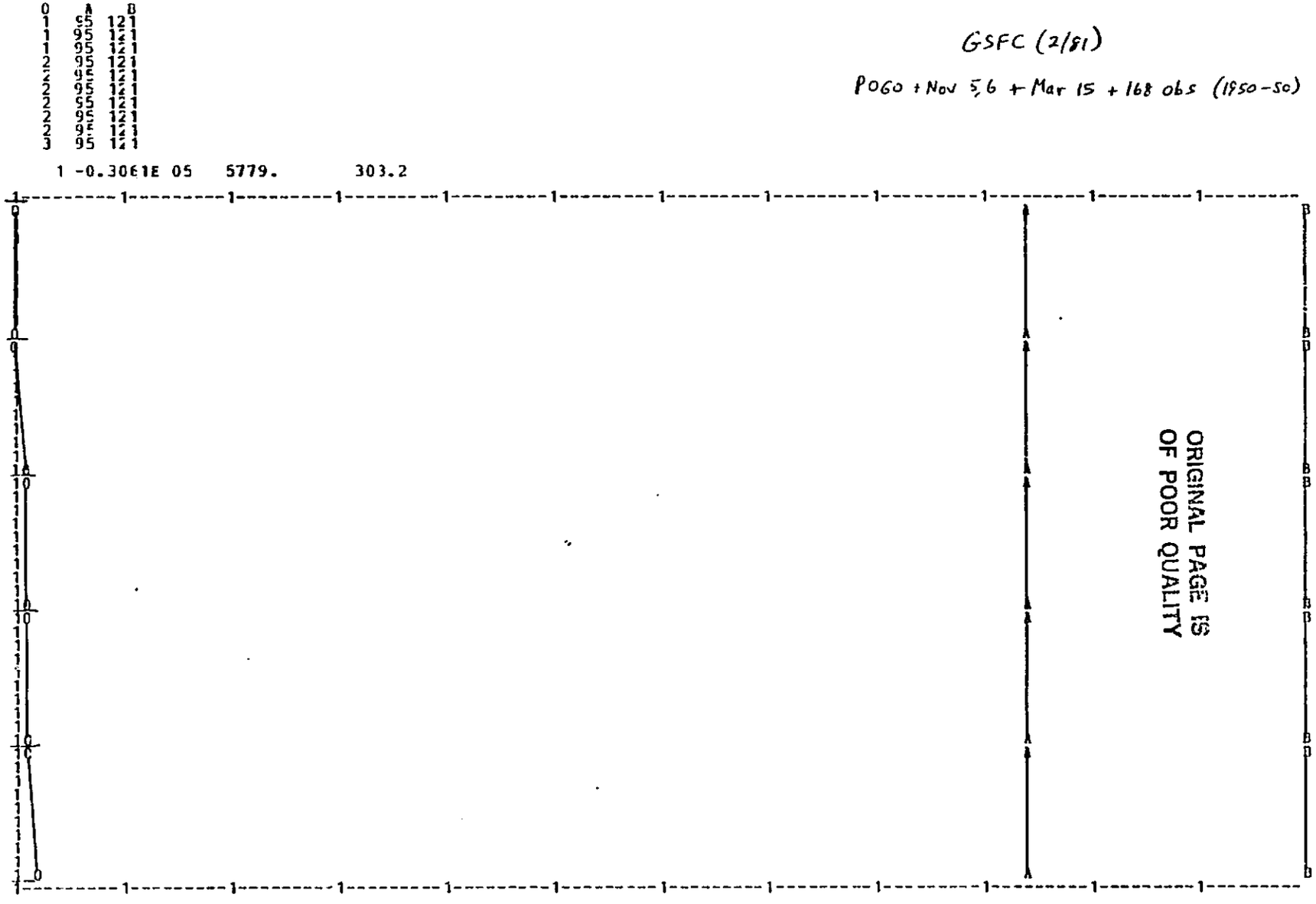

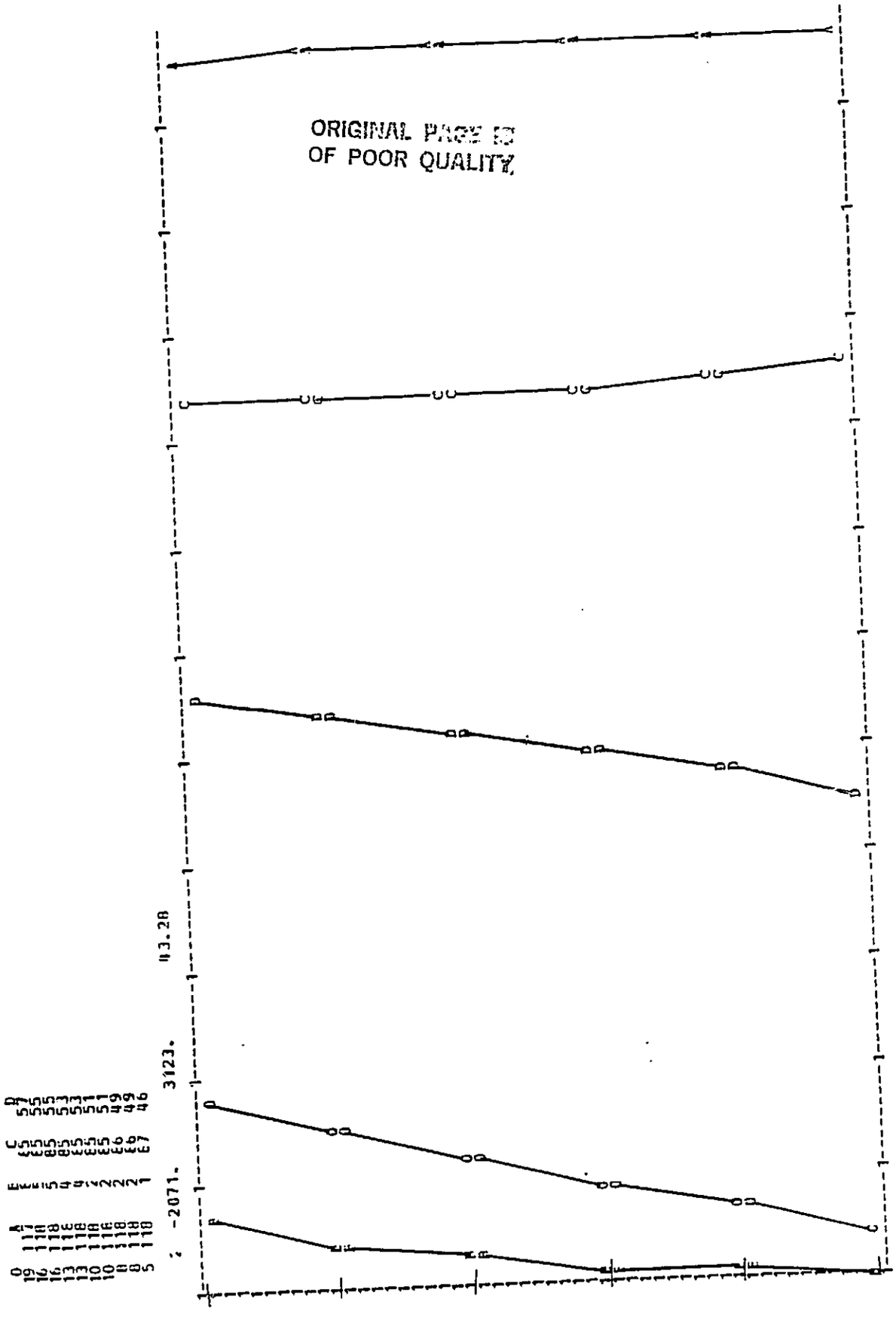
ORIGINAL PAGE IS
OF POOR QUALITY
3123.
-2071.

ORIGINAL PAGE IS
OF POOR QUALITY

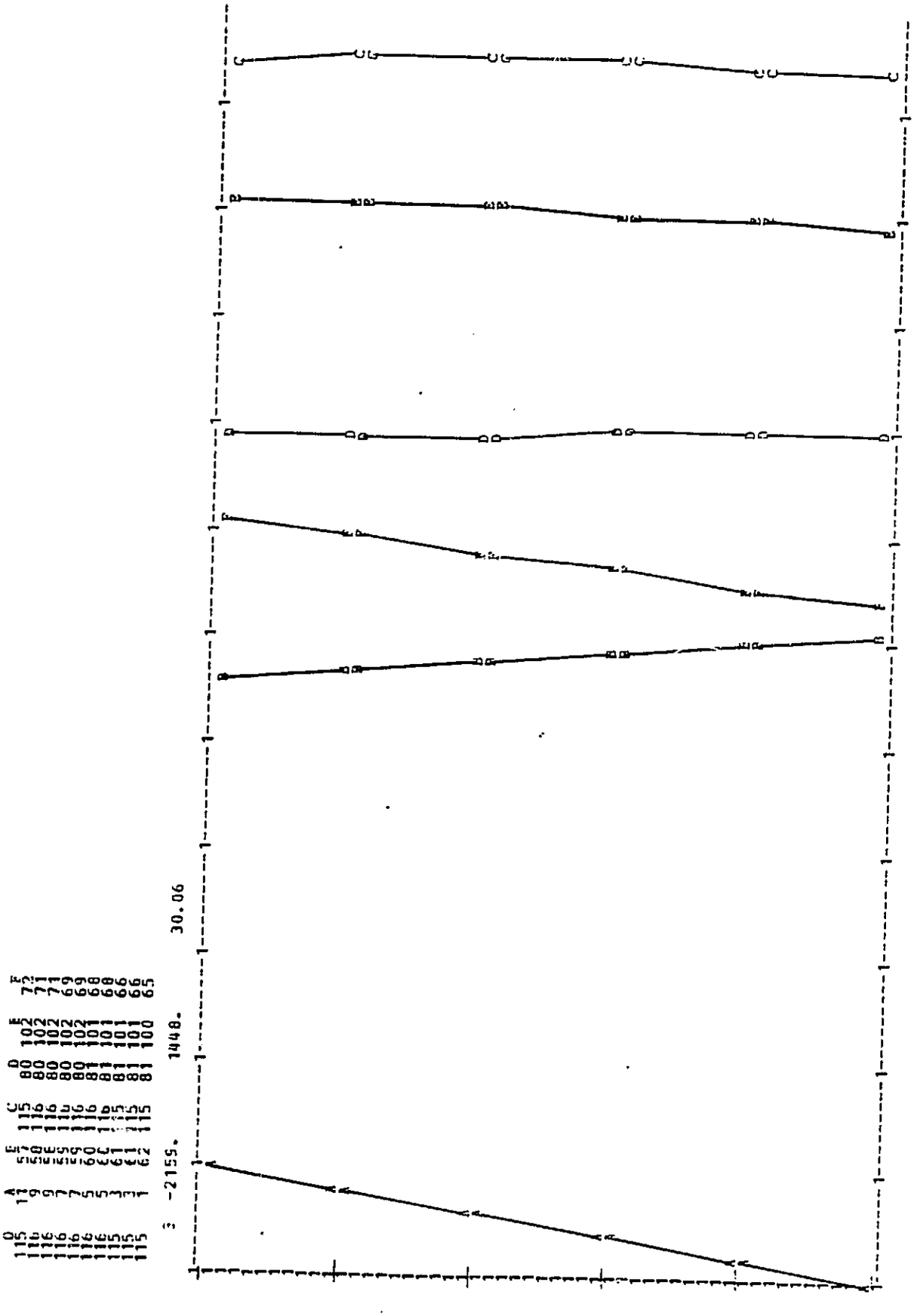

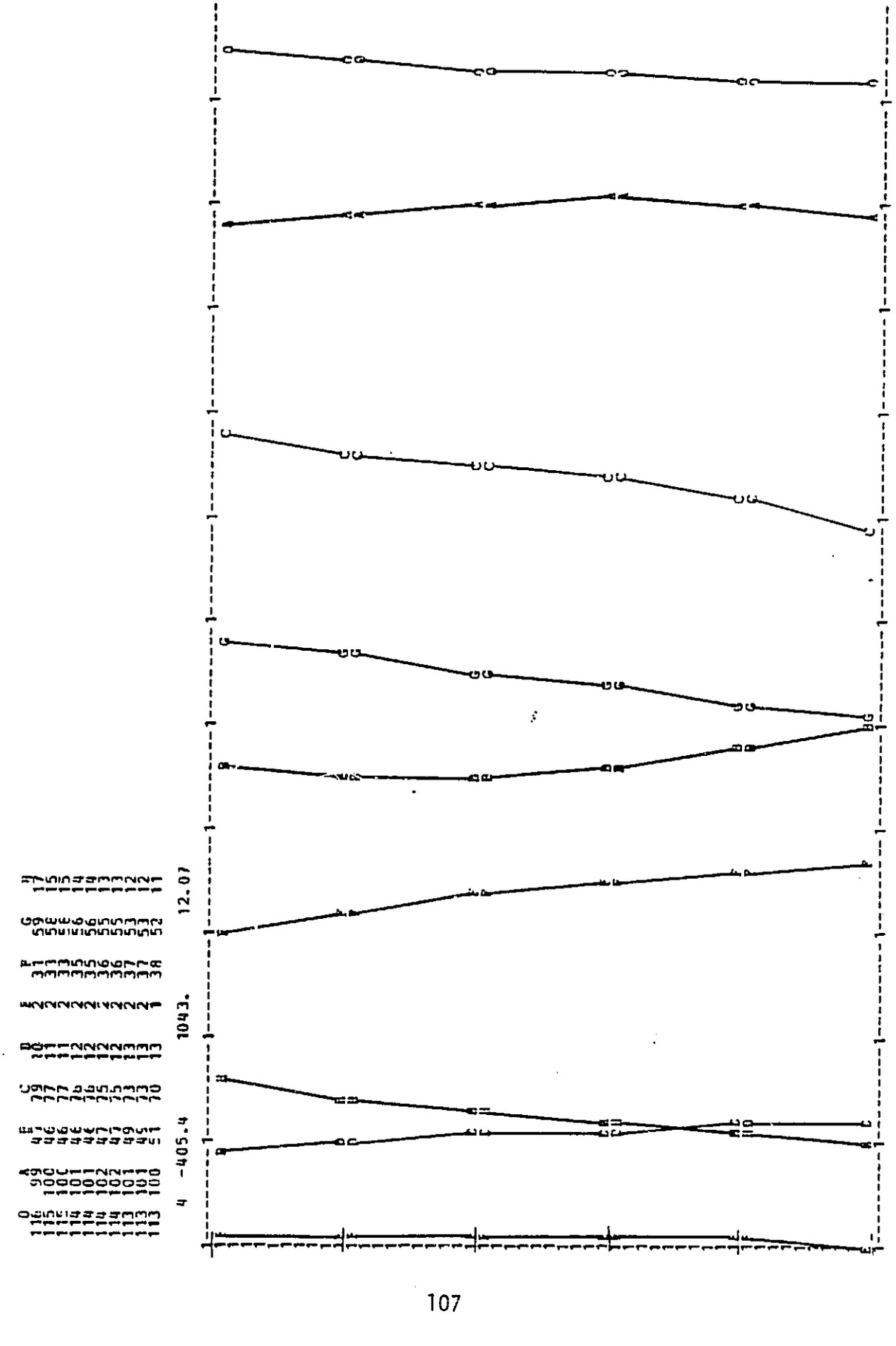

ORIGINAL PAGE IS
OF POOR QUALITY

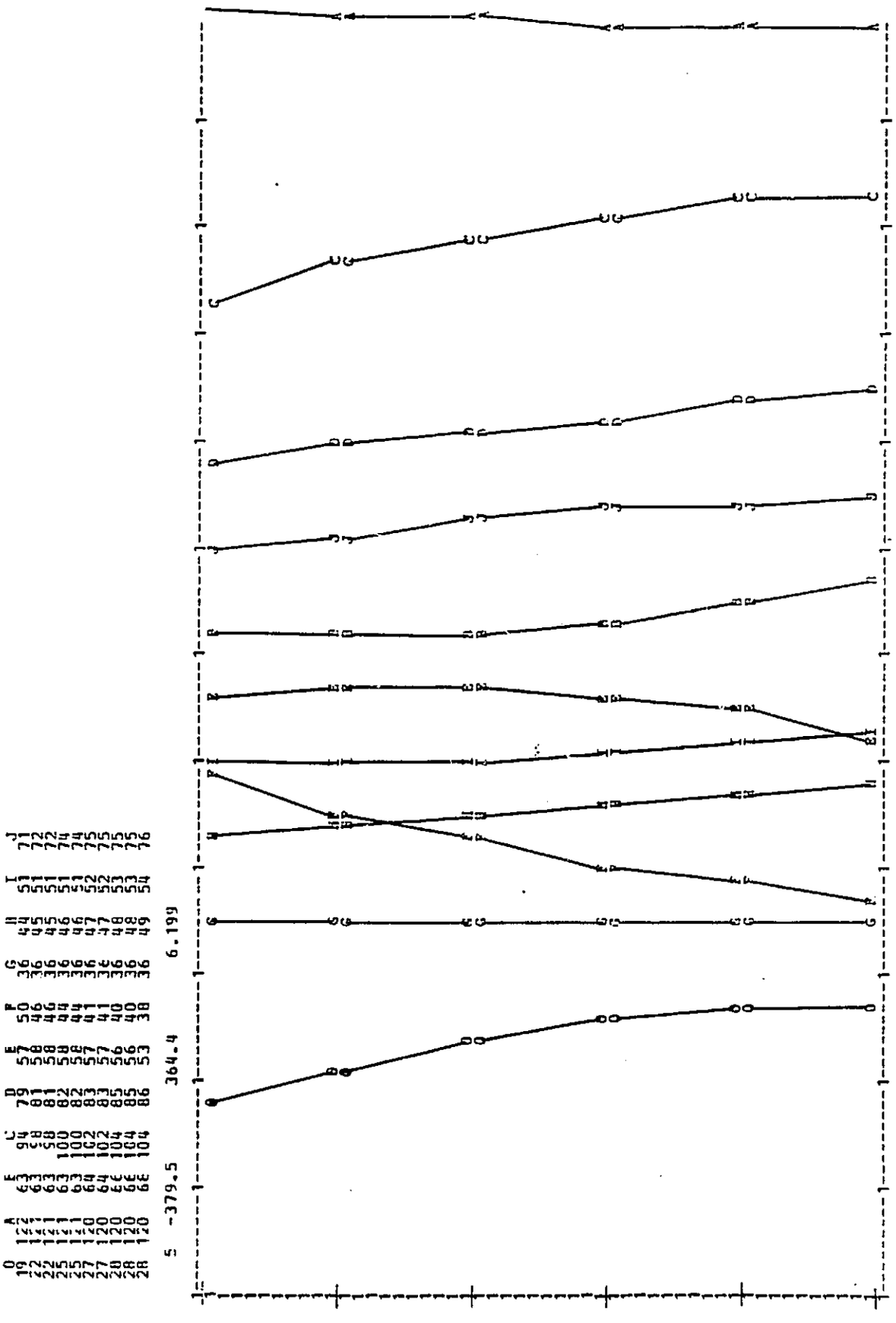

ORIGINAL PAGE IS
OF POOR QUALITY

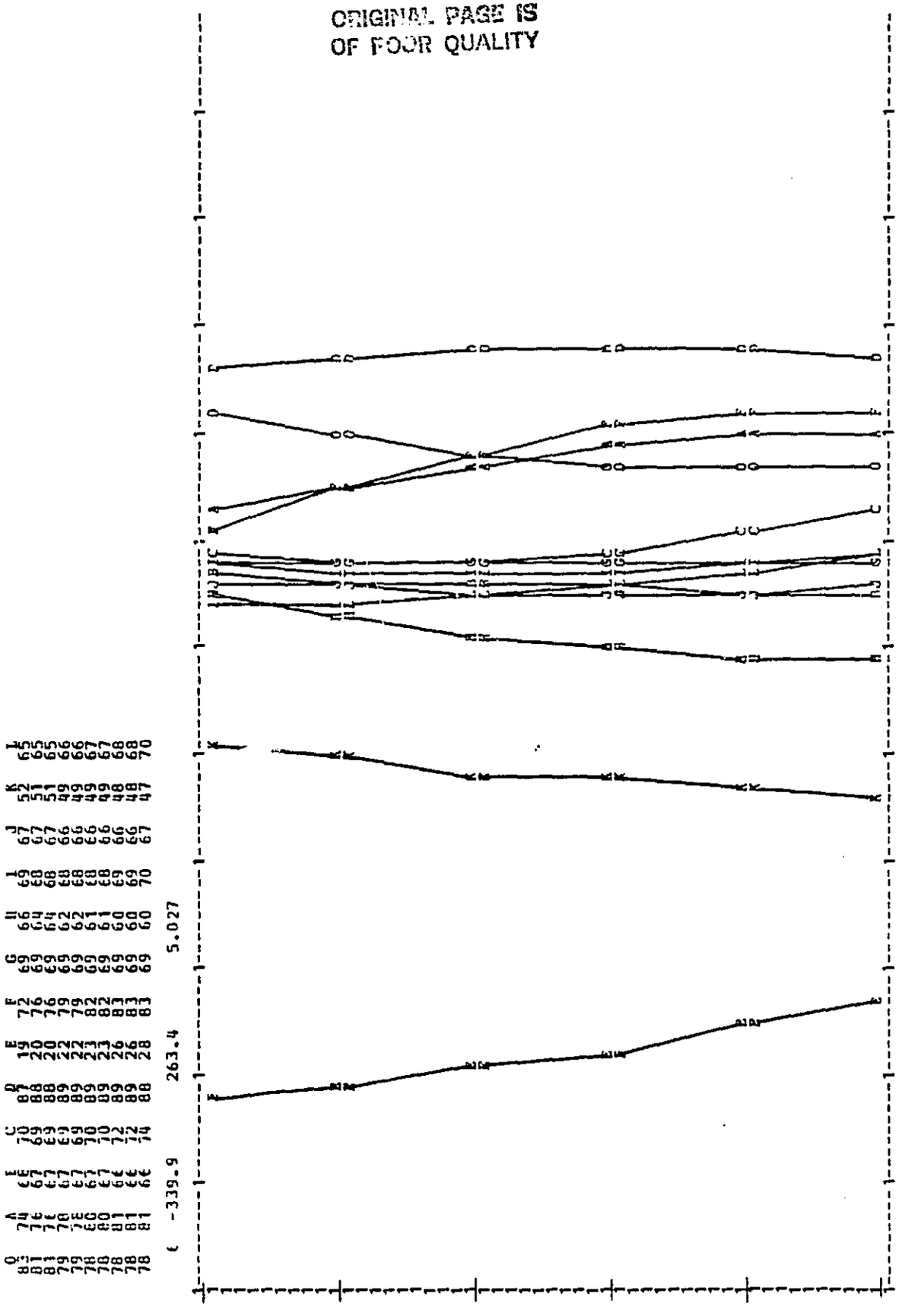

0	A	E	C	D	S	F	G	H	I	J	K	L	M	N
93	55	56	70	61	72	68	56	69	67	80	76	60	72	61
93	54	54	70	61	73	68	58	70	68	79	75	60	72	62
93	54	54	70	61	73	68	58	70	68	79	75	60	72	62
93	53	51	70	60	73	68	59	71	68	79	75	60	71	63
93	53	51	70	60	73	68	59	71	68	79	75	60	71	63
93	52	49	70	60	74	68	61	72	69	78	75	61	71	64
93	52	49	70	60	74	68	61	72	69	78	75	61	71	64
94	52	46	70	60	75	68	62	73	69	77	74	61	70	64
94	52	46	70	60	75	68	62	73	69	77	74	61	70	64
94	50	43	70	60	76	68	64	74	70	76	74	62	69	66

7 -202.2 151.4 2.947

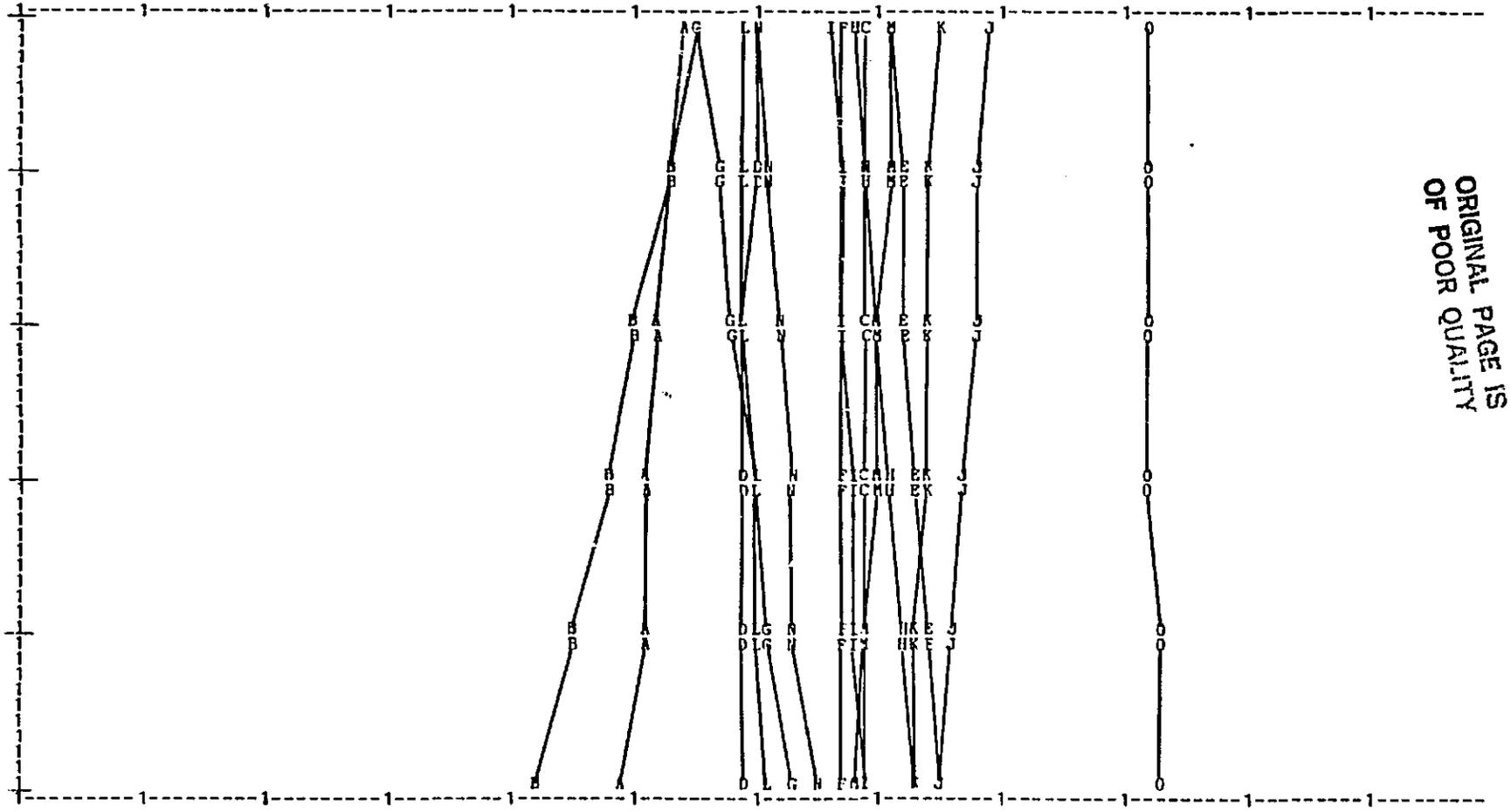

	O	A	B	C	D	E	F	G	H	I	J	K	L	M	N	O	P
62	64	64	65	60	59	59	64	63	59	66	64	58	70	69	65	61	57
63	64	64	65	61	59	59	64	62	59	66	64	58	70	68	64	61	57
63	64	64	65	61	59	59	64	62	59	66	64	58	70	68	64	61	57
64	64	64	65	61	58	59	64	62	58	65	64	59	69	67	63	61	57
64	64	64	65	61	58	59	64	62	58	65	64	59	69	67	63	61	57
65	64	64	64	61	58	59	64	61	57	65	64	60	68	66	62	61	58
65	64	64	64	61	58	59	64	61	57	65	64	60	68	66	62	61	58
66	64	64	64	62	58	59	63	61	57	64	64	61	68	65	61	62	58
66	64	64	64	62	58	59	63	61	57	64	64	61	68	65	61	62	58
67	64	64	64	62	57	59	63	60	56	63	64	62	67	65	59	62	58

8 -216.9 209.7 3.555

ORIGINAL PAGE IS
OF POOR QUALITY

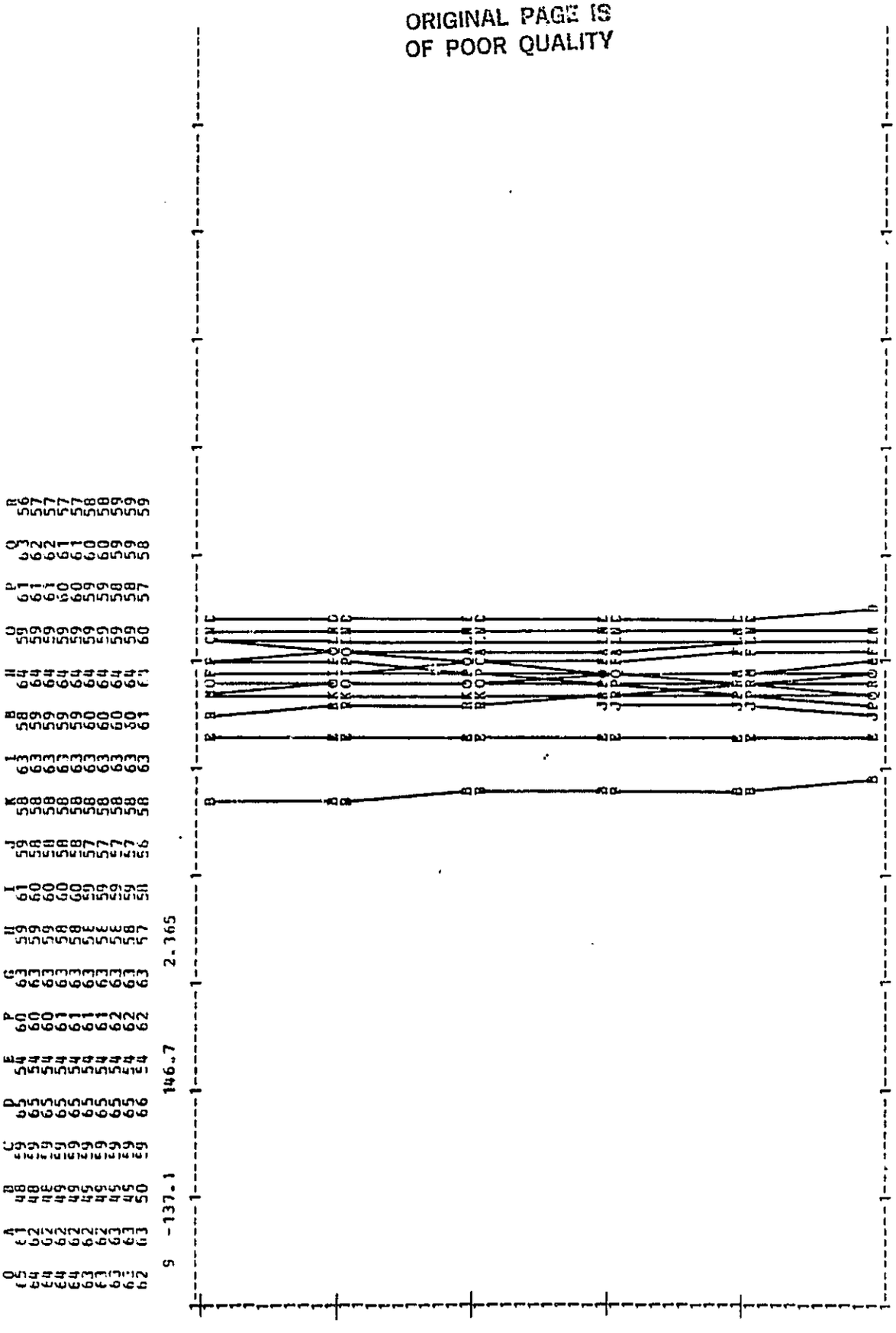

ORIGINAL PAGE IS
OF POOR QUALITY

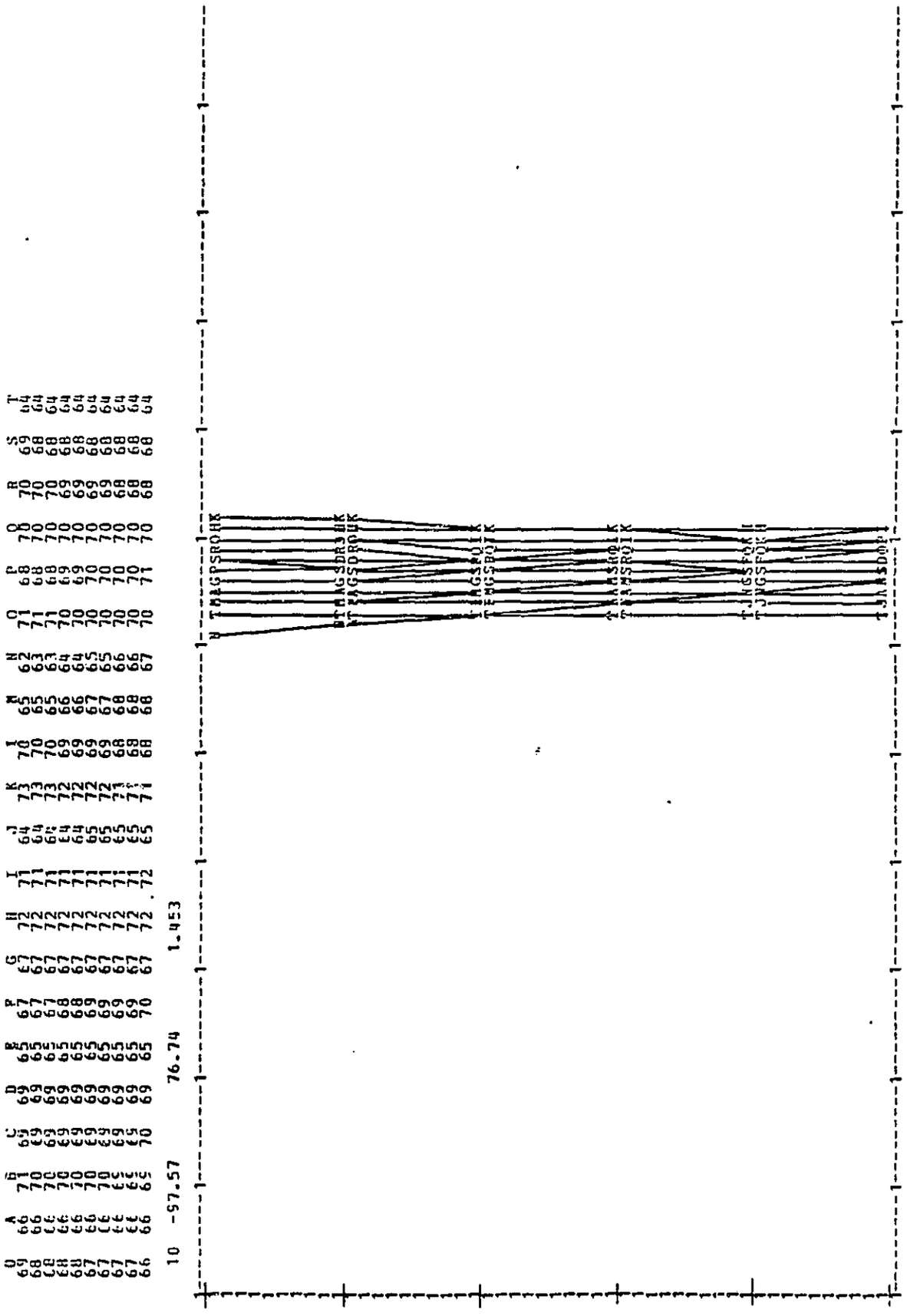

ORIGINAL PAGE IS
OF POOR QUALITY

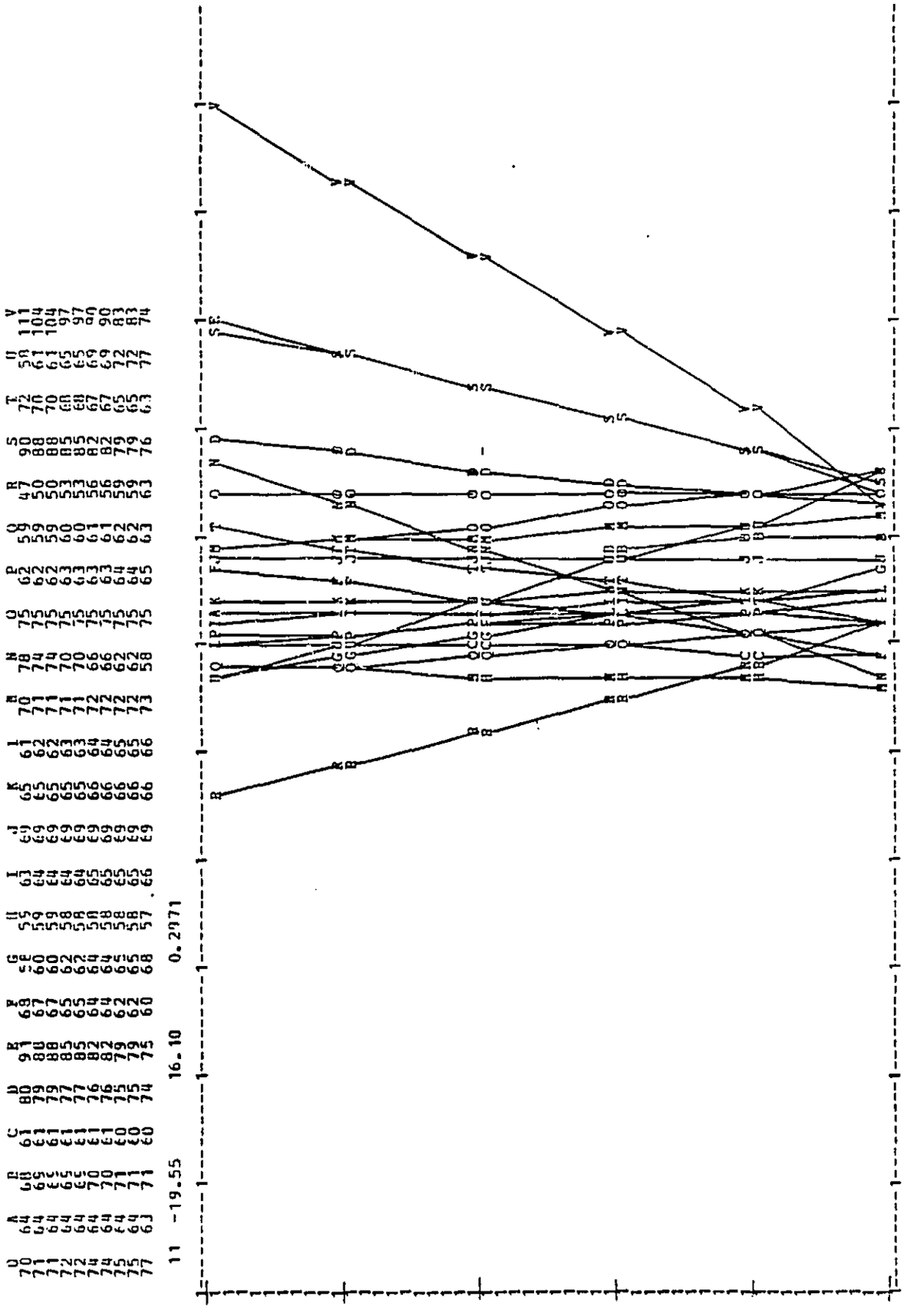

0	A	B	C	D	E	F	G	H	I	J	K	L	M	N	O	P	Q	R	S	T	U	V	W	X
59	58	64	44	57	62	66	74	62	61	74	60	53	69	67	56	77	73	68	58	53	59	77	59	68
58	59	63	47	58	61	67	72	61	62	72	59	55	67	65	57	74	70	67	58	53	60	74	59	67
58	59	63	47	58	61	67	72	61	62	72	59	55	67	65	57	74	70	67	58	53	60	74	59	67
57	60	63	50	60	61	68	69	60	62	69	59	56	65	64	58	71	67	65	59	54	60	72	59	66
57	60	63	50	60	61	68	69	60	62	69	59	56	65	64	58	71	67	65	59	54	60	72	59	66
56	60	63	54	61	61	69	67	59	63	66	59	58	63	63	59	67	65	64	60	55	61	69	60	65
56	60	63	54	61	61	69	67	59	63	66	59	58	63	63	59	67	65	64	60	55	61	69	60	65
55	61	63	57	62	60	70	65	58	63	63	58	60	61	62	60	64	62	62	61	56	61	67	60	64
55	61	63	57	62	60	70	65	58	63	63	58	60	61	62	60	64	62	62	61	56	61	67	60	64
54	62	62	61	63	60	71	62	57	64	60	58	63	59	61	61	61	59	61	61	57	62	64	61	63

12 -15.46 15.63 0.2591

ORIGINAL PAGE IS
OF POOR QUALITY